The Second *Swift* BAT Gamma-Ray Burst Catalog

T. Sakamoto[1,2,3], S. D. Barthelmy[3], W. H. Baumgartner[1,2,3], J. R. Cummings[1,2,3], E. E. Fenimore[4], N. Gehrels[3], H. A. Krimm[1,5,3], C. B. Markwardt[1,6,3], D. M. Palmer[4], A. M. Parsons[3], G. Sato[7], M. Stamatikos[8], J. Tueller[3], T. N. Ukwatta[9,3]

ABSTRACT

We present the second *Swift* Burst Alert Telescope (BAT) catalog of gamma-ray bursts (GRBs), which contains 476 bursts detected by the BAT between 2004 December 19 and 2009 December 21. This catalog (hereafter the BAT2 catalog) presents burst trigger time, location, 90% error radius, duration, fluence, peak flux, the time-averaged spectral parameters and the time-resolved spectral parameters measured by the BAT. In the correlation study of various observed parameters extracted from the BAT prompt emission data, we distinguish among long-duration GRBs (L-GRBs), short-duration GRBs (S-GRBs), and short-duration GRBs with extended emissions (S-GRBs with E.E.) to investigate for a possible distinct difference in the prompt emission properties. We compare the BAT prompt emission properties with the BATSE, the *BeppoSAX* and the *HETE*-2 GRB samples. We also correlate the observed prompt emission properties with the redshifts for the known redshift GRBs. The BAT T_{90} and T_{50} durations peak at 70 and 30 s, respectively. We confirm that the spectrum of the BAT S-GRBs are generally harder than those of the L-GRBs. The

[1]Center for Research and Exploration in Space Science and Technology (CRESST), NASA Goddard Space Flight Center, Greenbelt, MD 20771

[2]Joint Center for Astrophysics, University of Maryland, Baltimore County, 1000 Hilltop Circle, Baltimore, MD 21250

[3]NASA Goddard Space Flight Center, Greenbelt, MD 20771

[4]Los Alamos National Laboratory, P.O. Box 1663, Los Alamos, NM, 87545

[5]Universities Space Research Association, 10211 Wincopin Circle, Suite 500, Columbia, MD 21044-3432

[6]Department of Astronomy, University of Maryland, College Park, MD 20742

[7]Institute of Space and Astronautical Science, JAXA, Kanagawa 229-8510, Japan

[8]Center for Cosmology and Astro-Particle Physics, Department of Physics, The Ohio State University, 191 West Woodruff Avenue, Columbus, OH 43210

[9]Center for Nuclear Studies, Department of Physics, The George Washington University, Washington, D.C. 20052

time-averaged spectrum of the BAT S-GRBs with E.E. is similar to that of the L-GRBs. Whereas, the spectrum of the initial short spikes of the S-GRBs with E.E. is similar to that of the S-GRBs. We show that the BAT GRB samples are significantly softer than the BATSE bright GRBs. This is also consistent that the time-averaged $E_{\rm peak}^{\rm obs}$ of the BAT GRBs peak at 80 keV which is significantly smaller than those of the BATSE which peak at 320 keV. The time-averaged spectral properties of the BAT GRB samples are similar to those of the *HETE*-2 GRB samples. By the time-resolved spectral analysis, we find that 10% the BAT observed photon indices are outside of the allowed region from the synchrotron shock model. The observed duration of the BAT high redshift GRBs are not systematically longer than the moderate redshift GRBs. Furthermore, the observed spectra of the BAT high redshift GRBs are similar to or harder than the moderate redshift GRBs. The T_{90} and T_{50} distributions measured at the 140-220 keV band at the GRB rest frame form the BAT known redshift GRBs peak at 19 s and 8 s, respectively. We also report the update on the status of the on-orbit BAT calibrations.

Subject headings: gamma rays: bursts

1. Intruduction

The *Swift* mission (Gehrels et al. 2004) has revolutionized our understanding of gamma-ray bursts (GRBs) and their usage to study an early universe with the sophisticated on-board localization capability of the *Swift* Burst Alert Telescope (BAT; Barthelmy et al. (2005a)), the autonomously spacecraft slewing to point the X-Ray Telescope (XRT;Burrows et al. (2005a)), the UV/Optical Telescope (UVOT; Roming et al. (2005)) to the GRB location, and by the coordinations with multi-wavelength observatories on the ground. On April 23, 2009, *Swift* BAT detected GRB 090423 at the redshift of 8.2 which suggests massive stars were produced about 630 Myr after the Big Bang (Tanvir et al. 2009; Salvaterra et al. 2009). Extraordinary bright variable optical emission, which peaked at the visual magnitude of 5.3, while the prompt gamma-ray emission was still active for GRB 080319B has provided the first conclusive observational evidence that the synchrotron peak could be down in the optical band (Racusin et al. 2008). The wide variety in characteristics of the host galaxies for short duration bursts have been recognized due to the increasing number of their identifications (e.g., Berger 2009). Furthermore, the properties of the host galaxies of optically dark GRBs are in a great interest to understand the different environment of the GRB birth place comparing to GRBs with bright optical afterglows (e.g,. Perley et al.

2009).

The first BAT GRB catalog (the BAT1 catalog; Sakamoto et al. (2008)) consisted 237 bursts from 2004 December 19 to 2007 June 16. The BAT1 catalog contained burst trigger time, location, 90% error radius, duration, fluence, peak flux and time-averaged spectral parameters for 237 GRBs as measured by BAT. Here we present the second BAT GRB catalog (the BAT2 catalog), including 476 GRBs detected by BAT from 2004 December 19 to 2009 December 21. The GRB samples in the BAT1 catalog have been re-analyzed by the latest BAT software and the calibration files. Addition to the parameters in the BAT1 catalog, the BAT2 catalog includes the time-resolved spectral parameters. The catalog shows the correlations not only between observed prompt emission properties, but also between the observed prompt emission properties and the redshifts for known redshift GRBs. In §2, we summarize the updates on the in-orbit calibration of the BAT instrument. In §3, we describe the analysis methods for the catalog. In §4, we describe the content of the tables of the catalog and show the results of the prompt emission properties of the BAT GRBs based on the catalog. Our conclusions are summarized in §5. All quoted errors in this work are at the 90% confidence level.

2. Updates of In-orbit Calibrations

The BAT is a highly sensitive, large field of view (FOV) (2.2 sr for $> 10\%$ coded FOV), coded-aperture telescope that detects and localizes GRBs in real time. The BAT detector plane is composed of 32,768 pieces of CdZnTe (CZT: $4 \times 4 \times 2$ mm), and the coded-aperture mask is composed of $\sim$ 52,000 lead tiles ($5 \times 5 \times 1$ mm) with a 1 m separation between mask and detector plane. The energy range is 14–150 keV for imaging or mask-weighting, which is a technique to subtract the background based on the modulation resulting from the coded mask, with a non-coded response up to 350 keV. Further detailed descriptions, references and the in-orbit calibration status of the BAT can be found in the BAT1 GRB catalog.

We had two major updates on the energy calibration of the BAT since the publication of the BAT1 catalog. The first update is the identification of the problem in the energy response above 100 keV. The mobility-lifetime produces of electrons and holes ($\mu\tau$) which are used to model the characteristics of an individual CZT detector in the energy response function (Sato et al. 2005; Suzuki et al. 2005) have to be 1.7 larger than those originally determined. This fix eliminates the correction which we were applying above 100 keV to reproduce the canonical Crab spectrum and also reduces the amount of systematic errors (see Figure 1).

The second update is the correction to the gain change of the detectors. We have recognized shifts of peak energies in spectra from the on-board ^{241}Am tagged source towards low energies. An analysis of four years of on-board ^{241}Am spectra shows the shift is about 2.5 keV for the 59.5 keV peak. The BAT team has developed new calibration files to store the information (coefficient to convert from PHA channel to energy) to correct this gain change as a function of time. After applying the new gain correction, the scatter of the 59.5 keV line energy is ∼0.1 keV over the four-year period.

Figure 2 shows the Crab photon index and the flux in the 15-150 keV band as a function of the incident angle using the latest BAT software and calibration files. Both the photon index and the flux are within ±5% and ±10% respectively from the canonical Crab values over the BAT field of view. The deviation of the derived parameters from the Crab canonical values are larger toward the edge of the BAT field of view. Therefore, the larger systematic error in the spectral parameters could exist if the source is located at the edge of the field of BAT.

3. Analysis for the GRB catalog

We used the standard BAT software (HEASOFT 6.8) and the latest calibration database to process the BAT GRBs from December 2004 (GRB 041217) to December 2009 (GRB 091221). The GRBs included in the BAT1 catalog have been reprocessed. The BAT2 catalog samples also include bursts which were found in the ground processing. The burst pipeline script, `batgrbproduct`, was used to process the BAT event data. Since the burst emissions are longer than the duration of the event data for GRB 060124 and GRB 060218, we used both the event data and the survey data (Detector Plane Histogram data) to calculate the fluence and the time-averaged spectral parameters. We used a raw light curve data (quad-rate data) to measure the duration for the most of the bursts found on the ground process because only a partial event data are available for these bursts. In some cases, `battblocks`, which is one of the task runs in `batgrbproduct`, failed to find the burst interval. In those cases, we fitted the mask-weighted light curve in the full BAT energy range by a liner-rise exponential decay model ("BURS" model in ftools qdp[1]) to find the burst time intervals (T_{100}, T_{90}, T_{50} and peak 1-s intervals) and created the T_{100} and peak 1-s PHA files based on these time intervals. We put comments on Table 1 for the bursts which have a problem in either the data or the processing.

For the time-averaged spectral analysis, we used the time interval from the emission start

[1]http://heasarc.gsfc.nasa.gov/docs/software/ftools/others/qdp/qdp.html

time to the emission end time (T_{100} interval). Since the BAT energy response generator, `batdrmgen`, performs the calculation for a fixed single incident angle of the source, it is not appropriate to used the response for the fixed position if the GRB location at the detector plane is changing due to the spacecraft slewing. To take into account this problem, we created the detector energy response matrices (DRM) for each five-second period during the time interval taking into account the position difference of the GRB in detector coordinates especially during the spacecraft slew. We then weighted these DRMs by the five-second count rates and created the averaged DRM using `addrmf`. The weighted BAT DRM have been tested for subset of GRBs which simultaneously detected by the Konus-Wind and the *Suzaku* Wide-band All-sky Monitor instruments. The joint spectral analysis using the weighted BAT DRM for those GRBs shows no systematic trend in the derived parameters comparing to the spectral parameters derived by other GRB instruments (Sakamoto et al. 2010).

We extracted the time-resolved spectra for the intervals determined by `battblocks`. Since the first and the last intervals identified by `battblocks` are the pre- and post-burst backgrounds, the spectrum for these two intervals were not created. For the time-resolved spectral analysis, we created the DRM for each spectrum taking into account the GRB position in detector coordinates by updating the keyword of the spectral files using `batupdatephakw` before running `batdrmgen` to generating the DRM. We also created the individual DRM for the peak spectra for calculating the peak flux (see below).

The spectrum was fitted by a simple power-law (PL) model,

$$f(E) = K_{50}^{\rm PL} \left(\frac{E}{50\,{\rm keV}} \right)^{\alpha^{\rm PL}} \tag{1}$$

where $\alpha^{\rm PL}$ is the power-law photon index and $K_{50}^{\rm PL}$ is the normalization at 50 keV in units of photons cm^{-2} s^{-1} keV^{-1}, and by a cutoff power-law (CPL) model,

$$f(E) = K_{50}^{\rm CPL} \left(\frac{E}{50\,{\rm keV}} \right)^{\alpha^{\rm CPL}} \exp\left(\frac{-E\,(2+\alpha^{\rm CPL})}{E_{\rm peak}} \right) \tag{2}$$

where $\alpha^{\rm CPL}$ is the power-law photon index, $E_{\rm peak}$ is the peak energy in the νF_ν spectrum and $K_{50}^{\rm CPL}$ is the normalization at 50 keV in units of photons cm^{-2} s^{-1} keV^{-1}. All of the BAT spectra are acceptably fit by either a PL or a CPL model. The same criteria as in the BAT1 catalog, $\Delta\chi^2$ between a PL and a CPL fit is greater than 6 ($\Delta\chi^2 \equiv \chi^2_{\rm PL} - \chi^2_{\rm CPL} > 6$), was used to determine a CPL model is a better representative spectral model for the data. Note that none of the BAT spectra show a significant improvement in χ^2 with a Band function (Band et al. 1993) fit compared to that of a CPL model fit.

The fluence, the 1-s and the 20-ms peak fluxes were derived from the spectral fits. The fluences were calculated fitting the time-averaged spectrum by the best fit spectral model. The 1-s and 20-ms peak fluxes were calculated fitting the spectrum of the 1-s and the 20 ms interval bracketing the highest peak in the light curve. Those intervals were identified by `battblocks`. Similarly, we used the best fit spectral model for calculating the peak fluxes. Since the shortest burst emission which has been observed by BAT was around 20 ms, we chose this window size to measure the peak flux as the shortest time scale. Note that since the total number of photons for the 20-ms spectrum is generally small, we created the spectrum in 10 channels which are logarithmically equal-spaced from 14 keV to 150 keV to apply χ^2 fit to the spectrum. Since the duration of the 20-ms spectrum is extremely short, the spectral analysis of 29 GRBs showed an unacceptable reduced χ^2 ($\chi^2_\nu > 2$) either in a PL or a CPL fit. Furthermore, 31 GRBs could not create the 20-ms peak spectrum because `battblocks` failed to find the interval.

For the known-redshift GRBs, we calculated the T_{90} and T_{50} durations measured in the 140-220 keV band at the GRB rest frame. By fixing the energy range at the GRB rest frame, there is no need to apply the correction into the measured duration due to the difference in the GRB pulse widths as a function of the observed energy band (e.g., Fenimore et al. 1995). We created the light curves in the energy range from 140/(1+z) keV to 220/(1+z) keV by `batbinevt`. This energy band has been determined by the tradeoff between the redshift range from 0.1257 (GRB 060614) to 8.26 (GRB 090423) and the BAT observed energy range from 14 keV to 150 keV. We used the same algorithm in `batgrbproduct` to find the best T_{90} and T_{50} durations in the observed 140/(1+z) - 220/(1+z) keV band. Then, we divided the duration by (1+z) to correct for the time dilation effect due to the cosmic expansion.

4. The Catalog

The BAT2 catalog includes GRBs detected by BAT in five years of its operation between 2004 December 19 and 2009 December 31. The total number of GRBs including 25 GRBs found in ground processing (eight GRBs were found by the BAT slew survey; Copete et al. (2007)) and four possible GRBs is 476. 476 GRBs are listed in Table 1. The first column is the GRB name. The next column is the BAT trigger number. The next column specifies the BAT trigger time in UTC in the form of *YYYY-MM-DD hh:mm:ss.sss* where *YYYY* is year, *MM* is month, *DD* is day of month, *hh* is hour, *mm* is minute, and *ss.sss* is second. Note that the definition of the BAT trigger time is the start time of the foreground time interval of the image from which the GRB is detected on-board. The next four columns give the locations by the ground process in equatorial (J2000) coordinate, the signal-to-noise ratio

of the BAT image at the location, and the radius of the 90% confidence region in arcmin. The 90% error radius is calculated based on the signal-to-noise ratio of the image using the following equation which derived from the BAT hard X-ray survey process[2]

$$r_{90\%} = 10.92 \times \mathrm{SNR}^{-0.7} \text{ (arcmin)},$$

where SNR is the signal-to-noise ratio of the BAT image. However, due to the limitation of the BAT point spread function, we quote the minimum allowed value of $r_{90\%}$ as $1'$ in the catalog. The next two columns specify the burst durations which contain from 5% to 95% (T_{90}) and from 25% to 75% (T_{50}) of the total burst fluence. These durations are calculated in the 15–350 keV band.[3] The next two columns are the start and stop time from the BAT trigger time of the event data. The last column is the comments.

The energy fluences calculated in various energy bands are summarized in Table 2. The first column is the GRB name. The next column specifies the spectral model which used in deriving the fluences (PL: simple power-law model; Eq.(1), CPL: cutoff power-law model; Eq.(2)). The next five columns are the fluences in the 15-25 keV, the 25-50 keV, the 50-100 keV, the 100-150 keV, and the 15-150 keV band. The unit of the fluence is 10^{-8} ergs cm^{-2}. The next two columns specify the start and the stop time from the BAT trigger time which used to calculate the fluences. The last column is the comments. Note that fluences are not reported for GRBs with incomplete data.

Table 3 and 4 summarize the 1-s peak photon and energy fluxes in various energy bands. The first column is the GRB name. The next column specifies the spectral model used in deriving the 1-s peak flux. The next five column are the peak photon and energy fluxes in the 15-25 keV, the 25-50 keV, the 50-100 keV, the 100-150 keV, and the 15-150 keV band. The unit of the flux is photons cm^{-2} s^{-1} for the peak photon flux and 10^{-8} ergs cm^{-2} s^{-1} for the peak energy flux. The last two columns in Table 3 specify the start and the stop time from the BAT trigger time which were used to calculate the peak fluxes. The last column is the comments.

Table 5 shows the 20-ms peak energy and photon flux in the 15-150 keV band. The first column is the GRB name. The next column shows the spectral model used in deriving the flux. The next two columns are the peak energy flux and photon flux in the 15-150 keV band. The unit of the flux is photons cm^{-2} s^{-1} for the peak photon flux and 10^{-8} ergs cm^{-2} s^{-1} for the peak energy flux. The next two columns specify the start and the stop time from

[2]http://heasarc.gsfc.nasa.gov/docs/swift/analysis/bat_digest.html

[3]The coded mask is transparent to photons above 150 keV. Thus, photons above 150 keV are treated as background in the mask-weighted method. The effective upper boundary is $\sim$ 150 keV.

the BAT trigger time which were used to calculate the 20-ms peak flux. The last column is the comments.

The time-averaged spectral parameters are listed in Table 6. The first column is the GRB name. The next three columns are the photon index, the normalization at 50 keV in the unit of 10^{-4} photons cm^{-2} s^{-1} keV^{-1}, and χ^2 of the fit for a PL model. The next four columns are the photon index, $E_{\rm peak}^{\rm obs}$ in the unit of keV, the normalization at 50 keV in the unit of 10^{-3} photons cm^{-2} s^{-1} keV^{-1} and χ^2 of the fit in a CPL model. The spectral parameters in a CPL are only shown for the bursts which meet the criteria described in the section 3. The degree of freedom is 57 for a PL fit and 56 for a CPL fit except for GRB 060124 and GRB 060218 (see the comment column of the table). The last column is the comments.

The time-resolved spectral parameters are listed in Table 7. The total number of time-resolved spectra is 3323. The first column is the GRB name. The next two columns specify the start and the stop time from the BAT trigger time which were used to extract the spectrum. The next four columns are the photon index, the normalization at 50 keV in the unit of 10^{-4} photons cm^{-2} s^{-1} keV^{-1}, χ^2 and the energy flux in the 15-150 keV band in the unit of 10^{-8} ergs cm^{-2} s^{-1} of the fit for a PL model. The next five columns are the photon index, $E_{\rm peak}^{\rm obs}$ in the unit of keV, the normalization at 50 keV in the unit of 10^{-3} photons cm^{-2} s^{-1} keV^{-1}, χ^2, and the energy flux in the unit of 10^{-8} ergs cm^{-2} s^{-1} of the fit in a CPL model. The last column is the comment. Similar to the table of the time-averaged spectral parameters, we only show a CPL parameters for the fit which meet our $\Delta\chi^2$ criteria.

Table 8 shows the T_{90} and T_{50} durations measured in the 140-220 keV band at the GRB rest frame for the known redshift GRBs. The first column is the GRB name. The T_{90} and T_{50} durations at the GRB rest frame are in the second and the third columns. The last column is the comments.

Table 9 summarizes the redshift measurements of the *Swift* GRBs and their references.

4.1. Short GRB with an Extended Emission

The distinct class in short duration GRBs (S-GRBs) has been claimed based on the prompt emission properties, namely a S-GRB with an extended emission (E.E.)(e.g., Norris et al. 2000; Barthelmy et al. 2005b). The initial short spike of a S-GRB with an E.E. shows a negligible spectral lag which is one of the strong indications that the burst is indeed classified as a S-GRB (Norris et al. 2000). The BAT light curves of 9 S-GRBs with E.E.

included in this catalog[4] are shown in Figure 3. The initial short spike is usually composed from multiple pulses with a total duration of less than 2 seconds. The E.E. lasts from a few tens to a few hundreds of seconds. We distinguished among long GRBs (L-GRBs), S-GRBs and a S-GRBs with an E.E. throughout the paper to investigate the prompt emission properties of these three different classes of GRBs. The spectral parameter and the energy fluences of the initial short spike are reported on Table 10 and 11. Note that our definition of S-GRBs is whether T_{90} is smaller than 2 s or not. The GRBs classified as S-GRBs or S-GRBs with E.E. in our study are commented on Table 1.

4.2. BAT GRB Position and Sky Locations

Figure 4 shows the angular difference between the BAT ground position and the enhanced XRT position (Evans et al. 2009). The BAT ground position is within 1.1′, 1.8′ and 3.5′ from the XRT position for 68%, 90% and 99% of the bursts, respectively.

Figure 5 shows the sky map of the BAT 476 GRBs in galactic coordinates. L-GRBs, S-GRBs and S-GRBs with E.E. are marked in different colors. All GRBs are distributed uniformly in the sky. However, we do notice that several S-GRBs are located along the galactic plane region. These S-GRBs could be good candidates for previously unknown Soft Gamma-ray Repeaters or Anomalous X-ray Pulsars (e.g., Palmer et al. 2005; Sakamoto et al. 2009a).

4.3. Durations and Hardness

The histograms of T_{90} and T_{50} by the mask-weighted light curve in the BAT full energy band are shown in Figure 6. The average of the BAT T_{90} and T_{50} durations are 71 and 31 s, respectively. In Figure 7, we compare the T_{90} distributions of BAT, BATSE, *BeppoSAX* and *HETE*-2. The BATSE T_{90} are extracted from the 4B catalog (Paciesas et al. 1999), and they are measured in the 50-300 keV band. The *BeppoSAX* T_{90} are extracted from Frontera et al. (2009), and they are measured using the light curve of the GRBM instrument in the 40-700 keV band. The *HETE*-2 T_{90} are extracted from Pélangeon et al. (2008), and they are measured using the light curve of the FREGATE instrument in the 6-80 keV band. There is a clear shift in the peak of L-GRB populations by different instruments. The peak of

[4]According to Norris et al. (2010), GRB 090916 has been classified as a S-GRB with E.E. However, in our study, GRB 090916 was classified as a L-GRB due to unclear classification of this burst.

T_{90} distributions of L-GRBs from the BATSE, the *BeppoSAX* and the *HETE*-2 samples are around 10-30 s, whereas the BAT distribution is around 70 s. It is clear from this comparison that the duration measurement is sensitive to the sensitivity of instruments. Another distinct difference in the BATSE distribution comparing to that of the BAT, the *BeppoSAX* and the *HETE*-2 distributions is a clear bimodality between S-GRBs and L-GRBs (e.g., Kouveliotou et al. 1993). The lack of S-GRBs in the imaging instruments such as the BAT and the *HETE*-2 is the requirement of a larger number of photons to be able to "image" a GRB. This requirement is usually difficult to achieve for S-GRBs because S-GRBs are usually faint and their emissions are short. However, note that the BAT has been triggering and localizing S-GRBs in a much higher fraction than other GRB imaging instruments due to the large effective area and also the sophisticated flight software. As mentioned in Frontera et al. (2009), lack of S-GRBs in the *BeppoSAX* samples is likely to be due to the lower efficiency of the trigger system to S-GRBs.

Figure 8 shows the fluence ratio between the 50-100 keV and the 25-50 keV band versus the T_{90} and T_{50} durations of the BAT GRBs. It is clear from the figures that there is no large number of S-GRBs having soft spectra. The most of the S-GRBs are populated in the fluence ratio $\sim$2. On the other hand, the averaged fluence ratio of the L-GRBs is 1.3. Based on this comparison, we may conclude that the S-GRBs are generally harder than the L-GRBs. However, note that there is a large overlap in the hardness between L-GRBs and S-GRBs in the BAT samples. The S-GRBs with E.E. overlaps with the the L-GRB samples.

The comparisons in the fluence ratio-T_{90} plane for the BAT, the BATSE, the *BeppoSAX* the *HETE*-2 GRBs are shown in Figure 9. Both fluences and T_{90} values are extracted from the 4B catalog for the BATSE sample. For the *BeppoSAX* samples, we used the best fit simple power-law model in the catalog (Frontera et al. 2009) to calculate the fluence ratios in the 50-100 keV and the 25-50 keV band. For the *HETE*-2 sample, we calculated the fluences in those energy bands using the spectral parameters reported on Sakamoto et al. (2005) and Pélangeon et al. (2008). We only calculated the fluences for having the parameters in either a CPL or the Band function.[5] The T_{90} values of the *HETE*-2 sample are from Pélangeon et al. (2008). Although the GRB samples of different missions are overlaid each other, there is a large scatter especially in the BATSE sample. This could be either the BATSE was detecting a wider population of GRBs than those other missions or there is a systematic problem in the reported fluence values in the catalog.

[5]Because of this spectral model requirement, we are excluding a large number of X-ray flashes in the *HETE*-2 sample which usually a PL is the accepted model.

4.4. Peak Fluxes and Fluences

Figure 10 shows the distribution of the 1-s and the 20-ms peak photon flux versus the fluence in the 15-150 keV band. As we confirmed in the BAT1 catalog, there is a positive correlation between these two parameters. It is now clear that most of the BAT S-GRBs are populated in a low fluence but a high peak flux region by the correlation with the 20 ms peak flux. The systematically lower peak flux for the S-GRBs in the 1-s peak photon flux comparing to the 20-ms peak photon flux is due to the larger time window than the actual burst duration for calculating the flux. The S-GRB population in the region of a low fluence and a high peak flux for the BAT samples could be due to the selection effect of the imaging requirement in the trigger algorithm.

The distribution between the fluence in the 50-150 keV band versus that in the 15-50 keV band for the BAT GRBs is shown in the top of Figure 11. Assuming the Band function of the low energy photon index of -1 and the high energy photon of -2.5, 43% of the BAT GRBs has $E_{\rm peak}^{\rm obs} > 100$ keV , 50% of the BAT GRBs has 30 keV $< E_{\rm peak}^{\rm obs} \leq 100$ keV, and 7% of the BAT GRBs has $E_{\rm peak}^{\rm obs} \leq 30$ keV. The relatively same number of GRBs in the range of $E_{\rm peak}^{\rm obs} > 100$ keV and 30 keV $< E_{\rm peak}^{\rm obs} \leq 100$ keV is consistent with the *HETE*-2 GRB sample (Sakamoto et al. 2005). The systematically smaller number of GRBs with a soft spectrum ($E_{\rm peak}^{\rm obs} \leq 30$ keV) is likely due to luck of the sensitivity below 15 keV for the BAT. The S-GRBs are located in low fluences with a hard spectrum region with a small overlap with the L-GRBs in the figure. On the other hand, the S-GRBs with E.E. are populated in the same region with the L-GRBs. However, the fluences of the initial short spikes of the S-GRBs with E.E. are located at the similar region of S-GRBs. The bottom of Figure 11 compares the BAT, the BATSE, and the *HETE*-2 GRBs in the same fluence-fluence plane. The fluences for the BATSE sample and the *HETE*-2 are calculated using the best fit spectral parameters in a CPL model and the Band function reported on Kaneko et al. (2006) and Pélangeon et al. (2008) respectively. Majority of the BATSE samples are located at the high fluences with a hard spectrum region of the figure. The *HETE*-2 and the BAT samples are overlaid in this fluence-fluence plane.

4.5. Time-averaged Spectral Parameters

Figure 12 shows the histograms of the BAT time-averaged photon index in a PL fit for the L-GRBs, the S-GRBs, the S-GRBs with E.E. and the initial short spikes of the S-GRBs with E.E. The Gaussian fit to the histogram of the PL photon index of the L-GRBs shows the peak at -1.6 with σ of 0.3. This BAT photon index based on a PL fit is systematically steeper than typical low-energy photon index α (~ -1) and also shallower

than high-energy photon index β (~ -2.5) based on the Band function fit (e.g., Kaneko et al. 2006). As demonstrated in the detailed spectral simulation study of Sakamoto et al. (2009b), the distribution of the BAT photon index in a PL fit reflects the fact that more than half of $E_{\rm peak}^{\rm obs}$ in the BAT GRBs are located within the BAT energy range (15-150 keV). This is consistent with the discussion in section 4.4 that 50% of $E_{\rm peak}^{\rm obs}$ in the BAT GRBs are located 30 keV $< E_{\rm peak}^{\rm obs} \leq$ 100 keV assuming typical spectral parameters of the Band function. The histogram of a PL photon index of the S-GRBs has a shift toward a shallower index comparing to that of the L-GRBs. The time-averaged PL photon index for the S-GRBs is -1.2. The Kolmogorov-Smironov (K-S) test probabilities in the comparison between the time-averaged PL photon index between the L-GRBs and the S-GRBs is 10^{-7}. Therefore, there is a significant difference in the time-averaged PL photon index between the L-GRBs and the S-GRBs. Although a number of sample is limited, the time-averaged PL photon index of S-GRBs with E.E. is consistent with the L-GRBs. On the other hand, the PL photon index of the initial short spikes of the S-GRBs with E.E. is much more consistent with that of the S-GRBs.

Figure 13 shows the distribution of the BAT time-averaged photon index in a PL fit versus the fluence in the 15-150 keV band. Similar to the trend in Figure 11 and 12, the S-GRBs are located in a lower fluence and a harder spectral region comparing to the L-GRBs. The time-averaged properties of the S-GRBs with E.E. overlay with the L-GRBs in the PL photon index - fluence plane. The initial short spikes of the S-GRBs with E.E. seem consistent with the properties of S-GRBs in this plane, but in the systematically higher fluence region than the S-GRBs.

The low-energy photon index α and $E_{\rm peak}^{\rm obs}$ based on a CPL fit are compared among the BAT, the BATSE and the *HETE*-2 GRBs in Figure 14. 77 out of 456 time-averaged spectra (17%) show a significant improvement of χ^2 in a CPL fit over a PL fit ($\Delta\chi^2 > 6$). The BATSE and the *HETE*-2 spectral parameters based on a CPL fit are extracted from Kaneko et al. (2006) and Pélangeon et al. (2008) respectively. The low-energy photon index α is consistent among the all instruments. However, most of the $E_{\rm peak}^{\rm obs}$ on the BATSE GRBs are larger than 100 keV, whereas, the majority of $E_{\rm peak}^{\rm obs}$ in the BAT and the *HETE*-2 GRBs are less than 100 keV. This is more clearly represented in the histograms of $E_{\rm peak}^{\rm obs}$ shown in Figure 15. The Gaussian fits to the log-normal $E_{\rm peak}^{\rm obs}$ histograms of the BAT, the BATSE and the *HETE*-2 samples reveal the peak at 79 keV, 320 keV, and 65 keV with σ in $\log(E_{\rm peak}^{\rm obs})$ of 0.18, 0.22, and 0.31 respectively. The K-S test probabilities in the log-normal $E_{\rm peak}^{\rm obs}$ distributions for the BAT and the BATSE, and the BAT and the *HETE*-2 are 9×10^{-21} and 0.15 respectively. As clearly see in these histograms, although the peak and the width of the $E_{\rm peak}^{\rm obs}$ distributions differ among the instruments, they are overlapping. Moreover, there is no sign of a bimodal $E_{\rm peak}^{\rm obs}$ distribution by the measurement in a single instrument.

Therefore, we may conclude that "true" $E_{\rm peak}^{\rm obs}$ has a single broad log-normal distribution. The difference of the $E_{\rm peak}^{\rm obs}$ distributions among the GRB instruments is very likely due to the instrumental selection effect.

4.6. Time-resolved Spectral Parameters

We used the spectral fit results of 3284 out of 3323 spectra based on the goodness of the fit and also the constrains of the spectral parameters in the BAT time-resolved spectral study. Figure 16 compares the distributions of the photon index in a PL fit between the time-resolved and the time-averaged spectra. The best fit parameters in the Gaussian fit to those histograms are the peak at -1.53 with σ of 0.47 and the peak at -1.57 with σ of 0.32 for the time-resolved and the time-averaged spectra respectively. The K-S test probability for the time-resolved and the time-averaged PL photon index distribution is 10^{-4}. Therefore, there is a marginal difference in the photon index of a PL fit between the time-resolved and the time-averaged spectra especially in their widths of the distributions.

Figure 17 shows the comparison of $E_{\rm peak}^{\rm obs}$ in a CPL fit between the time-resolved and the time-averaged spectra. 472 out of 3284 time-resolved spectra show a significant improvement of χ^2 in a CPL fit over a PL fit ($\Delta\chi^2 > 6$). The Gaussian fits to those log-normal $E_{\rm peak}^{\rm obs}$ histograms show the peak of 68 keV with $\log(E_{\rm peak}^{\rm obs})$ of 0.23 and the peak of 77 keV with $\log(E_{\rm peak}^{\rm obs})$ of 0.19 between the time-resolved and the time-averaged spectra. We found the K-S probability of 0.04 for the comparison in $E_{\rm peak}^{\rm obs}$ distributions between the time-resolved and the time-averaged spectra. Therefore, there is no significant difference between $E_{\rm peak}^{\rm obs}$ based on a CPL fit in the BAT time-resolved and the time-averaged spectra.

Ghirlanda et al. (2009) suggested a possible resemblance in the low-energy photon index α of the S-GRBs and the initial part of the spectrum of the L-GRBs in the BATSE GRBs. As shown in figure 12, since we do see a significant difference in the time-averaged photon index in a PL fit in the BAT data between the L-GRBs and the S-GRBs, it is worth investigating this possibility by our time-resolved spectral results of the BAT. Figure 18 shows the histograms of the BAT photon index in a PL fit for the initial 0.1-2 s spectra of the L-GRBs and the time-averaged photon index of the S-GRBs. The K-S test probability of the comparison in the initial PL photon indices of the L-GRBs and the time-averaged photon indices of the S-GRBs is 0.02. Furthermore, the K-S test probability of the comparison in the initial PL photon indices of the L-GRBs and the time-averaged photon indices of the L-GRBs is 0.002. Therefore, there is a weak indication of a resemblance in the spectral parameter between the PL photon indices in the initial 0.1-2 s intervals of the L-GRBs and the time-averaged PL photon indices of the S-GRBs in the BAT data.

One of the important question in the prompt emission is whether the observed spectrum is correctly represented by the synchrotron shock model (SSM) or not (Rees & Mészáros 1992; Sari et al. 1996). According to Preece et al. (1998), 23% of the BATSE time-resolved spectra have low-energy photon indices which violate the SSM limit from $-3/2$ to $-2/3$ (so called "line of death" problem). Although the BAT photon index based on a PL fit does not represent the low-energy photon index α of the Band function if $E_{\rm peak}^{\rm obs}$ is located inside the BAT energy range (see section 4.5), the BAT photon index should be the actual low energy photon index α if $E_{\rm peak}^{\rm obs}$ is located above the BAT energy range. Therefore, even if a majority of the photon index is derived by a PL fit, the BAT time-resolved spectra are the interesting dataset to investigate the line of death problem. Figure 19 shows the distribution between the BAT photon index versus the energy flux in the 15-150 keV of the time-resolved spectra based on a PL fit. We only used the results which the 90% error of the photon index has been constrained within ± 0.5. Out of 2968 data in the figure, 18 spectra (0.6%) are exceeding the hard side of the line of death ($>-2/3$) either in $>1.6\ \sigma$ but $<3.2\ \sigma$, or $\geq 3.2\ \sigma$ level. Figure 20 shows the distribution of the low-energy photon index α and $E_{\rm peak}^{\rm obs}$ of the BAT time-resolved spectra which show a significant improvement of χ^2 in a CPL fit over a PL fit. Same as in the PL fit samples, we only used the results that the low-energy photon index α is constrained within ± 0.5 in the 90% confidence level. The low-energy photon index of 23 out of 234 spectra are harder than $-2/3$ in $>1.6\ \sigma$ but $<3.2\ \sigma$, or $\geq 3.2\ \sigma$ level. There is only one time-resolved spectrum (GRB 090618 from 110.5 s to 112.272 s from the trigger time) which violates the softer side of the line of death ($<-3/2$) at the significance level of $>1.6\ \sigma$ but $<3.2\ \sigma$. Therefore, the total fraction of the BAT spectra in the CPL samples which violate the line of death is 10%. Although there are the spectra which violate the line of death in the BAT data, it is likely that the number of the BAT spectra which violate the limit is a factor of two smaller than the BATSE result. Figure 21, 22 and 23 show the BAT light curves with hatches for the time intervals exceeding the line of death. We noticed that the intervals exceeding the line of death are a bright spike in the light curve. Furthermore, in some bursts, the rising part of the light curve (e.g. GRB 080318B) is exceeding the limit. Although it is hard to conclude which part of the light curve violating the line of death due to a small number of sample in our study, we do see a general trend that 1) a bright peak and 2) a rising part of a peak in the light curve are tend to be exceeding the line of death limit. This is consistent with the BATSE results that the initial part of the FRED pulses tend to violate the line of death (Lu et al. 2010).

One of the interesting indication of the spectral feature in the time-resolved spectroscopy of the *Fermi* GRB 090902B which has a strong GeV detection by the Large Area Telescope is the presence of underlining power-law component addition to the Band function component (Abdo et al. 2009). The extra power-law component emerges not only in the GeV energy

range but also in <50 keV energy range in the observe spectra. To investigate such a spectral feature in the BAT time-resolved spectra, we perform the BAT spectral simulations by inputing the spectral parameters of the interval b (from 4.6 s to 9.6 s) reported on Abdo et al. (2009): the Band parameters of $\alpha = 0.07$, $\beta = -3.9$ and $E_{\rm peak}^{\rm obs} = 908$ keV, and the extra power-law photon index of -1.94. We simulate 10,000 spectra by the BAT energy response of 30° off-axis case using `xspec fakeit` command. We also created the simulated background spectrum using the real data and subtracted it from the simulated spectra. The systematic error has been applied to the spectrum using `batphasyserr`. The simulated spectra are fit by a PL and a CPL model. Figure 24 shows one of the example of the simulated spectrum fit by a PL model. Since the input spectrum has a steep power-law (photon index of -1.94) and then break to a very flat power-law (photon index of 0.07) around 50 keV, the BAT simulated spectrum shows a significant deviation from a PL fit. In this example, the reduced χ^2 in a PL fit is 2.93. None of a CPL fit to the simulated spectra shows a significant improvement over a PL fit. Figure 25 shows the reduced χ^2 distribution of the BAT simulated spectra inputting the spectral parameters of the *Fermi* GRB 090902B interval b fit by a PL model. The Gaussian fit to the histogram shows the peak of 2.58 with σ of 0.28. 99.97% of the simulated spectra show the reduced $\chi^2 \geq 1.7$. On the other hand, the reduced χ^2 distributions of the time-averaged and the time-resolved spectra of the actual BAT GRBs either by a PL or a CPL fit are well centroid around 1 (Figure 26). There are only two time-resolved spectra (out of 3284 spectra) which show the reduced χ^2 > 1.7. By eye inspection, the residuals from the best fit model for these two spectra are not similar to the residual seen in Figure 25. The worst reduced χ^2 of the time-averaged spectra of the BAT GRBs is 1.54. Therefore, we concluded that we could not confirm the existence of the extra power-law component which extends below 50 keV like *Fermi* GRB 090902B in the BAT GRB spectra. Although GRB 090902B and also other *Fermi* GRBs which claim to have detections of the extra power-law component could be a special type of GRBs which have never been observed by the BAT, we believe that confirmations from other GRB instruments are required to validate the existence of the extra power-law component, especially whether this component is visible at the hard X-ray range, in the spectrum.

4.7. Observed Properties vs. Redshifts

Figure 27 shows the distribution between the observed BAT T_{90} duration versus the redshifts. The trajectories of the observed T_{90} for three known redshift GRBs are calculated assuming the observed duration changes only by the time-dilation effect as a function of redshift. If the time-dilation effect is the dominant effect to the observed duration, we would expect the duration of a high-redshift GRB tends to be longer as shown in those trajectories.

However, there is no such a clear indication in the BAT observed T_{90} duration as a function of redshifts.

Figure 28 shows the distribution between the observed photon index of the time-averaged spectra in a PL fit versus the redshifts. If there is an intrinsic spectral shape at the GRB rest frame, we would expect the observed spectra should be softer if the redshift goes higher. The overlaid trajectories in the figure show the expected BAT observed PL photon index as a function of redshift in the case of $E_{\rm peak}^{\rm src}$ of 300 keV, 100 keV and 30 keV. We used the $E_{\rm peak}$-Γ relation (Sakamoto et al. 2009b) to convert $E_{\rm peak}^{\rm obs}$ into the BAT PL photon index in these estimations. As can be seen in the figure, there is no clear trend that the BAT PL photon index goes softer as the redshift goes higher. The photon index of high redshift GRBs are consistent with a majority of GRBs or even harder in the BAT data. This is suggesting that there is no intrinsic spectral shape in the GRB rest frame at least in the *Swift* known-redshift samples. Furthermore, the redshifts of the BAT GRBs which have soft spectra (photon index < -2) are less than 3.5. This might be indicating that redshifts of GRBs with soft spectra such X-ray flashes (Heise et al. 2001; Kippen et al. 2001; Sakamoto et al. 2005) could not be very high.

The distributions of the peak flux and the fluence as a function of redshifts are shown in Figure 29 and 30. Although the peak flux and the fluence measured in the narrow BAT energy band are not bolometric measurement, there is no obvious correlation between those parameters and the redshifts. The fluence and the peak flux of the low redshift GRBs are scattered from the lowest to the highest values. The high redshift GRBs are located in the small peak flux and the fluence region, but they are not the dimmest populations of the BAT known redshift GRBs.

4.8. Rest-frame Properties

Figure 31 shows the distribution of T_{90} and T_{50} durations measured in the 140-220 keV band at the GRB rest frame as a function of redshifts. The averaged T_{90} and T_{50} durations at the rest frame are 18.5 s and 8.0 s respectively. The correlation coefficients between T_{90} and T_{50} and the redshifts are 0.09 in 122 samples (the null probability of 0.3) and 0.1 in 121 samples (the null probability of 0.3) respectively. Therefore, there is no clear trend between the duration at the GRB rest fame and the redshifts.

Figure 32 shows the correlation between $E_{\rm peak}^{\rm src}$ and the isotropic-equivalent energy $E_{\rm iso}$. The $E_{\rm peak}^{\rm src}$ and $E_{\rm iso}$ values of the GRB samples from BASTE, *BeppoSAX* and *HETE*-2 are extracted from Amati (2006). We only selected the *Swift* GRB samples which we reported

the time-averaged CPL fits in this catalog and also have redshift measurements. For those samples, we fit the spectrum in the Band function to measured $E_{\rm peak}^{\rm src}$ and $E_{\rm iso}$ which is integrated over the 1 keV - 10 MeV band at the GRB rest frame. We used the same cosmological parameters of Amati (2006) in the calculation of $E_{\rm iso}$ for the *Swift* GRBs. Table 12 summarized the values of $E_{\rm peak}^{\rm src}$ and $E_{\rm iso}$ of *Swift* GRBs. As shown in Figure 32, the *Swift* GRB samples are consistent with the samples from other GRB missions, and following the relation originally proposed by Amati et al. (2002).

5. Summary

The BAT2 catalog including 476 GRBs detected by BAT during 5 years of its operation. We presented the observed temporal and spectral properties of the BAT GRBs mainly based on the BAT event data. In this catalog, not only the time-averaged but also the time-resolved spectral properties of the BAT GRBs were presented. We also distinguished among L-GRBs, S-GRBs, and S-GRBs with E.E. to investigate the possible distinct characteristics in the prompt emission properties. The comparisons in the prompt emission properties with the BATSE, the *BeppoSAX* and the *HETE*-2 GRB samples were shown. The observed prompt emission properties for the BAT known redshift GRBs were also presented.

We showed that the BAT T_{90} and T_{50} duration peaked around 70 s and 30 s, respectively, whereas the BATSE, the *BeppoSAX* and the *HETE*-2 T_{90} duration peaked around 10-30 s which could be understood by the difference in the sensitivity of the instruments. We confirmed that the spectrum of the BAT S-GRBs are generally harder than those of the L-GRBs. The hardness of the S-GRBs with E.E. for the entire emission is comparable to that of the L-GRBs. Whereas, the hardness of the initial short spikes of the S-GRBs with E.E. is comparable to that of the S-GRBs. By comparing the BAT GRBs with the BATSE and the *HETE*-2 samples in the fluences between the 50-150 keV and the 15-50 keV band, we showed that the majority of the BAT GRBs are systematically softer than the bright BATSE GRBs. Whereas, the *HETE*-2 samples overlap with the BAT GRBs in this fluence-fluence plane. We confirmed the harder photon index by a PL fit in the BAT S-GRBs comparing to that of the L-GRBs by the time-averaged spectral analysis. The distribution of the time-averaged PL photon index of the S-GRBs with E.E. is consistent with that of the L-GRBs. However, the PL photon index of the initial short spikes of the S-GRBs with E.E. is much more similar to that of the S-GRBs. The time-averaged $E_{\rm peak}^{\rm obs}$ of the BAT GRBs based on a CPL fit showed a log-normal distribution in the peak around 80 keV which is significantly smaller than that of the BATSE GRBs which peak around 320 keV. There is no significant difference in the $E_{\rm peak}^{\rm obs}$ based on a CPL fit between the time-averaged and the time-resolved

spectra in the BAT data. We confirmed that 10% of the BAT photon indices in the BAT time-resolved spectra are outside the allowed range of the line of death (the limit from the SSM). The intervals which are violating the line of death are at a bright peak and/or a rising part of a peak. The BAT observed T_{90} of known high redshift GRBs are not systematically longer. The observed spectra of the BAT high redshift GRBs are similar to or harder than the moderate *Swift* redshift GRBs. The T_{90} and T_{50} durations measured at the 140-220 keV band at the GRB rest frame for the BAT known redshift samples are peaked at 19 s and 8 s, respectively. The BAT GRB samples are consistent with the $E^{\rm src}_{\rm peak}$-$E_{\rm iso}$ relation (Amati relation).

REFERENCES

Abdo, A.A. et al. 2009, ApJ, 706, L128

Amati, L. et al. 2002, A&A, 390, 81

Amati, L. 2006, MNRAS, 372, 233

Band, D.L., 1993, ApJ, 413, 281

Gehrels, N. et al. 2004, ApJ, 611, 1005

Ghirlanda et al. 2009, A&A, 496, 585

Barthelmy, S. D., et al. 2005, Space Sci. Rev., 120, 143

Barthelmy, S. D., et al. 2005, Nature, 438, 994

Berger, E. 2009, ApJ, 690, 231

Burrows, S. D., et al. 2005a, Space Sci. Rev., 120, 165

Copete, A. et al. 2007, GCN Circ. 6653, http://gcn.gsfc.nasa.gov/gcn3/6653.gcn3

Evans, P.A., et al. 2009, MNRAS, 397, 1177

Fenimore, E. E., in't Zand, J.J.M., Norris, J.P., Bonnel, J.T., & Nemiroff, R.J. 1995, ApJ, 448, L101

Frontera, F., et al. 2009, ApJS, 180, 192

Heise, J., in't Zand, J., Kippen, R.M., & Woods, P.M. 2001, in Gamma-Ray Bursts in the Afterglow Era, ed. E. Costa, F. Frontera, & J. Hjorth (Berlin:Springer), 16

Kaneko, Y. et al. 2006, ApJS, 166, 298

Kippen, R.M., Woods, P.M., Heise, J., in't Zant, J.J.M., Briggs, M.S., Preece, R.D. 2003, in API Conf. Proc. 662, Gamma-Ray Burst and Afterglow Astronomy 2001, ed. G.R.Ricker & R.K. Vanderspek (New York: AIP), 244

Kouveliotou, C., et al. 1993, ApJ, 413, L101

Lu, R.-J., Hou, S.-J., Liang, En-Wei 2010, ApJ in press

Norris, J.P., Marani, G.F., & Bonnelll, J.T. 2000, ApJ, 534, 248

Norris, J.P., Gehrels, N., Scargle, J.D. 2010, ApJ, submitted (arXiv/0910.2456)

Paciesas, W.S. et al. 1999, ApJS, 122, 465

Palmer, D.M. et al. 2005, Nature, 434, 1107

Pélangeon, A. et al., A&A,

Preece, R.D. et al., 1998, ApJL, 506, 23

Perley, D.A., et al. 2009, ApJ, 138, 1690

Racusin, J.L. et al. 2008, Nature, 455, 183

Rees, M.J. & Mészáros, P., 1992, MNRAS, 258, 41

Roming, P.W.A. et al. 2005, Space Sci. Rev., 120, 95

Sakamoto, T. et al. 2005, ApJ, 629, 311

Sakamoto, T. et al. 2008, ApJS, 175, 179

Sakamoto, T. et al. 2009a, in AIP Conf. Proc. 1133, Gamma-Ray Bursts 6th Huntsville Symposium, ed. C. Meegan, M. Gehrels & C. Kouveliotou (New York: AIP), 503

Sakamoto, T. et al. 2009b, ApJ, 693, 922

Sakamoto, T. et al. 2010, Submitted to PASJ

Sari, R. et al. 1998, ApJL, 506, 23

Sato, G. et al. 2005, NIM A, 541, 372

Suzuki, M. et al. 2005, IEEE Trans. Nucl. Sci., 52, 1033

Tanvir, N.R., et al. 2009, Nature, 461, 1254

Salvaterra, R. et al. 2009, Nature, 461, 1258

This preprint was prepared with the AAS LaTeX macros v5.2.

Table 1. BAT GRB summary

GRB Name	Trigger Number	Trigger time	R.A. (°)	Dec. (°)	SN_{img} (σ)	Error ($'$)	T_{90} (s)	T_{50} (s)	Start (s)	Stop (s)	Note
041217	100116	2004-12-17 07:28:25.920	164.790	-17.944	19.3	1.4	5.65	2.71	-2	18	
041219A	100318	2004-12-19 01:42:18.000	6.154	62.847	—	—	—	—	—	—	(1)
041219B	100367	2004-12-19 15:38:48.000	167.674	-33.458	—	—	—	—	—	—	(1)
041219C	100380	2004-12-19 20:30:34.000	343.882	-76.786	13.2	1.8	10.00	4.00	-3	17	
041220	100433	2004-12-20 22:58:26.599	291.301	60.596	31.9	1.0	5.58	2.20	-300	302	
041223	100585	2004-12-23 14:06:17.956	100.186	-37.072	83.7	1.0	109.08	29.20	-299	303	
041224	100703	2004-12-24 20:20:57.698	56.192	-6.666	11.4	2.0	177.17	37.68	-299	303	
041226	100815	2004-12-26 20:34:18.976	79.647	73.343	5.6	3.3	89.50	52.72	-299	303	
041228	100970	2004-12-28 10:49:14.142	336.649	5.027	36.5	1.0	52.16	19.54	-299	303	
050117	102861	2005-01-17 12:52:36.037	358.490	65.934	53.8	1.0	166.65	83.51	-299	303	
050124	103647	2005-01-24 11:30:02.876	192.876	13.041	35.0	1.0	3.93	1.88	-299	303	
050126	103780	2005-01-26 12:00:54.073	278.134	42.395	15.2	1.6	48.00	16.00	-299	303	
050128	103906	2005-01-28 04:19:55.191	219.584	-34.762	26.3	1.1	28.00	8.00	-300	303	
050202	104298	2005-02-02 03:35:14.800	290.583	-38.733	9.7	2.2	0.11	0.05	-299	243	(2)
050215A	106106	2005-02-15 02:15:28.543	348.411	49.322	7.8	2.6	66.41	49.00	-120	302	
050215B	106107	2005-02-15 02:33:43.199	174.467	40.792	15.4	1.6	10.62	4.74	-240	229	
050219A	106415	2005-02-19 12:40:01.049	166.413	-40.685	34.5	1.0	23.84	10.06	-299	303	
050219B	106442	2005-02-19 21:05:51.256	81.300	-57.759	29.7	1.0	28.74	6.91	-300	302	
050223	106709	2005-02-23 03:09:06.068	271.391	-62.468	16.7	1.5	21.68	10.58	-299	303	
050306	107547	2005-03-06 03:33:11.876	282.313	-9.151	30.5	1.0	158.43	73.72	-299	303	
050315	111063	2005-03-15 20:59:42.518	306.480	-42.589	25.4	1.1	95.57	24.36	-300	302	
050318	111529	2005-03-18 15:44:37.170	49.697	-46.388	30.9	1.0	40.0	20.8	-300	32	(3)
050319	111622	2005-03-19 09:31:18.449	154.172	43.580	8.2	2.5	151.74	124.57	-300	302	
050326	112453	2005-03-26 09:53:56.135	6.881	-71.374	72.3	1.0	29.44	19.39	-300	303	
050401	113120	2005-04-01 14:20:15.326	247.872	2.186	28.6	1.0	33.30	25.92	-300	302	
050406	113872	2005-04-06 15:58:48.407	34.417	-50.181	8.3	2.5	4.79	1.64	-300	302	
050410	114299	2005-04-10 12:14:33.553	89.757	79.606	23.5	1.2	64.00	32.00	-299	243	
050412	114485	2005-04-12 05:44:02.894	181.099	-1.187	16.7	1.5	26.46	9.50	-299	303	

[1]The event data are not available.

[2]Short duration GRB.

[3]The event data of the part of the burst emission are not available.

Table 2. BAT GRB energy fluence

GRB Name	Spectral Model	S(15-25)	S(25-50)	S(50-100)	S(100-150)	S(15-150)	Start (s)	Stop (s)	Note
		(10^{-8} ergs cm^{-2})							
041217	CPL	30.0 ± 3.1	72.1 ± 3.3	106.0 ± 5.3	61.1 ± 8.1	270.0 ± 12.1	+0.82	+7.89	
041219A	—	—	—	—	—	—	—	—	(1)
041219B	—	—	—	—	—	—	—	—	(1)
041219C	PL	25.5 ± 2.0	34.5 ± 1.6	34.4 ± 2.5	20.0 ± 2.3	114.0 ± 5.8	+0.00	+12.00	
041220	PL	5.9 ± 0.6	9.8 ± 0.7	12.3 ± 1.2	8.6 ± 1.3	36.6 ± 2.8	-0.21	+6.81	
041223	PL	153.0 ± 5.8	347.0 ± 7.7	624.0 ± 10.4	576.0 ± 15.3	1700.0 ± 27.2	-10.54	+145.94	
041224	CPL	133.0 ± 11.0	261.0 ± 10.4	309.0 ± 14.2	149.0 ± 21.1	853.0 ± 34.3	-109.63	+116.27	
041226	PL	3.8 ± 1.5	7.4 ± 1.8	11.0 ± 3.4	8.9 ± 4.3	31.0 ± 8.2	-1.34	+93.50	
041228	PL	52.8 ± 4.2	90.2 ± 4.2	118.0 ± 6.1	84.7 ± 7.1	345.0 ± 14.8	-0.40	+66.78	
050117	CPL	112.0 ± 7.1	226.0 ± 5.9	318.0 ± 9.2	211.0 ± 15.6	867.0 ± 23.0	+4.28	+215.86	
050124	CPL	12.7 ± 1.7	30.3 ± 2.0	46.3 ± 3.1	28.5 ± 4.5	118.0 ± 6.9	-3.90	+3.07	
050126	PL	10.1 ± 1.8	20.3 ± 2.2	31.6 ± 4.0	26.1 ± 5.0	88.0 ± 10.0	-11.44	+36.56	
050128	CPL	51.2 ± 6.3	125.0 ± 6.8	201.0 ± 11.3	133.0 ± 15.2	511.0 ± 23.7	-7.56	+25.44	
050202	PL	0.4 ± 0.1	0.7 ± 0.1	1.1 ± 0.2	0.9 ± 0.3	3.2 ± 0.6	+0.00	+0.14	
050215A	PL	7.1 ± 1.9	14.4 ± 2.2	23.0 ± 4.0	19.4 ± 5.5	63.9 ± 9.9	-0.32	+71.07	
050215B	PL	6.1 ± 0.9	7.4 ± 0.8	6.6 ± 1.4	3.5 ± 1.1	23.5 ± 3.2	-1.98	+10.86	
050219A	CPL	33.9 ± 3.7	102.0 ± 4.5	173.0 ± 7.5	98.4 ± 10.6	408.0 ± 15.9	-5.81	+29.98	
050219B	CPL	186.0 ± 16.8	413.0 ± 15.5	604.0 ± 23.7	381.0 ± 29.3	1580.0 ± 49.5	-35.59	+38.57	
050223	PL	12.2 ± 1.6	18.4 ± 1.6	20.7 ± 2.8	13.3 ± 2.8	64.6 ± 6.6	-12.01	+16.57	
050306	CPL	135.0 ± 14.6	287.0 ± 13.6	426.0 ± 21.1	294.0 ± 27.5	1140.0 ± 33.9	-3.42	+187.84	
050315	PL	75.9 ± 5.4	97.8 ± 4.2	92.0 ± 6.2	51.3 ± 5.5	317.0 ± 14.3	-56.24	+69.18	
050318	—	—	—	—	—	—	—	—	(2)
050319	PL	27.8 ± 3.7	39.3 ± 3.6	41.1 ± 6.5	24.9 ± 6.0	133.0 ± 14.9	-134.09	+27.76	
050326	PL	90.4 ± 3.5	192.0 ± 4.3	321.0 ± 5.9	280.0 ± 8.5	884.0 ± 15.2	-9.84	+32.42	
050401	PL	94.8 ± 7.3	191.0 ± 8.7	298.0 ± 11.9	247.0 ± 15.4	831.0 ± 30.8	-7.68	+29.06	
050406	CPL	2.2 ± 0.5	3.4 ± 0.8	1.1 ± 0.8	0.35	6.7 ± 1.4	-2.50	+3.90	(3)
050410	CPL	59.6 ± 6.9	128.0 ± 7.3	164.0 ± 10.8	82.9 ± 15.6	435.0 ± 24.9	-27.02	+36.98	
050412	PL	3.3 ± 0.7	9.6 ± 1.2	23.2 ± 2.0	26.8 ± 3.7	62.9 ± 5.7	-8.28	+22.16	
050416A	CPL	19.7 ± 2.5	13.3 ± 2.2	5.9 ± 2.0	1.8 ± 0.9	40.7 ± 5.6	+0.03	+10.14	
050416B	CPL	10.3 ± 2.3	27.9 ± 2.7	45.6 ± 4.6	27.2 ± 6.8	111.0 ± 10.1	+0.06	+4.20	
050418	CPL	77.9 ± 6.4	143.0 ± 5.7	181.0 ± 8.2	109.0 ± 12.8	511.0 ± 19.9	-8.35	+80.50	
050421	PL	2.1 ± 0.8	3.7 ± 0.9	4.9 ± 1.7	3.6 ± 1.9	14.3 ± 4.0	+0.05	+18.11	
050422	PL	7.2 ± 1.5	14.1 ± 1.8	21.2 ± 3.3	17.1 ± 4.1	59.6 ± 8.1	-11.30	+68.70	
050502B	PL	7.0 ± 0.8	12.1 ± 0.9	16.2 ± 1.8	11.8 ± 2.0	47.1 ± 4.2	-17.32	+3.18	
050505	PL	30.0 ± 4.0	58.8 ± 4.8	89.3 ± 7.1	72.5 ± 8.9	251.0 ± 18.1	-10.06	+52.51	
050507	—	—	—	—	—	—	—	—	(2)
050509A	PL	8.3 ± 1.0	10.4 ± 0.8	9.7 ± 1.5	5.3 ± 1.3	33.6 ± 3.3	-6.26	+8.06	
050509B	PL	0.08 ± 0.03	0.16 ± 0.04	0.26 ± 0.08	0.2 ± 0.1	0.7 ± 0.2	+0.00	+0.03	
050525A	CPL	220.0 ± 9.8	440.0 ± 7.6	555.0 ± 8.8	299.0 ± 8.1	1510.0 ± 20.0	-0.12	+12.68	
050528	PL	12.1 ± 2.2	14.3 ± 2.0	12.1 ± 3.0	6.2 ± 2.3	44.7 ± 7.0	-8.20	+4.98	
050603	PL	66.3 ± 5.4	147.0 ± 7.1	257.0 ± 11.2	233.0 ± 16.1	703.0 ± 28.9	-17.77	+33.23	
050607	PL	12.5 ± 1.8	17.9 ± 1.7	19.0 ± 3.0	11.7 ± 2.8	61.2 ± 6.82	-11.37	+36.63	

[1]The event data are not available.

[2]The event data of the part of the burst emission are not available.

[3]S(100-150) is an upper limit.

Table 3. BAT GRB 1-s peak photon flux

GRB Name	Spectral Model	F^p_{ph}(15-25)	F^p_{ph}(25-50)	F^p_{ph}(50-100)	F^p_{ph}(100-150)	F^p_{ph}(15-150)	Start (s)	Stop (s)	Note
		(photons cm^{-2} s^{-1})							
041217	PL	2.09 ± 0.25	2.24 ± 0.17	1.70 ± 0.14	0.796 ± 0.106	6.82 ± 0.48	+3.26	+4.26	
041219A	—	—	—	—	—	—	—	—	(1)
041219B	—	—	—	—	—	—	—	—	(1)
041219C	PL	0.88 ± 0.14	0.78 ± 0.04	0.48 ± 0.03	0.19 ± 0.02	2.33 ± 0.23	+2.00	+3.00	
041220	PL	0.52 ± 0.03	0.58 ± 0.02	0.46 ± 0.02	0.22 ± 0.02	1.78 ± 0.13	-0.02	+0.98	
041223	PL	1.51 ± 0.11	2.20 ± 0.10	2.38 ± 0.10	1.48 ± 0.05	7.58 ± 0.29	+35.01	+36.01	
041224	PL	0.82 ± 0.14	0.95 ± 0.10	0.79 ± 0.04	0.40 ± 0.03	2.95 ± 0.29	-0.06	+0.94	
041226	PL	0.09 ± 0.02	0.11 ± 0.02	0.09 ± 0.02	0.05 ± 0.01	0.34 ± 0.05	+3.31	+4.31	
041228	PL	0.63 ± 0.15	0.56 ± 0.04	0.34 ± 0.03	0.13 ± 0.02	1.65 ± 0.24	+22.03	+23.03	
050117	PL	0.51 ± 0.03	0.70 ± 0.03	0.70 ± 0.03	0.41 ± 0.03	2.32 ± 0.16	+87.22	+88.22	
050124	CPL	4.20 ± 0.63	11.9 ± 0.9	19.5 ± 1.5	11.1 ± 2.2	46.6 ± 3.3	-0.1	+0.9	
050126	PL	0.64	0.91	1.56	2.21	4.22	+12.1	+13.1	(3,4,5,6,7)
050128	PL	6.73 ± 1.02	13.9 ± 1.3	22.2 ± 2.2	18.7 ± 2.8	61.6 ± 5.66	+5.4	+6.4	
050202	PL	0.58 ± 0.31	1.09 ± 0.34	1.57 ± 0.55	1.22 ± 0.69	4.46 ± 1.31	-0.4	+0.6	
050215A	PL	0.27 ± 0.16	0.78 ± 0.28	1.86 ± 0.46	2.11 ± 0.80	5.02 ± 1.27	+5.6	+6.6	
050215B	PL	0.78 ± 0.20	1.24 ± 0.23	1.47 ± 0.42	0.98 ± 0.42	4.47 ± 1.00	+0.1	+1.1	
050219A	PL	2.78 ± 0.47	6.38 ± 0.67	11.6 ± 1.2	10.7 ± 1.7	31.4 ± 3.1	+9.5	+10.5	
050219B	CPL	23.0 ± 2.6	50.7 ± 3.1	69.6 ± 4.9	40.2 ± 5.9	184.0 ± 10.0	+2.8	+3.8	
050223	PL	0.65 ± 0.26	1.22 ± 0.30	1.76 ± 0.55	1.37 ± 0.67	5.00 ± 1.32	+1.6	+2.6	
050306	PL	2.88 ± 0.71	6.39 ± 0.96	11.1 ± 1.5	10.0 ± 2.0	30.4 ± 3.9	+107.9	+108.9	
050315	PL	2.67 ± 0.38	3.47 ± 0.36	3.30 ± 0.57	1.85 ± 0.48	11.3 ± 1.4	+24.6	+25.6	
050318	—	—	—	—	—	—	—	—	(3)
050319	PL	1.99 ± 0.35	2.69 ± 0.36	2.68 ± 0.60	1.56 ± 0.52	8.92 ± 1.43	+0.6	+1.6	
050326	PL	8.13 ± 0.40	21.0 ± 0.6	43.6 ± 1.4	44.8 ± 2.1	117.0 ± 3.6	-0.1	+0.9	
050401	CPL	6.88 ± 1.53	21.2 ± 2.1	41.7 ± 4.1	29.6 ± 5.3	99.2 ± 7.9	+24.3	+25.3	
050406	PL	0.53 ± 0.18	0.65 ± 0.20	0.57 ± 0.32	0.30 ± 0.25	2.04 ± 0.75	+0.5	+1.5	
050410	PL	1.91 ± 0.62	2.98 ± 0.68	3.51 ± 1.12	2.33 ± 1.10	10.7 ± 2.7	-3.5	-2.5	
050412	PL	0.23 ± 0.11	0.74 ± 0.22	1.98 ± 0.38	2.47 ± 0.72	5.42 ± 1.07	+1.1	+2.1	
050416A	CPL	8.64 ± 0.92	9.44 ± 1.13	1.75 ± 0.94	—	19.9 ± 1.9	+0.0	+1.0	(6)
050416B	PL	4.27 ± 0.82	10.6 ± 1.3	21.2 ± 2.1	21.2 ± 3.1	57.3 ± 5.4	+0.1	+1.1	
050418	PL	2.79 ± 0.38	6.57 ± 0.55	12.3 ± 1.0	11.7 ± 1.4	33.4 ± 2.5	+0.7	+1.7	
050421	PL	0.48 ± 0.19	0.82 ± 0.21	1.05 ± 0.41	0.75 ± 0.45	3.10 ± 0.97	+0.4	+1.4	
050422	PL	0.36 ± 0.19	0.51 ± 0.20	0.55 ± 0.38	$0.80 \pm ---$	1.76 ± 0.87	+60.2	+61.2	(6)
050502B	CPL	1.12 ± 0.20	3.10 ± 0.32	4.47 ± 0.52	2.01 ± 0.81	10.7 ± 1.2	+0.2	+1.2	
050505	PL	1.39 ± 0.43	3.29 ± 0.64	6.17 ± 0.95	5.89 ± 1.32	16.7 ± 2.5	+1.0	+2.0	
050507	—	—	—	—	—	—	—	—	(2)

[1]The event data are not available.

[2]The event data of the part of the burst emission are not available.

[3]F^p_{ph}(15-25) is an upper limit.

[4]F^p_{ph}(25-50) is an upper limit.

[5]F^p_{ph}(50-100) is an upper limit.

[6]F^p_{ph}(100-150) is an upper limit.

[7]F^p_{ph}(15-150) is an upper limit.

Table 4. BAT GRB 1-s peak energy flux

GRB Name	Spectral Model	F^p_{ene}(15-25)	F^p_{ene}(25-50)	F^p_{ene}(50-100)	F^p_{ene}(100-150)	F^p_{ene}(15-150)	Note
		(10^{-8} ergs cm^{-2} s^{-1})					
041217	PL	6.5 ± 0.8	12.7 ± 0.9	19.3 ± 1.7	15.7 ± 2.1	54.2 ± 4.2	
041219A	—	—	—	—	—	—	(1)
041219B	—	—	—	—	—	—	(1)
041219C	PL	2.7 ± 0.4	4.4 ± 0.4	5.4 ± 0.7	3.7 ± 0.8	16.3 ± 1.8	
041220	PL	1.6 ± 0.2	3.3 ± 0.3	5.2 ± 0.5	4.4 ± 0.7	14.5 ± 1.3	
041223	PL	4.8 ± 0.4	12.8 ± 0.6	27.7 ± 1.2	29.4 ± 1.9	74.6 ± 3.2	
041224	PL	2.5 ± 0.4	5.4 ± 0.6	9.0 ± 1.0	7.9 ± 1.3	24.9 ± 2.6	
041226	PL	0.3 ± 0.1	0.6 ± 0.2	1.1 ± 0.4	1.0 ± 0.5	2.9 ± 0.9	
041228	PL	2.0 ± 0.5	3.1 ± 0.5	3.8 ± 0.8	2.6 ± 0.8	11.4 ± 1.8	
050117	PL	1.6 ± 0.2	4.0 ± 0.3	8.1 ± 0.6	8.2 ± 1.0	21.9 ± 1.7	
050124	CPL	4.2 ± 0.6	11.9 ± 0.9	19.5 ± 1.5	11.1 ± 2.2	46.6 ± 3.3	
050126	PL	0.6	0.9	1.6	2.2	4.2	(3,4,5,6,7)
050128	PL	6.7 ± 1.0	13.9 ± 1.3	22.2 ± 2.2	18.7 ± 2.8	61.6 ± 5.7	
050202	PL	0.6 ± 0.3	1.1 ± 0.3	1.6 ± 0.6	1.2 ± 0.7	4.5 ± 1.3	
050215A	PL	0.3 ± 0.2	0.8 ± 0.3	1.9 ± 0.5	2.1 ± 0.8	5.0 ± 1.3	
050215B	PL	0.8 ± 0.2	1.2 ± 0.2	1.5 ± 0.4	1.0 ± 0.4	4.5 ± 1.0	
050219A	PL	2.8 ± 0.5	6.4 ± 0.7	11.6 ± 1.2	10.7 ± 1.7	31.4 ± 3.1	
050219B	CPL	23.0 ± 2.6	50.7 ± 3.1	69.6 ± 4.9	40.2 ± 5.9	184.0 ± 10.0	
050223	PL	0.7 ± 0.3	1.2 ± 0.3	1.8 ± 0.6	1.4 ± 0.7	5.0 ± 1.3	
050306	PL	2.9 ± 0.7	6.4 ± 1.0	11.1 ± 1.5	10.0 ± 2.0	30.4 ± 3.9	
050315	PL	2.7 ± 0.4	3.5 ± 0.4	3.3 ± 0.6	1.9 ± 0.5	11.3 ± 1.4	
050318	—	—	—	—	—	—	(2)
050319	PL	2.0 ± 0.4	2.7 ± 0.4	2.7 ± 0.6	1.6 ± 0.5	8.9 ± 1.4	
050326	PL	8.1 ± 0.4	21.0 ± 0.6	43.6 ± 1.4	44.8 ± 2.1	117.0 ± 3.6	
050401	CPL	6.9 ± 1.5	21.2 ± 2.1	41.7 ± 4.1	29.6 ± 5.3	99.2 ± 7.9	
050406	PL	0.5 ± 0.2	0.7 ± 0.2	0.6 ± 0.3	0.3 ± 0.3	2.0 ± 0.8	
050410	PL	1.9 ± 0.6	3.0 ± 0.7	3.5 ± 1.1	2.3 ± 1.1	10.7 ± 2.7	
050412	PL	0.2 ± 0.1	0.7 ± 0.2	2.0 ± 0.4	2.5 ± 0.7	5.4 ± 1.1	
050416A	CPL	8.6 ± 0.9	9.4 ± 1.1	1.8 ± 0.9	0.1	19.9 ± 1.9	(6)
050416B	PL	4.3 ± 0.8	10.6 ± 1.3	21.2 ± 2.1	21.2 ± 3.1	57.3 ± 5.4	
050418	PL	2.9 ± 0.4	6.6 ± 0.6	12.3 ± 1.0	11.7 ± 1.4	33.4 ± 2.5	
050421	PL	0.5 ± 0.2	0.8 ± 0.2	1.1 ± 0.4	0.8 ± 0.5	3.1 ± 1.0	
050422	PL	0.4 ± 0.2	0.5 ± 0.2	0.6 ± 0.4	0.8	1.8 ± 0.9	
050502B	CPL	1.1 ± 0.2	3.1 ± 0.3	4.5 ± 0.5	2.0 ± 0.8	10.7 ± 1.2	
050505	PL	1.4 ± 0.4	3.3 ± 0.6	6.2 ± 1.0	5.9 ± 1.3	16.7 ± 2.5	
050507	—	—	—	—	—	—	(2)

[1]The event data are not available.

[2]The event data of the part of the burst emission are not available.

[3]F^p_{ene}(15-25) is an upper limit.

[4]F^p_{ene}(25-50) is an upper limit.

[5]F^p_{ene}(50-100) is an upper limit.

[6]F^p_{ene}(100-150) is an upper limit.

[7]F^p_{ene}(15-150) is an upper limit.

Table 5. BAT GRB 20-msec peak photon and energy flux

GRB Name	Spectral Model	F^p_{ene}(15-150) (10^{-8} ergs cm^{-2} s^{-1})	F^p_{ph}(15-150) (photons cm^{-2} s^{-1})	Start (s)	Stop (s)	Note
041217	CPL	75.5 ± 31.0	9.5 ± 3.3	+3.63	+3.65	
041219A	—	—	—	—	—	(1)
041219B	—	—	—	—	—	(1)
041219C	PL	20.8 ± 10.8	4.1 ± 1.6	+8.13	+8.15	
041220	PL	33.0 ± 11.8	3.1 ± 1.0	+0.25	+0.27	
041223	PL	124.0 ± 27.1	11.3 ± 2.2	+24.30	+24.32	
041224	CPL	44.6 ± 18.5	5.9 ± 2.1	+0.68	+0.70	
041226	PL	13.1 ± 7.1	1.4 ± 0.7	+2.75	+2.77	
041228	—	—	—	+2.49	+2.51	(2)
050117	CPL	41.9 ± 16.6	4.0 ± 1.2	+88.02	+88.04	
050124	CPL	69.1 ± 20.4	9.6 ± 2.6	+0.36	+0.38	
050126	PL	28.5 ± 13.2	2.9 ± 1.2	+3.44	+3.46	
050128	PL	154.0 ± 54.7	14.7 ± 4.5	+6.18	+6.20	
050202	PL	41.9 ± 15.3	4.3 ± 1.4	+0.08	+0.10	
050215A	PL	16.7 ± 10.3	1.9 ± 1.0	+0.40	+0.42	
050215B	PL	17.0 ± 10.8	1.6 ± 0.9	+1.52	+1.54	
050219A	PL	71.5 ± 31.1	6.9 ± 2.5	+10.52	+10.54	
050219B	PL	344.0 ± 103.0	36.4 ± 9.6	+3.06	+3.08	
050223	CPL	13.7 ± 7.5	2.4 ± 1.0	+7.74	+7.76	
050306	CPL	70.3 ± 35.6	7.5 ± 3.7	+107.96	+107.98	
050315	PL	22.7 ± 11.2	3.2 ± 1.4	+9.86	+9.88	
050318	—	—	—	—	—	(3)
050319	CPL	18.7 ± 7.3	3.6 ± 1.3	+0.65	+0.67	
050326	PL	161.0 ± 30.1	16.0 ± 2.4	+0.48	+0.50	
050401	—	—	—	+25.17	+25.19	(2)
050406	PL	11.3	1.3 ± 0.6	+0.60	+0.62	(4)
050410	CPL	81.0	5.0 ± 2.6	+7.84	+7.86	(4)
050412	PL	12.6 ± 6.7	1.5 ± 0.6	+21.66	+21.68	
050416A	CPL	25.0 ± 12.1	7.4 ± 3.3	+0.72	+0.74	
050416B	PL	62.0 ± 32.8	8.6 ± 4.2	+0.20	+0.22	
050418	CPL	46.1 ± 20.3	5.7 ± 2.0	+2.35	+2.37	
050421	PL	15.4 ± 9.1	1.4 ± 0.8	+1.33	+1.35	
050422	PL	12.9 ± 7.5	1.6 ± 0.7	+2.52	+2.54	
050502B	PL	22.2 ± 9.0	2.4 ± 0.9	+0.89	+0.91	
050505	PL	33.8 ± 18.3	4.7 ± 2.2	-8.37	-8.35	
050507	—	—	—	—	—	(3)
050509A	PL	11.4 ± 6.0	1.7 ± 0.7	-4.93	-4.91	
050509B	PL	31.4 ± 10.3	3.7 ± 1.0	+0.01	+0.03	
050525A	CPL	494.0 ± 47.4	53.8 ± 3.9	+1.02	+1.04	
050528	CPL	28.8 ± 15.2	3.6 ± 2.0	-5.01	-4.99	

[1]The event data are not available.

[2]Reduced χ^2 is greater than 2.

[3]The event data of the part of the burst emission are not available.

[4]F^p_{ene}(15-150) is an upper limit.

Table 6. BAT time-averaged spectral parameters

GRB	$\alpha^{\rm PL}$	$K_{50}^{\rm PL}$(a)	χ^2	$\alpha^{\rm CPL}$	$E_{\rm peak}^{\rm obs}$ (keV)	$K_{50}^{\rm CPL}$(b)	χ^2	Note
041217	$-1.452^{+0.064}_{-0.064}$	$417.0^{+15.4}_{-15.4}$	73.2	$-0.663^{+0.309}_{-0.29}$	$91.5^{+22.8}_{-12.0}$	$97.5^{+37.3}_{-25.7}$	49.2	
041219A	—	—	—	—	—	—	—	(1)
041219B	—	—	—	—	—	—	—	(1)
041219C	$-2.007^{+0.087}_{-0.089}$	$103.0^{+5.4}_{-5.4}$	44.6	—	—	—	—	
041220	$-1.672^{+0.120}_{-0.122}$	$56.2^{+3.9}_{-4.0}$	30.5	—	—	—	—	
041223	$-1.153^{+0.030}_{-0.03}$	$106.0^{+1.8}_{-1.8}$	33.4	—	—	—	—	
041224	$-1.731^{+0.058}_{-0.058}$	$43.2^{+1.4}_{-1.4}$	62.8	$-0.984^{+0.281}_{-0.264}$	$68.9^{+11.7}_{-7.0}$	$10.1^{+3.7}_{-2.6}$	36.9	
041226	$-1.416^{+0.430}_{-0.417}$	$3.4^{+0.8}_{-0.8}$	85.1	—	—	—	—	
041228	$-1.617^{+0.077}_{-0.077}$	$55.1^{+2.3}_{-2.3}$	64.6	—	—	—	—	
050117	$-1.519^{+0.042}_{-0.042}$	$44.5^{+0.9}_{-0.9}$	44.4	$-1.171^{+0.182}_{-0.172}$	$130.3^{+70.6}_{-26.7}$	$6.4^{+1.3}_{-1.0}$	32.2	
050124	$-1.412^{+0.085}_{-0.085}$	$181.0^{+9.2}_{-9.2}$	55.2	$-0.698^{+0.404}_{-0.37}$	$100.2^{+48.4}_{-18.3}$	$38.8^{+20.3}_{-12.5}$	43.6	
050126	$-1.360^{+0.169}_{-0.168}$	$18.8^{+1.9}_{-1.9}$	72.3	—	—	—	—	
050128	$-1.368^{+0.071}_{-0.071}$	$162.0^{+6.9}_{-6.9}$	63.1	$-0.716^{+0.333}_{-0.313}$	$113.7^{+50.8}_{-20.2}$	$31.6^{+12.3}_{-8.5}$	49.5	
050202	$-1.357^{+0.296}_{-0.292}$	$246.0^{+42.8}_{-42.8}$	44.7	—	—	—	—	
050215A	$-1.326^{+0.267}_{-0.261}$	$9.1^{+1.2}_{-1.2}$	43.0	—	—	—	—	
050215B	$-2.173^{+0.209}_{-0.223}$	$19.6^{+3.0}_{-3.1}$	57.6	—	—	—	—	
050219A	$-1.305^{+0.056}_{-0.056}$	$121.0^{+4.1}_{-4.1}$	100.7	$-0.122^{+0.300}_{-0.282}$	$90.6^{+11.3}_{-7.9}$	$40.4^{+13.8}_{-9.8}$	39.0	
050219B	$-1.508^{+0.050}_{-0.05}$	$230.0^{+6.8}_{-6.8}$	79.4	$-0.919^{+0.236}_{-0.224}$	$107.9^{+30.2}_{-15.2}$	$41.4^{+10.6}_{-8.1}$	57.9	
050223	$-1.826^{+0.158}_{-0.163}$	$24.6^{+2.4}_{-2.5}$	49.3	—	—	—	—	
050306	$-1.467^{+0.065}_{-0.065}$	$63.4^{+2.4}_{-2.4}$	59.5	$-1.086^{+0.281}_{-0.265}$	$140.3^{+171.5}_{-35.8}$	$9.3^{+2.9}_{-2.1}$	53.3	
050315	$-2.087^{+0.084}_{-0.085}$	$27.2^{+1.3}_{-1.3}$	52.3	—	—	—	—	
050318	—	—	—	—	—	—	—	(2)
050319	$-1.934^{+0.171}_{-0.178}$	$8.9^{+1.0}_{-1.0}$	43.4	—	—	—	—	
050326	$-1.261^{+0.033}_{-0.032}$	$210.0^{+3.6}_{-3.6}$	46.9	—	—	—	—	
050401	$-1.358^{+0.064}_{-0.064}$	$232.0^{+8.6}_{-8.6}$	41.4	—	—	—	—	
050406	$-2.404^{+0.317}_{-0.365}$	$12.4^{+3.5}_{-3.5}$	73.6	$0.406^{+2.594}_{-1.754}$	$29.4^{+6.2}_{-3.2}$	$82.7^{+2170.0}_{-76.5}$	65.6	
050410	$-1.616^{+0.080}_{-0.08}$	$76.3^{+3.7}_{-3.7}$	66.4	$-0.812^{+0.386}_{-0.355}$	$75.6^{+21.0}_{-10.2}$	$19.0^{+10.1}_{-6.2}$	49.9	
050412	$-0.729^{+0.173}_{-0.165}$	$17.1^{+1.6}_{-1.6}$	30.3	—	—	—	—	
050416A	$-3.180^{+0.285}_{-0.319}$	$30.6^{+8.1}_{-7.7}$	58.6	$-0.972^{+2.279}_{-1.012}$	$13.7^{+7.9}_{-12.6}$	4870	52.2	(6)
050416B	$-1.327^{+0.128}_{-0.128}$	$285.0^{+21.7}_{-21.7}$	72.4	$-0.391^{+0.679}_{-0.585}$	$95.7^{+65.5}_{-19.4}$	$76.2^{+75.1}_{-34.4}$	64.3	
050418	$-1.665^{+0.060}_{-0.06}$	$63.4^{+2.1}_{-2.1}$	57.1	$-1.292^{+0.260}_{-0.246}$	$99.8^{+86.7}_{-21.2}$	$9.6^{+3.1}_{-2.2}$	50.2	
050421	$-1.593^{+0.412}_{-0.429}$	$8.5^{+2.1}_{-2.2}$	47.9	—	—	—	—	
050422	$-1.408^{+0.204}_{-0.205}$	$7.7^{+0.9}_{-0.9}$	41.5	—	—	—	—	
050502B	$-1.587^{+0.133}_{-0.135}$	$24.5^{+2.0}_{-2.0}$	67.9	—	—	—	—	
050505	$-1.396^{+0.118}_{-0.117}$	$41.4^{+2.9}_{-2.9}$	43.8	—	—	—	—	
050507	—	—	—	—	—	—	—	
050509A	$-2.114^{+0.165}_{-0.174}$	$25.2^{+2.7}_{-2.8}$	54.5	—	—	—	—	

[a]In the unit of 10^{-4} ph cm^{-2} s^{-1} keV^{-1}.

[b]In the unit of 10^{-3} ph cm^{-2} s^{-1} keV^{-1}.

[1]The event data are not available.

[2]The event data of the part of the burst emission are not available.

[6]$K_{50}^{\rm CPL}$ is an upper limit.

Table 7. BAT time-resolved spectral parameters

GRB	Start (s)	Stop (s)	$\alpha^{\rm PL}$	$K_{50}^{\rm PL}$(a)	χ^2	F_{PL}(15-150)(b)	$\alpha^{\rm CPL}$	$E_{\rm peak}^{\rm obs}$ (keV)	$K_{50}^{\rm CPL}$(c)	χ^2	F_{CPL}(15-150)(b)	Note
041217	0.824	5.812	$-1.385^{+0.064}_{-0.064}$	$499.0^{+18.8}_{-18.8}$	78.2	48.4 ± 1.9	$-0.517^{+0.319}_{-0.297}$	$93.6^{+21.1}_{-11.8}$	$126.0^{+49.2}_{-33.3}$	50.2	46.3 ± 2.1	
041217	5.812	7.888	$-1.763^{+0.191}_{-0.198}$	$210.0^{+25.5}_{-25.9}$	54.5	19.3 ± 2.5	—	—	—	—	—	
041219C	0.000	6.000	$-1.912^{+0.094}_{-0.096}$	$139.0^{+7.8}_{-7.8}$	52.7	12.7 ± 0.7	—	—	—	—	—	
041219C	6.000	9.000	$-2.168^{+0.169}_{-0.179}$	$88.8^{+10.4}_{-10.7}$	54.4	8.3 ± 0.9	—	—	—	—	—	
041219C	9.000	12.000	$-2.060^{+0.300}_{-0.332}$	$45.1^{+9.5}_{-9.9}$	42.3	4.2 ± 0.8	—	—	—	—	—	
041220	-0.208	1.728	$-1.479^{+0.116}_{-0.117}$	$126.0^{+8.3}_{-8.3}$	52.0	12.0 ± 0.9	—	—	—	—	—	
041220	1.728	2.936	$-1.862^{+0.236}_{-0.25}$	$59.1^{+9.4}_{-9.7}$	53.9	5.4 ± 0.9	—	—	—	—	—	
041220	2.936	6.812	$-2.029^{+0.360}_{-0.408}$	$19.3^{+5.0}_{-5.3}$	40.1	1.8 ± 0.4	—	—	—	—	—	
041223	-10.536	-0.544	$-1.363^{+0.388}_{-0.381}$	$17.1^{+4.0}_{-4.0}$	61.5	1.7 ± 0.4	—	—	—	—	—	
041223	-0.544	-0.124	$-1.529^{+0.400}_{-0.408}$	$88.9^{+21.9}_{-22.3}$	48.5	8.4 ± 2.3	—	—	—	—	—	
041223	-0.124	2.196	$-0.771^{+0.082}_{-0.081}$	$292.0^{+13.6}_{-13.7}$	57.6	34.6 ± 1.7	—	—	—	—	—	
041223	2.196	3.104	$-0.977^{+0.303}_{-0.286}$	$93.1^{+15.7}_{-15.8}$	49.6	10.2 ± 1.8	—	—	—	—	—	
041223	3.104	4.220	$-1.155^{+0.148}_{-0.146}$	$188.0^{+16.2}_{-16.2}$	58.1	19.4 ± 1.9	—	—	—	—	—	
041223	4.220	4.864	$-0.896^{+0.100}_{-0.098}$	$466.0^{+27.4}_{-27.4}$	53.7	52.3 ± 3.4	—	—	—	—	—	
041223	4.864	5.372	$-1.148^{+0.153}_{-0.152}$	$296.0^{+26.8}_{-26.9}$	61.6	30.5 ± 3.1	—	—	—	—	—	
041223	5.372	9.768	$-1.159^{+0.092}_{-0.092}$	$158.0^{+8.0}_{-8.0}$	48.5	16.2 ± 0.9	—	—	—	—	—	
041223	9.768	11.524	$-1.415^{+0.360}_{-0.365}$	$48.2^{+10.3}_{-10.4}$	54.7	4.6 ± 1.1	—	—	—	—	—	
041223	11.524	12.840	$-1.105^{+0.191}_{-0.188}$	$126.0^{+13.2}_{-13.3}$	66.2	13.1 ± 1.5	—	—	—	—	—	
041223	12.840	13.192	$-0.701^{+0.168}_{-0.162}$	$337.0^{+33.6}_{-34.0}$	69.8	41.1 ± 4.1	—	—	—	—	—	
041223	13.192	14.400	$-0.937^{+0.183}_{-0.176}$	$133.0^{+14.7}_{-14.7}$	77.0	14.7 ± 1.7	—	—	—	—	—	
041223	14.400	14.680	$-1.094^{+0.204}_{-0.201}$	$269.0^{+34.1}_{-34.1}$	63.5	28.2 ± 4.0	—	—	—	—	—	
041223	14.680	15.348	$-1.071^{+0.315}_{-0.301}$	$96.1^{+18.4}_{-18.4}$	62.3	10.1 ± 2.1	—	—	—	—	—	
041223	15.348	16.188	$-0.976^{+0.111}_{-0.11}$	$372.0^{+22.9}_{-22.9}$	69.7	40.6 ± 2.8	—	—	—	—	—	
041223	16.188	17.436	$-1.138^{+0.150}_{-0.147}$	$173.0^{+14.9}_{-14.9}$	62.4	17.9 ± 1.7	—	—	—	—	—	
041223	17.436	20.056	$-0.934^{+0.074}_{-0.073}$	$294.0^{+12.5}_{-12.6}$	67.4	32.6 ± 1.5	$-0.456^{+0.323}_{-0.3}$	$189.8^{+204.7}_{-53.3}$	$47.5^{+17.4}_{-12.1}$	59.7	31.9 ± 1.6	
041223	20.056	21.108	$-0.994^{+0.102}_{-0.101}$	$369.0^{+20.9}_{-20.9}$	52.2	40.0 ± 2.5	—	—	—	—	—	
041223	21.108	21.684	$-0.867^{+0.101}_{-0.099}$	$549.0^{+32.2}_{-32.3}$	64.9	62.4 ± 4.0	—	—	—	—	—	
041223	21.684	22.524	$-1.146^{+0.135}_{-0.134}$	$258.0^{+20.3}_{-20.3}$	59.6	26.5 ± 2.3	—	—	—	—	—	
041223	22.524	23.104	$-0.951^{+0.118}_{-0.116}$	$399.0^{+27.8}_{-27.8}$	60.6	44.0 ± 3.4	—	—	—	—	—	

[a]In the unit of 10^{-4} ph cm^{-2} s^{-1} keV^{-1}.

[b]In the unit of 10^{-8} ergs cm^{-2} s^{-1}.

[c]In the unit of 10^{-3} ph cm^{-2} s^{-1} keV^{-1}.

Table 8: BAT GRB T_{90} and T_{50} durations in the 140-220 keV band at the GRB rest frame.

GRB	T_{90}^{src} (s)	T_{50}^{src} (s)	Note
050126	8.73	4.80	
050223	—	—	(1)
050315	13.99	6.93	
050318	5.68	3.02	
050319	33.29	28.15	
050401	8.37	6.53	
050416A	—	—	(1)
050505	11.37	4.55	
050509B	—	—	(1)
050525A	4.24	2.89	
050603	2.53	0.57	
050724	—	—	(1)
050730	28.67	13.00	
050801	1.10	0.79	
050802	4.72	2.29	
050814	24.81	7.91	
050820A	—	—	(2)
050904	26.48	12.50	
050908	1.11	0.50	
050922C	1.56	0.63	
051016B	—	—	(1)
051109A	11.78	8.36	
051111	18.82	6.27	
051221A	0.17	0.08	
060115	28.80	19.86	
060124	3.94	2.73	
060206	1.10	0.43	
060210	35.74	6.24	
060218	—	—	(2)
060223A	1.93	0.70	
060418	19.28	6.43	
060502A	6.69	2.95	
060505	—	—	(1)
060510B	44.87	19.78	

[1]battblocks failed because of the weak signal in the light curve.

[2]The event data of the part of the burst emission are not available.

Table 9: Redshifts of Swift GRBs

GRB	Redshift	Note
050126	1.290	(2)
050223	0.584	(3)
050315	1.950	(4)
050318	1.444	(4)
050319	3.2425	(1)
050401	2.8983	(1)
050416A	0.6528	(5)
050505	4.275	(6)
050509B	0.226	(7)
050525A	0.606	(8)
050603	2.821	(9)
050724	0.258	(10)
050730	3.9693	(10)
050801	1.38	(1)
050802	1.7102	(1)
050814	5.3	(11)
050820A	2.6147	(1)
050824	0.8278	(1)
050826	0.296	(12)
050904	6.295	(13)
050908	3.3467	(1)
050922C	2.1995	(1)
051016B	0.9364	(14)
051109A	2.346	(15)

[1]Fynbo et al. ApJS, 185, 526 (2009)
[2]Berger E. et al. ApJ, 629, 328 (2005)
[3]Pellizza, L.J. et al. A&A, 459, L5 (2006)
[4]Berger, E. et al. ApJ, 634, 501 (2005)
[5]Soderberg, A.M. et al. ApJ, 661, 982 (2007)
[6]Berger, E. et al. ApJ, 642, 979 (2006)
[7]Gehrels, N. et al. Nature, 437, 851 (2005)
[8]Della Valle, M. et al. ApJ, 642, L103 (2006)
[9]Berger, E. et al. GCN Circ. 3520
[10]Berger, E. et al. Nature, 438, 988 (2005)
[11]Jakobsson, P. et al. A&A, 447, 897 (2006)
[12]Mirabal, N. et al. ApJ, 661, L127 (2007)
[13]Kawai, N. et al. Nature, 440, 184 (2006)
[14]Soderberg, A.M. et al. GCN Circ. 4186

Table 10. Spectral parameters of the initial short spikes of the short GRBs with E.E.

GRB	start (s)	stop (s)	$\alpha^{\rm PL}$	$K_{50}^{\rm PL}$(a)	χ^2
050724	-0.024	0.416	$-1.50^{+0.14}_{-0.14}$	$515.2^{+40.9}_{-41.1}$	50.9
051227	-0.848	0.828	$-0.94^{+0.23}_{-0.25}$	$61.0^{+7.9}_{-8.0}$	65.6
061006	-23.24	-22.20	$-0.86^{+0.07}_{-0.07}$	$445.3^{+17.7}_{-17.8}$	50.8
061210	-0.004	0.080	$-0.69^{+0.12}_{-0.12}$	$2755.1^{+209.0}_{-209.8}$	58.2
070714B	-1	-2	$-0.98^{+0.08}_{-0.08}$	$158.2^{+7.2}_{-7.2}$	43.0
071227	-0.144	1.872	$-0.90^{+0.22}_{-0.24}$	$98.6^{+12.1}_{-12.3}$	51.0
080503	-0.048	0.436	$-1.62^{+0.23}_{-0.23}$	$130.6^{+19.3}_{-19.6}$	66.0
090510	-0.128	0.384	$-0.87^{+0.19}_{-0.20}$	$699.9^{+78.0}_{-78.6}$	36.6
090715A	-0.12	0.84	$-0.99^{+0.19}_{-0.20}$	$348.9^{+38.3}_{-38.8}$	55.0

[a]In the unit of 10^{-4} ph cm^{-2} s^{-1} keV^{-1}.

Table 11. BAT GRB energy fluence of the initial short spkes of the short GRB with E.E.

GRB Name	Spectral Model	S(15-25)	S(25-50)	S(50-100)	S(100-150)	S(15-150)
		(10^{-8} ergs cm^{-2})				
050724	PL	2.9 ± 0.4	5.3 ± 0.4	7.5 ± 0.8	5.7 ± 0.9	21.5 ± 1.9
051227	PL	0.8 ± 0.2	2.0 ± 0.3	4.2 ± 0.6	4.3 ± 1.0	11.3 ± 1.6
061006	PL	3.3 ± 0.3	8.9 ± 0.4	19.6 ± 0.8	21.0 ± 1.4	52.7 ± 2.3
061210	PL	1.4 ± 0.2	4.2 ± 0.4	10.5 ± 0.8	12.4 ± 1.5	28.4 ± 2.4
070714B	PL	3.7 ± 0.4	9.4 ± 0.5	19.2 ± 1.0	19.5 ± 1.6	51.8 ± 2.6
071227	PL	1.4 ± 0.4	3.9 ± 0.6	8.3 ± 1.1	8.8 ± 1.8	22.4 ± 2.9
080503	PL	0.9 ± 0.2	1.5 ± 0.2	2.0 ± 0.4	1.5 ± 0.4	5.9 ± 0.9
090510	PL	2.5 ± 0.6	6.9 ± 1.0	15.1 ± 1.8	16.2 ± 3.0	40.7 ± 4.8
090715	PL	2.7 ± 0.6	6.7 ± 0.9	13.4 ± 1.5	13.5 ± 2.4	36.3 ± 4.0

Table 12. $E_{\rm peak}^{\rm src}$ and $E_{\rm iso}$ values for *Swift* GRBs.

GRB	z	$E_{\rm peak}^{\rm src}$ (keV)	$E_{\rm iso}$ (10^{52} erg)
050416A	0.6528	22^{+5}_{-4}	$0.12^{+0.01}_{-0.02}$
050525A	0.606	129^{+6}_{-7}	$2.6^{+0.9}_{-0.2}$
060115	3.5328	297^{+92}_{-111}	$6.5^{+6.7}_{-1.5}$
060206	4.0559	410^{+195}_{-179}	$4.5^{+3.2}_{-1.0}$
060707	3.4240	274^{+66}_{-77}	$4.7^{+18.8}_{-0.8}$
060908	1.8836	414^{+399}_{-120}	$8.1^{+1.9}_{-4.5}$
060927	5.4636	276^{+97}_{-54}	13^{+3}_{-3}
071010B	0.947	88^{+21}_{-21}	$2.6^{+0.5}_{-0.4}$
071117	1.3308	112^{+315}_{-52}	$6.5^{+1.6}_{-4.4}$
080413B	1.1014	163^{+51}_{-46}	$1.7^{+2.2}_{-0.3}$
080603B	2.6892	277^{+95}_{-111}	$6.6^{+6.2}_{-1.2}$
080605	1.6403	766^{+1100}_{-243}	31^{+20}_{-12}
080916A	0.6887	200^{+120}_{-51}	$1.8^{+1.8}_{-1.0}$
090205	4.6497	214^{+58}_{-87}	$0.9^{+0.7}_{-0.3}$
090423	8.26	410^{+115}_{-88}	$9.5^{+2.6}_{-1.9}$
090424	0.544	236^{+127}_{-49}	$4.3^{+2.4}_{-1.4}$
090926B	1.24	175^{+24}_{-20}	$5.4^{+2.8}_{-2.0}$
091018	0.971	$55^{+6.8}_{-17}$	$0.7^{+0.3}_{-0.1}$
091029	2.752	229^{+94}_{-59}	$8.5^{+4.5}_{-2.5}$

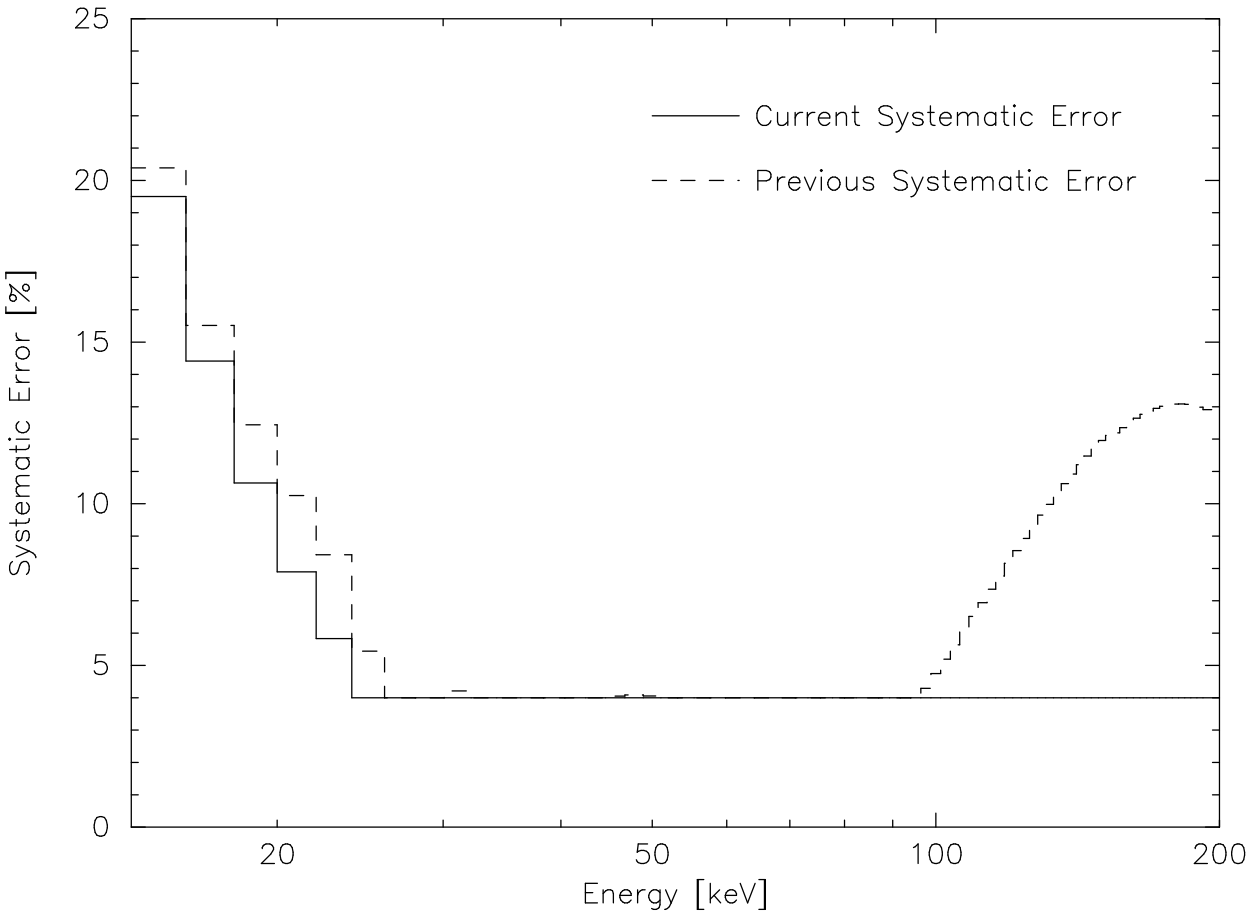

Fig. 1.— Systematic error as a function of energy. The current systematic error is shown in a solid line and the previous systematic error (used in the analysis of the BAT1 catalog) is shown in a dashed line.

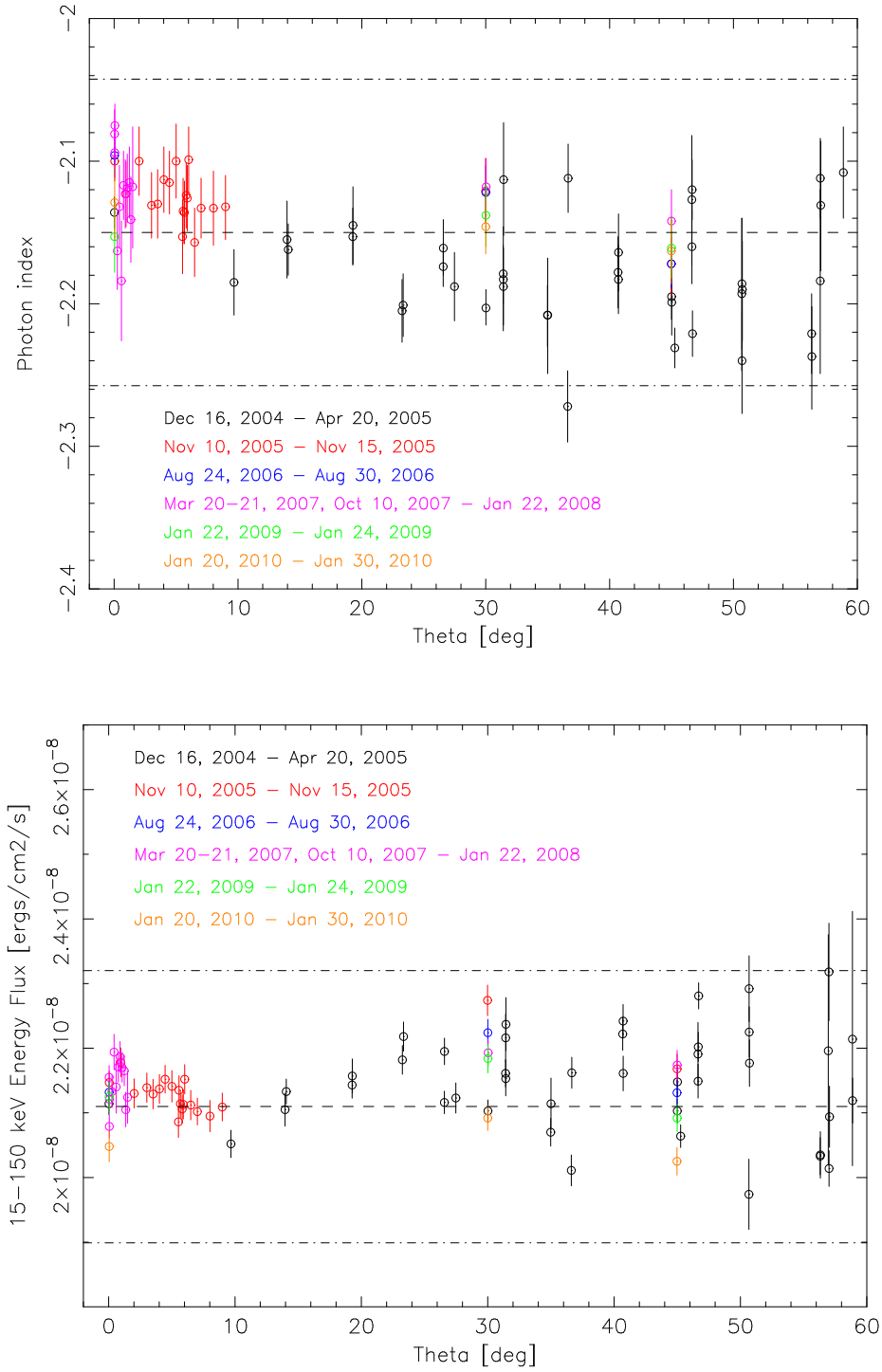

Fig. 2.— Power-law photon index (top) and the flux in the 15-150 keV band as a function of the incident angle of the Crab observed in different time periods. The horizontal dashed lines are the Crab canonical values of -2.15 for the photon index and 2.11×10^{-8} ergs cm^{-2} s^{-1} for the flux. The dashed dotted lines are $\pm 5\%$ of the photon index and $\pm 10\%$ of the flux canonical values.

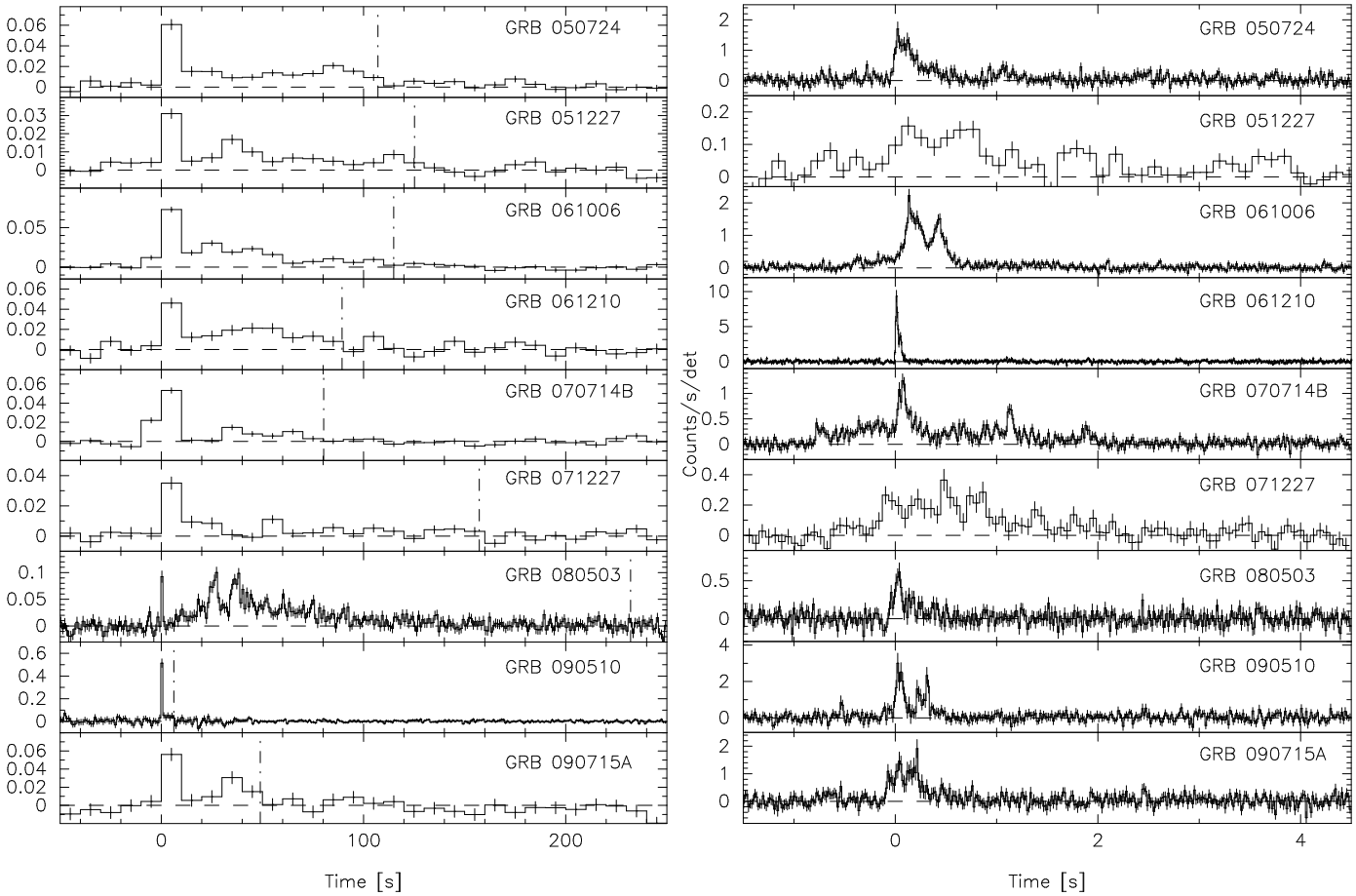

Fig. 3.— The BAT mask-weighted light curves of the 15-150 keV band in a course binning (left) and a fine binning (right) for short GRBs with extended emissions. The vertical dash-dotted lines in course binning light curves are showing the emission end time found by `battblocks`.

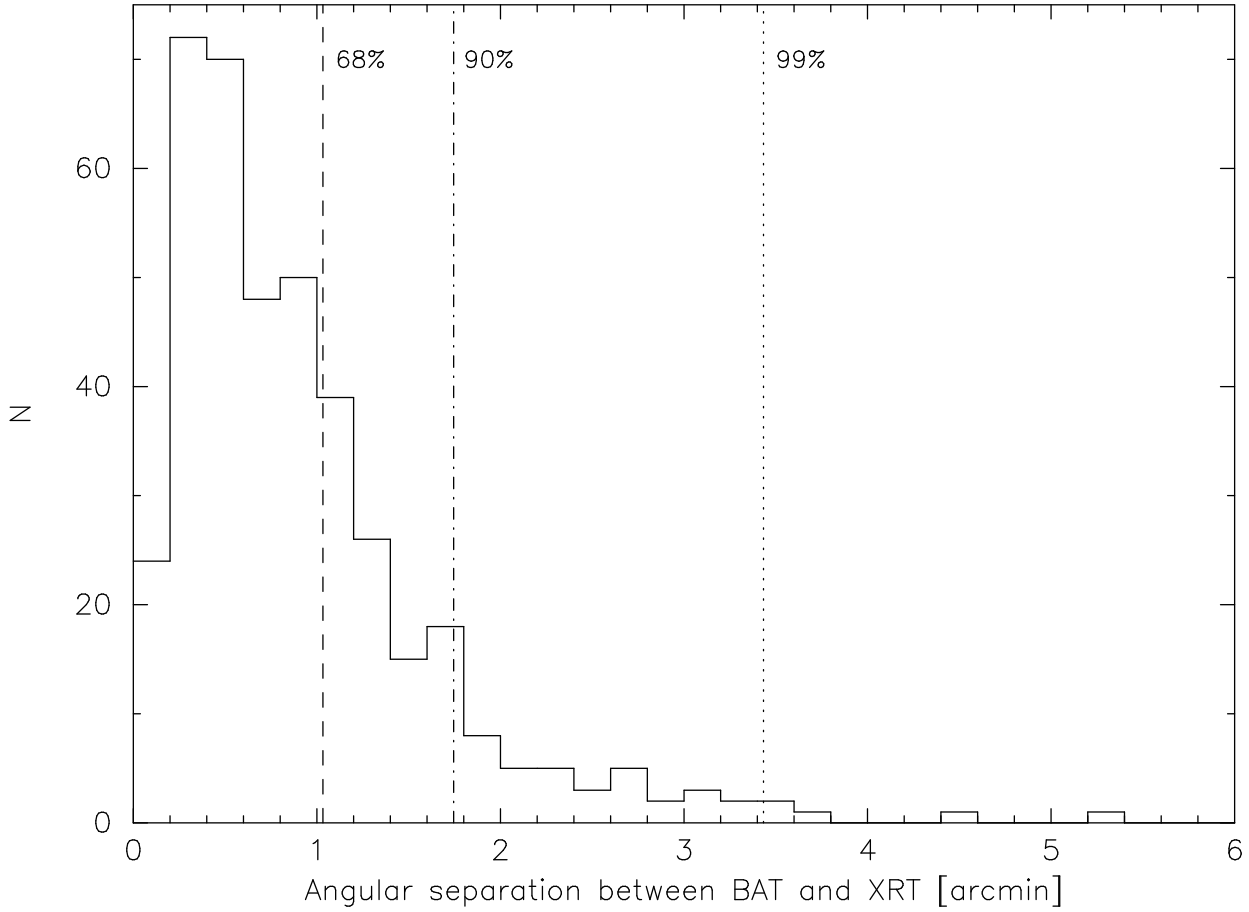

Fig. 4.— The histogram of the angular difference between the BAT ground position and the XRT position. 68%, 90% and 99% of BAT ground positions are within 1.1′, 1.8′ and 3.5′ from the XRT position, respectively.

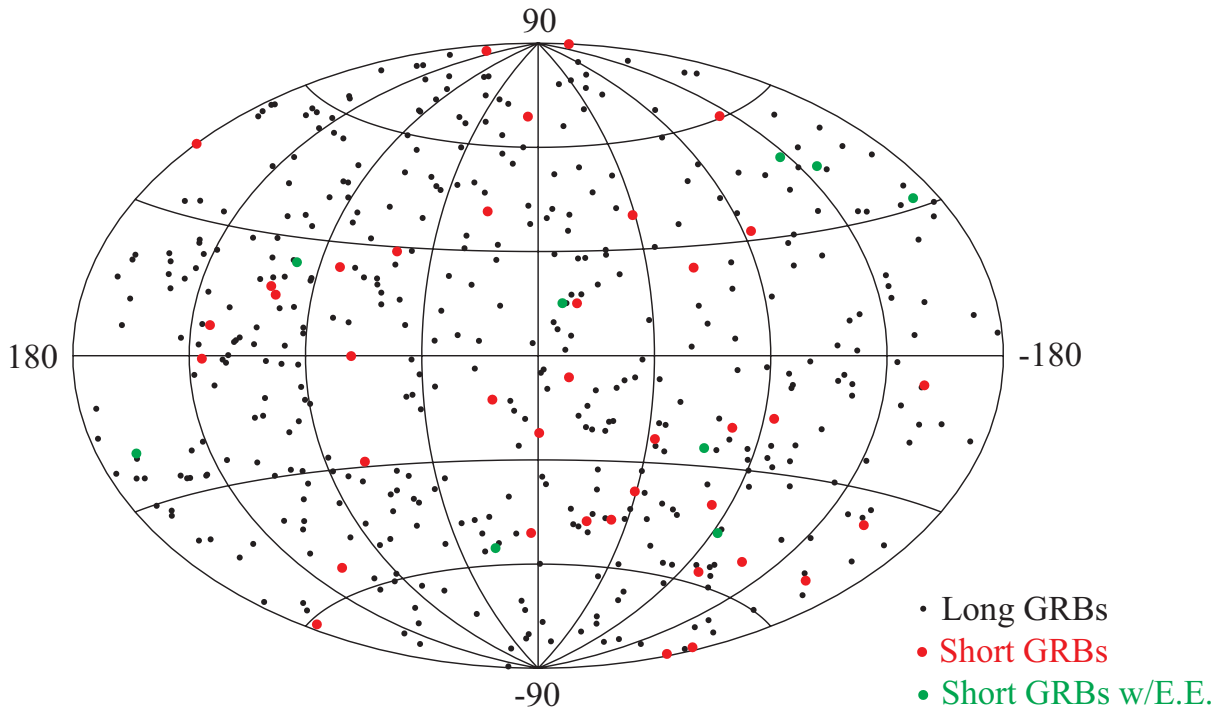

Fig. 5.— Sky distribution of the 476 BAT bursts in Galactic coordinates with long GRBs in black, short GRBs in red and short GRBs with extended emissions in green.

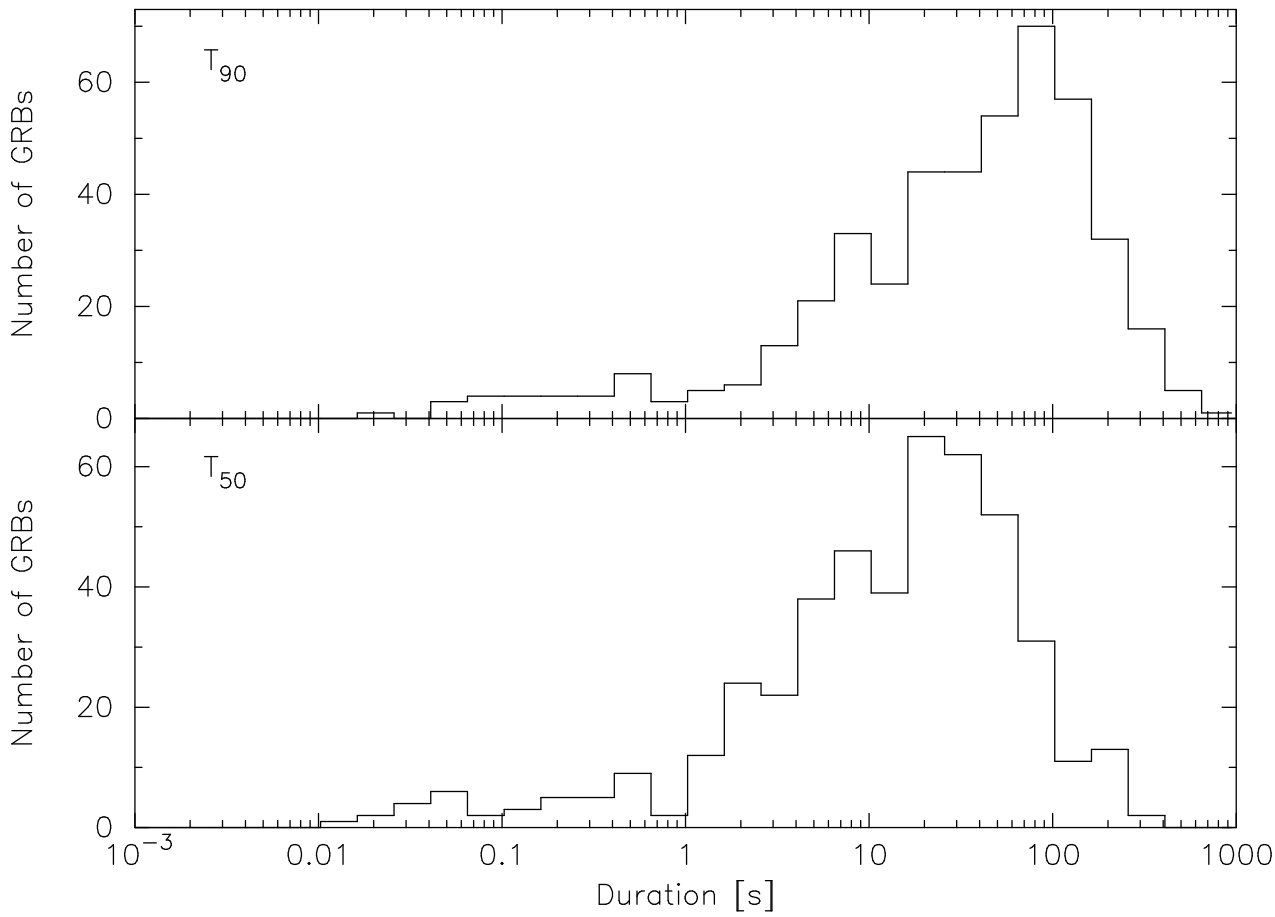

Fig. 6.— T_{90}(*top*) and T_{50}(*bottom*) distributions from the BAT mask-weighted light curves in the 15-350 keV band.

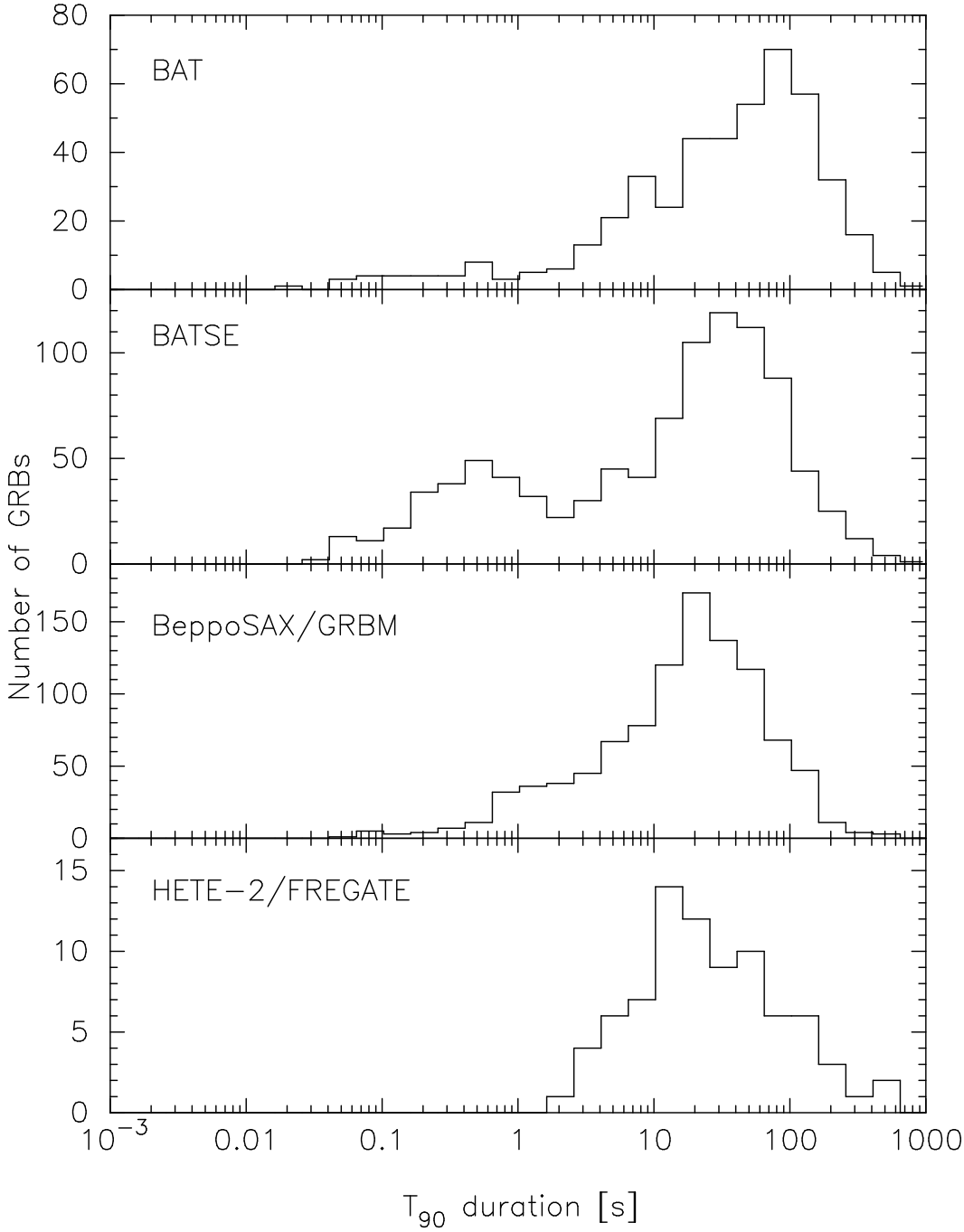

Fig. 7.— T_{90} distribution of BAT by the mask-weighted light curve in the 15-350 keV band, BATSE by the light curve in the 50-350 keV band, *BeppoSAX* by the light curve of the GRBM instrument in the 40-700 keV band, and HETE-2 by the light curve of the FREGATE instrument in the 6-80 keV band from top to bottom.

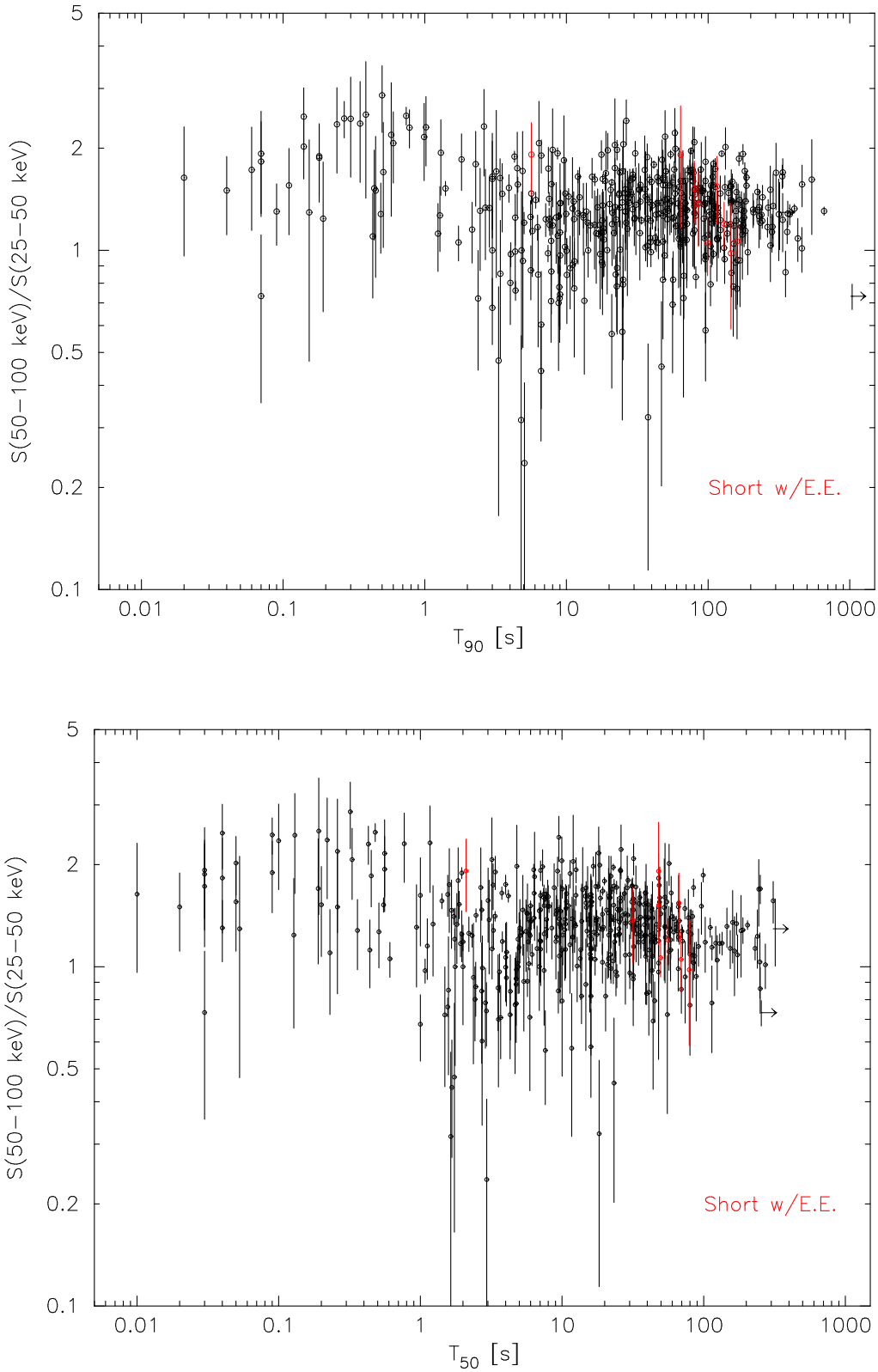

Fig. 8.— The fluence ratio between the 50-100 keV and the 25-50 keV bands and T_{90}(*top*) and T_{50}(*bottom*). Short GRBs with an E.E. are shown in red.

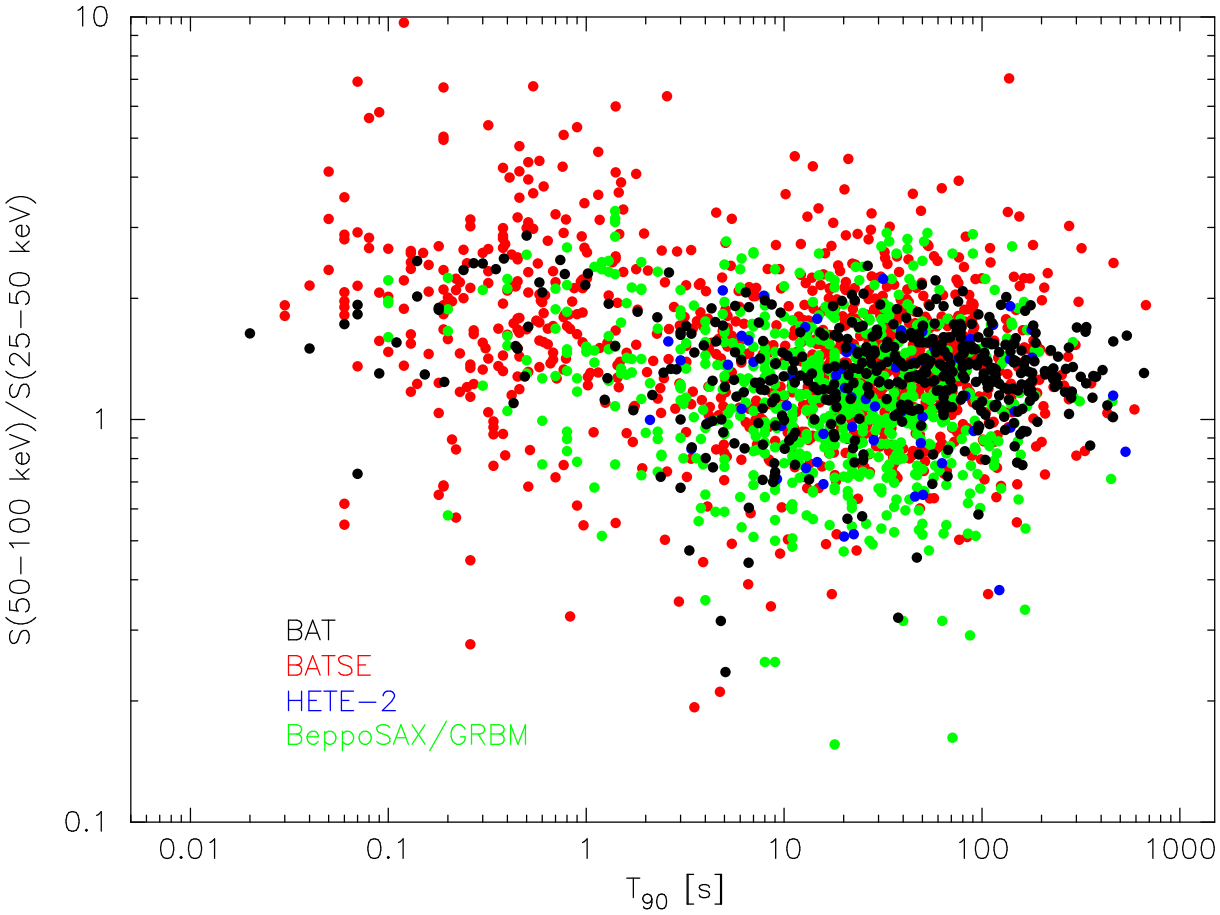

Fig. 9.— The fluence ratio between the 50-100 keV and the 25-50 keV bands and T_{90} for BAT (black), BATSE (red), *HETE*-2 (blue) and *BeppoSAX* (green) GRBs.

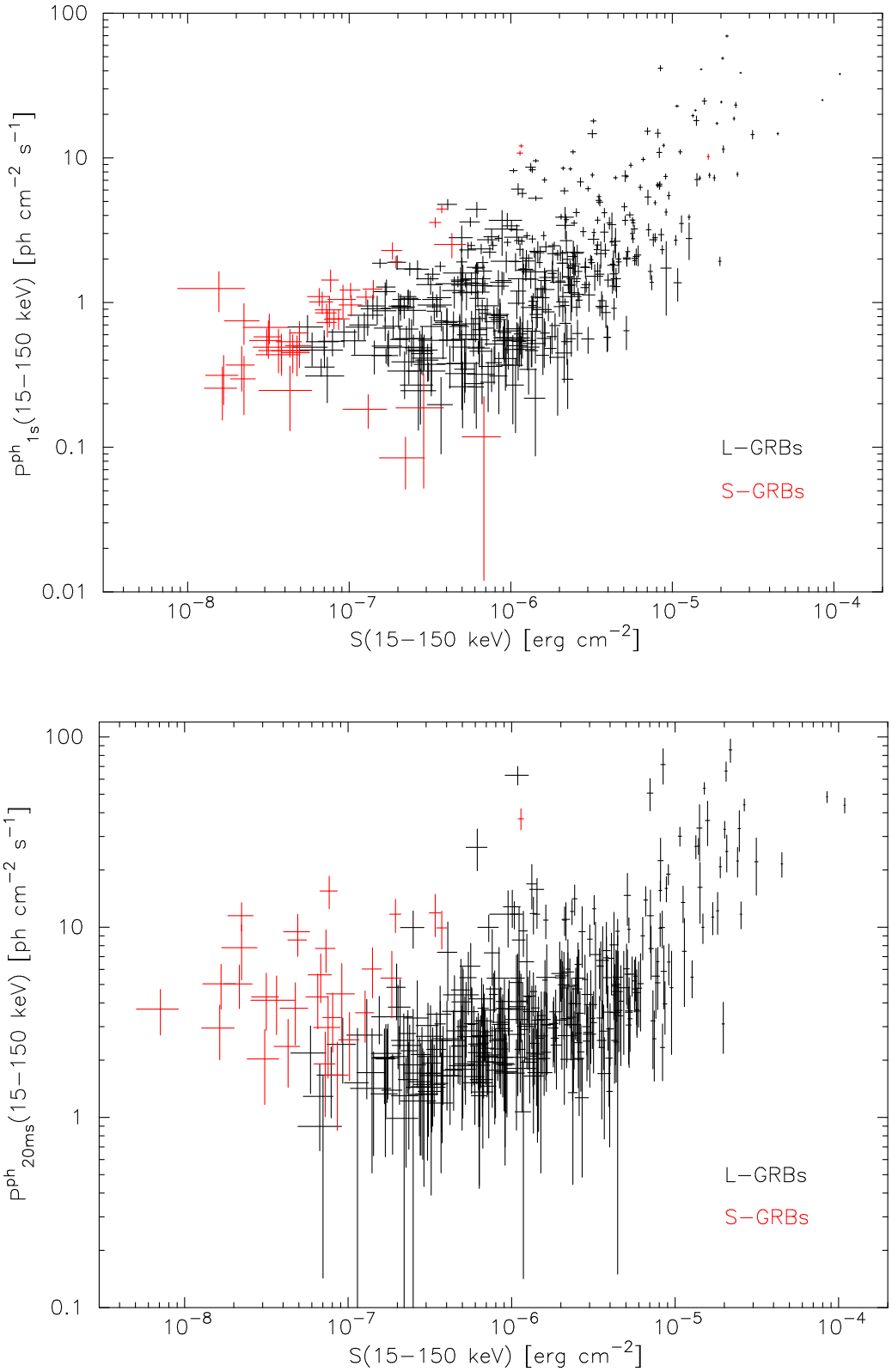

Fig. 10.— Distributions of 1 s peak photon flux (top) and 20 ms peak photon flux (bottom) in the 15-150 keV band and the energy fluence in the 15-150 keV band.

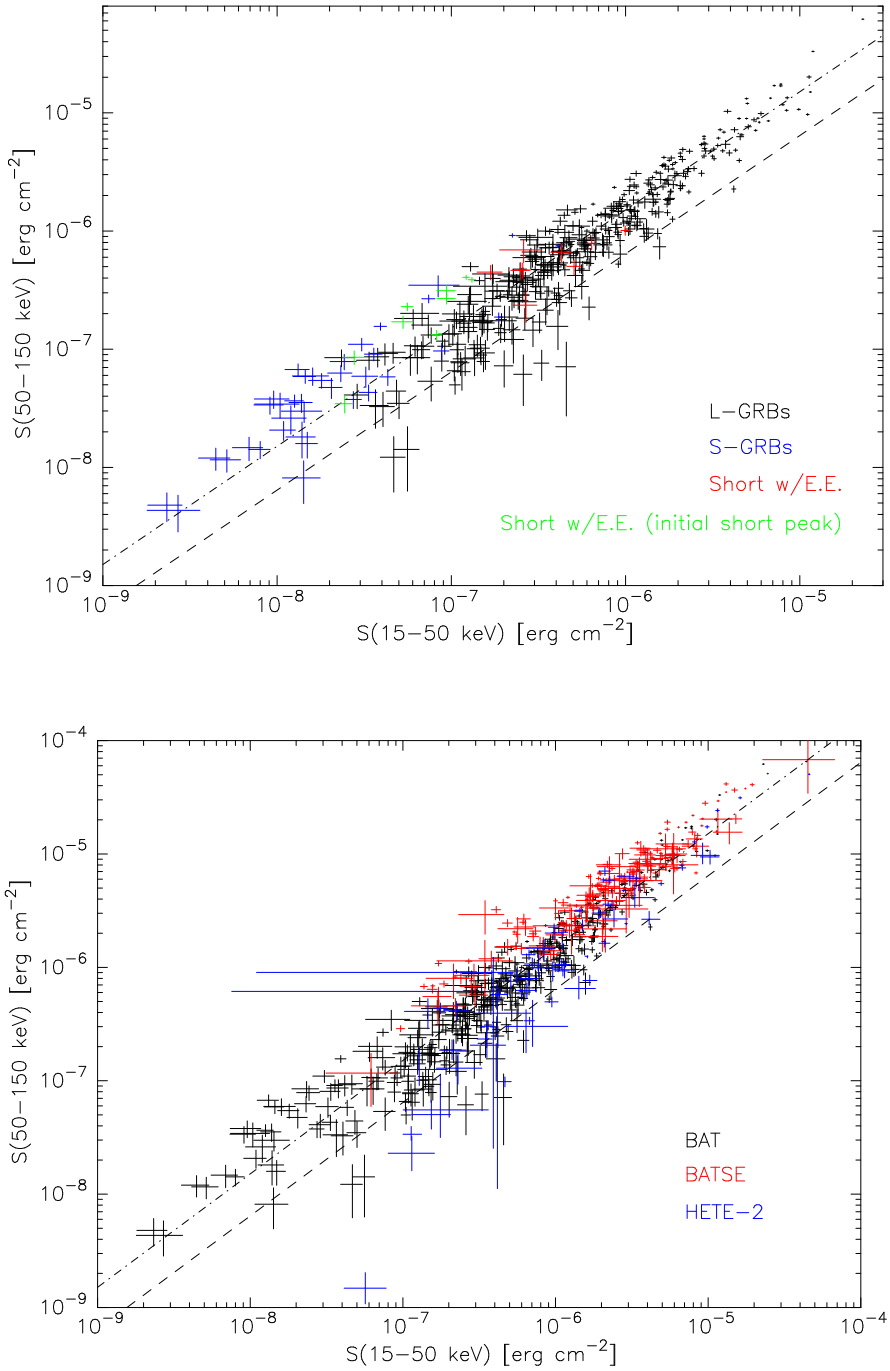

Fig. 11.— *Top*: Distribution of the energy fluence in the 50-150 keV band vs. that in the 50-150 keV band for the BAT GRBs. L-GRBs are in black, S-GRBs are in blue, S-GRBs with E.E. are in red, and the initial short spikes of S-GRBs with E.E. are in green. The dashed-dotted line is the case of the Band function of $\alpha = -1$, $\beta = -2.5$, and $E_{\rm peak}^{\rm obs} = 100$ keV. The dashed line is the case of the Band function of $\alpha = -1$, $\beta = -2.5$, and $E_{\rm peak}^{\rm obs} = 30$ keV. *Bottom*: Distribution in the same plane as top among different missions. The BAT sample is in black, the BATSE sample is in red, and the HETE-2 sample is in blue. The dashed-dotted and dashed lines are same as top.

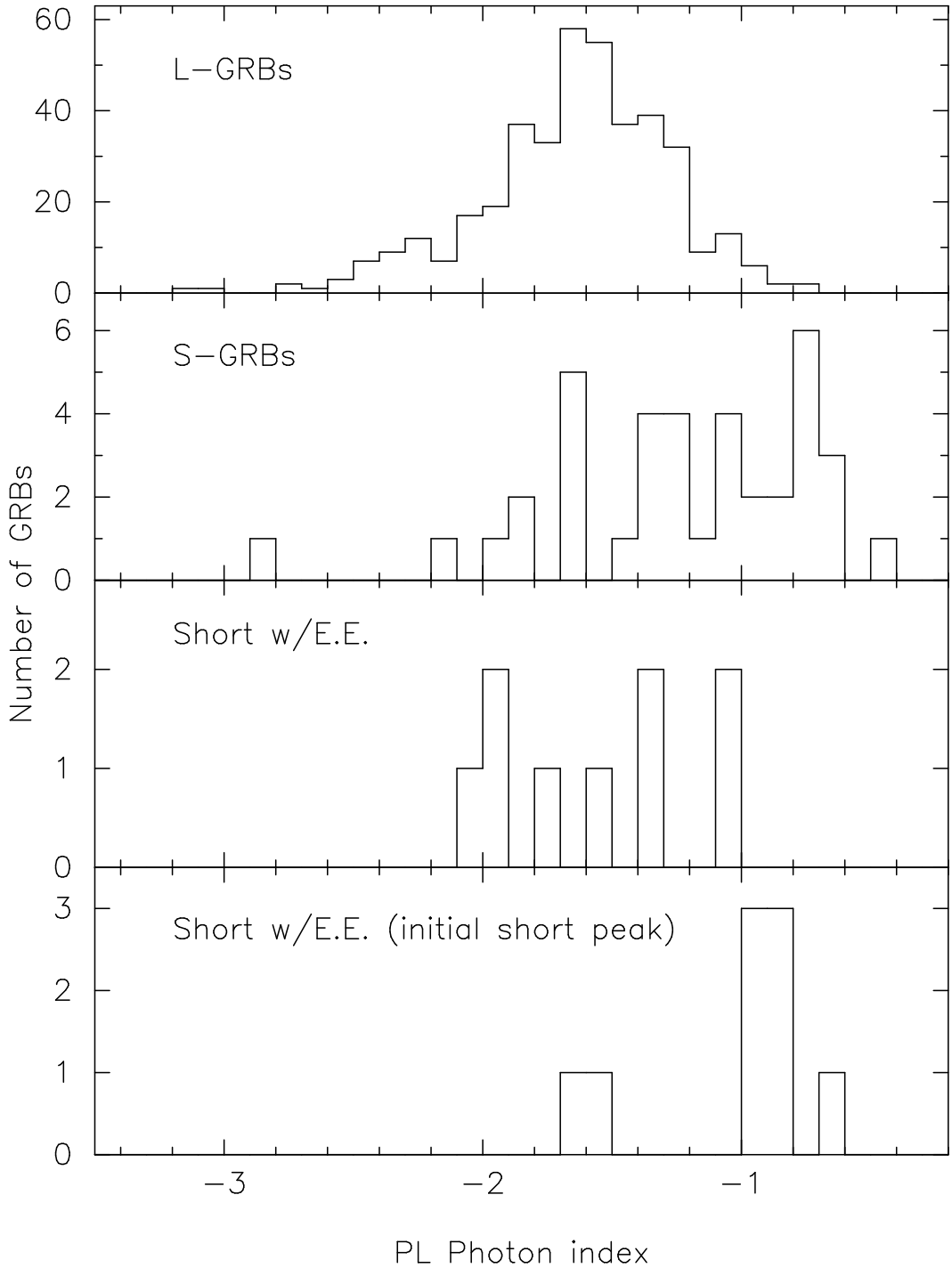

Fig. 12.— Histograms of the BAT time-averaged photon index in a PL fit for the L-GRBs, the S-GRBs, the S-GRBs with E.E. and the initial short spikes of the S-GRBs with E.E. from top to bottom.

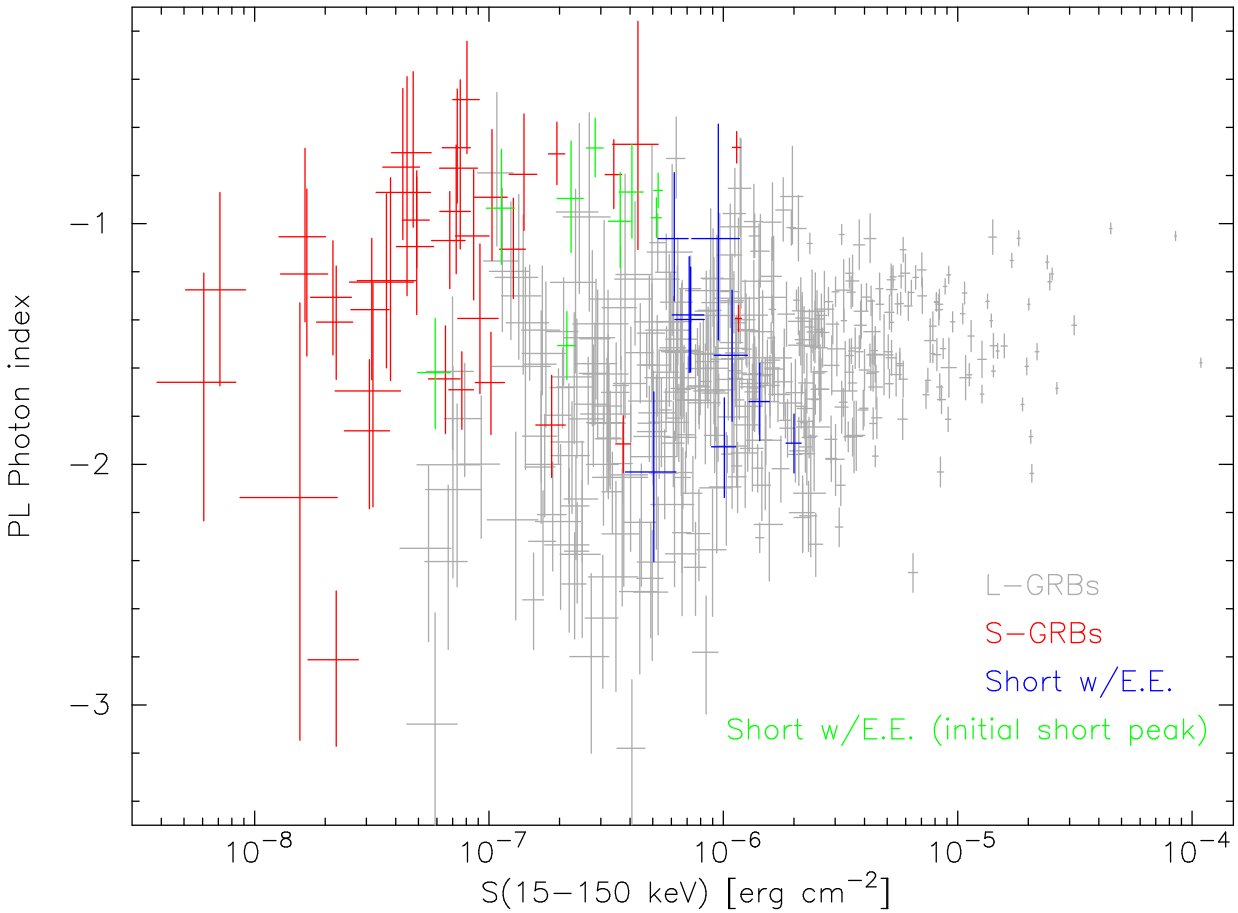

Fig. 13.— Distribution of the BAT PL photon index vs. the energy fluence in the 15-150 keV band for the L-GRBs (light gray), the S-GRBs (red), the S-GRBs with E.E. (blue) and the initial short spikes of the S-GRBs with E.E.(green).

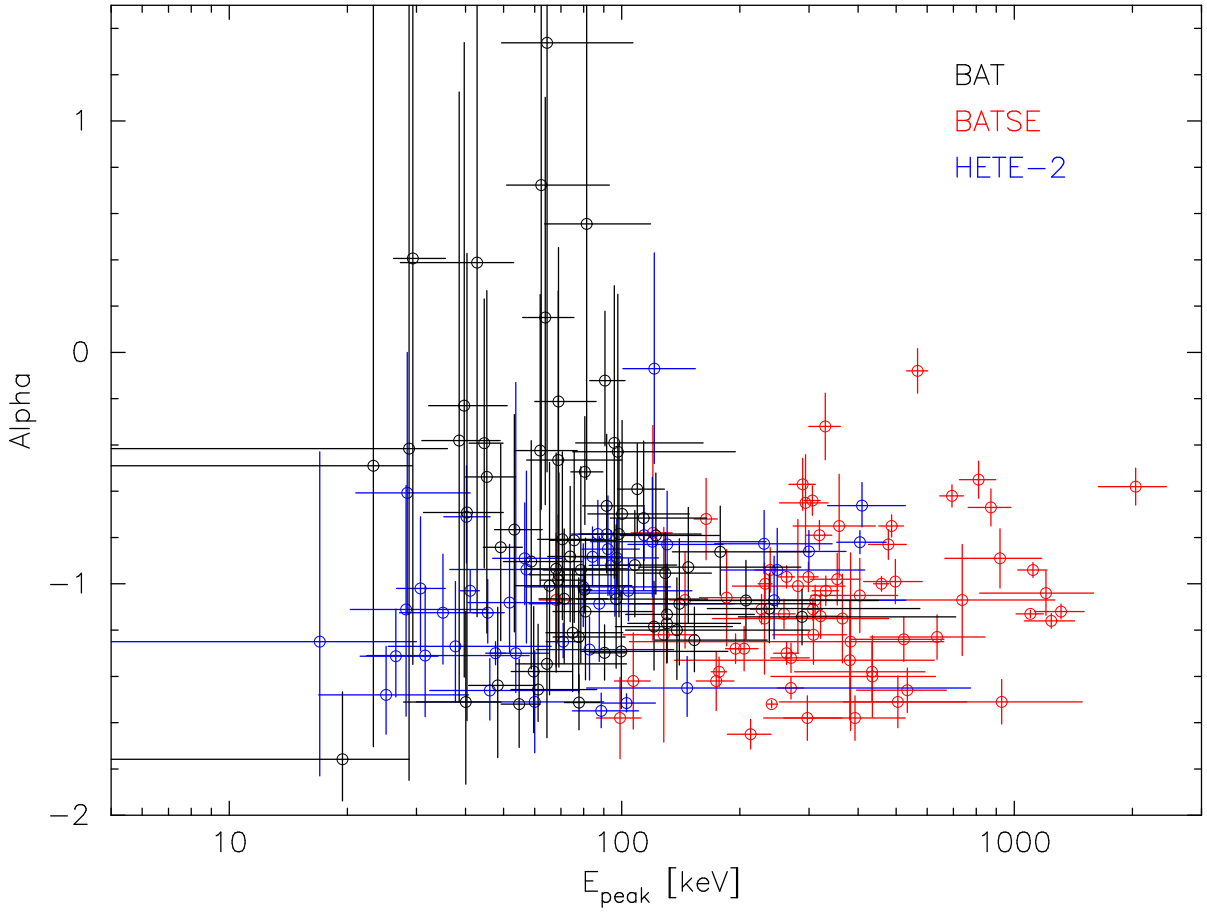

Fig. 14.— Distributions of the photon index α and $E_{\rm peak}$ in a CPL fit for the BAT (black), the BATSE (red) and the HETE-2 (blue) GRBs.

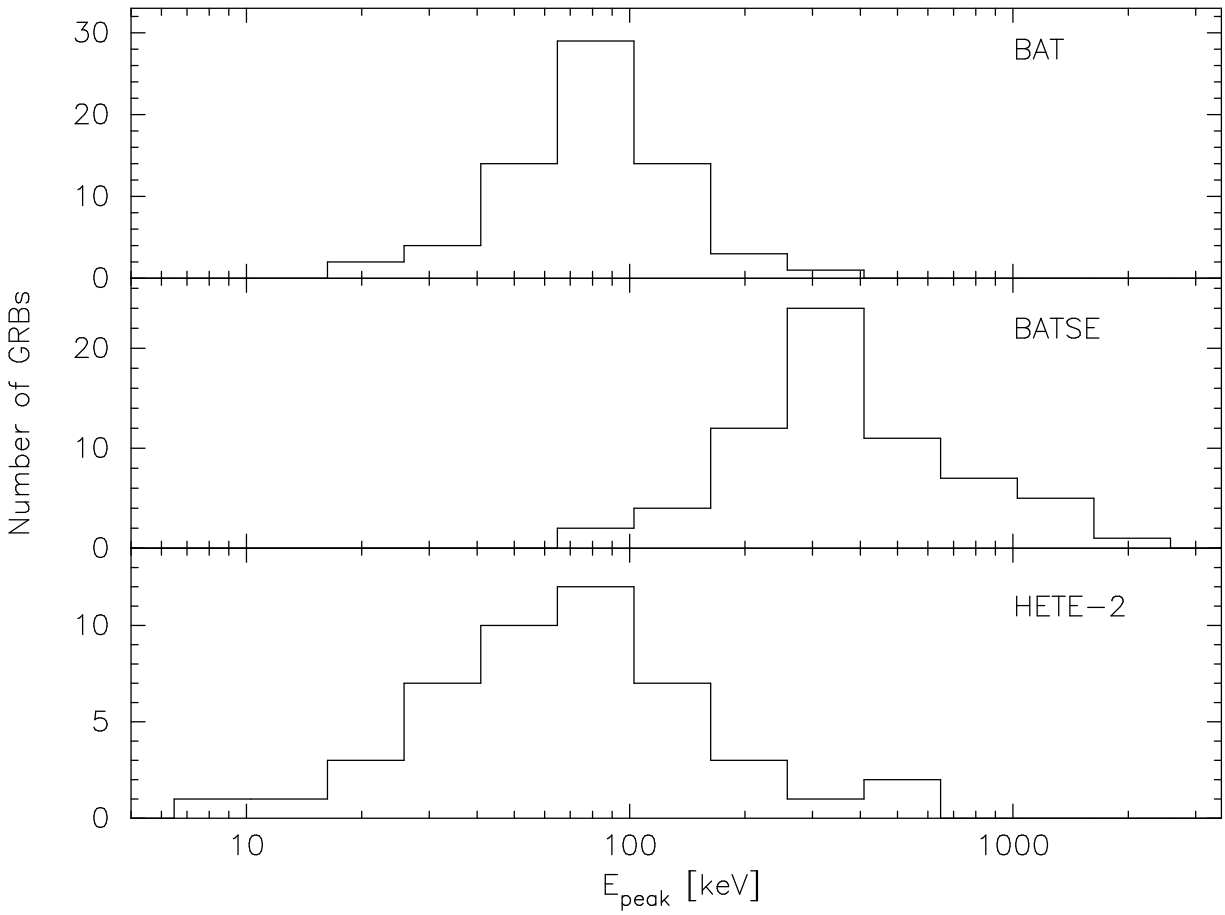

Fig. 15.— Histograms of $E_{\rm peak}$ in a CPL fit for the BAT (top), the BATSE (middle) and the HETE-2 (bottom) GRBs.

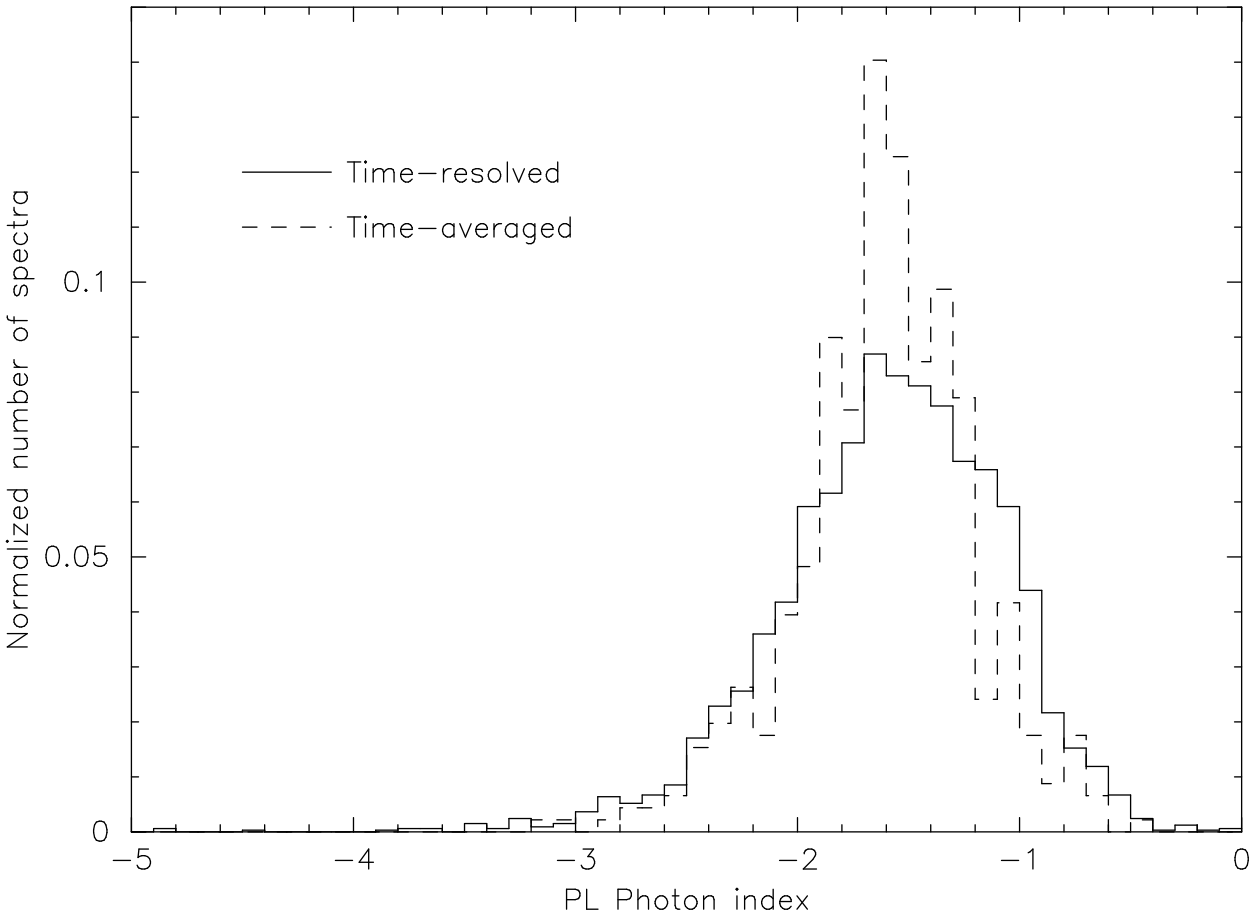

Fig. 16.— Histograms of the BAT photon index in a PL fit for the time-resolved (solid) and the time-averaged (dash) spectra. The histograms are normalized by a total number of spectra.

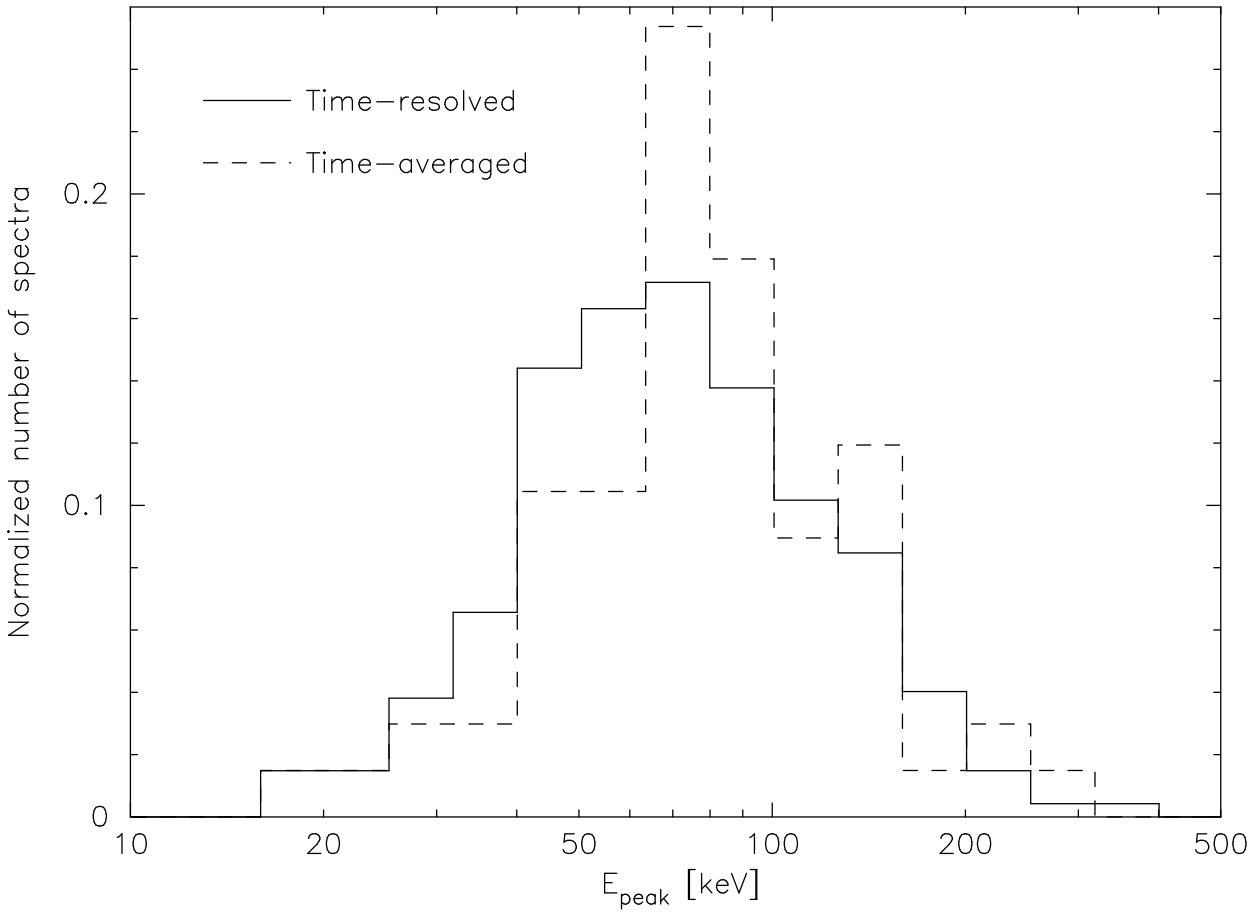

Fig. 17.— Histograms of the BAT $E_{\rm peak}$ in a CPL fit for the time-resolved (solid) and the time-averaged (dash) spectra. The histograms are normalized by a total number of spectra.

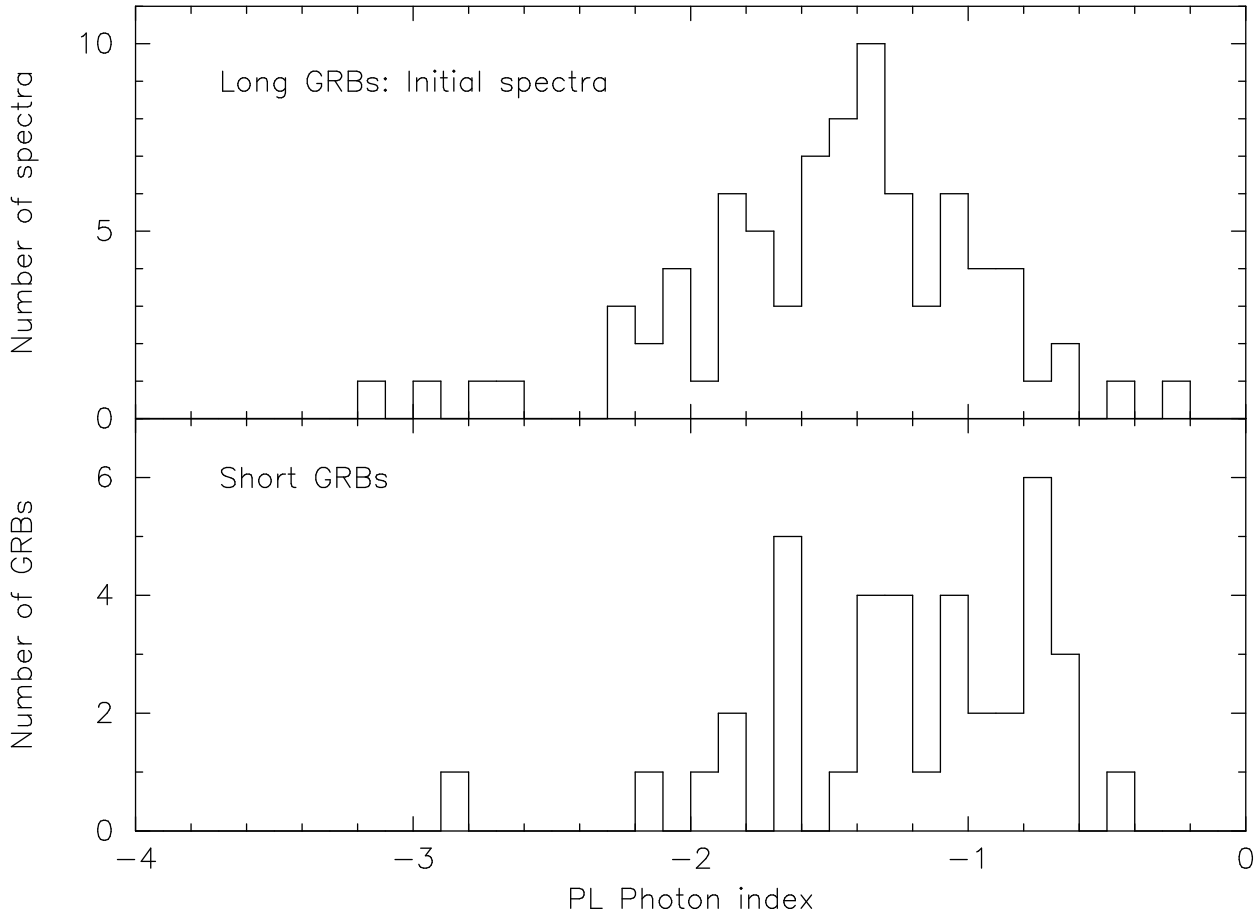

Fig. 18.— Histograms of the BAT photon index in a PL fir for initial 0.1-2 s spectra of long GRBs (top) and for short GRBs (bottom).

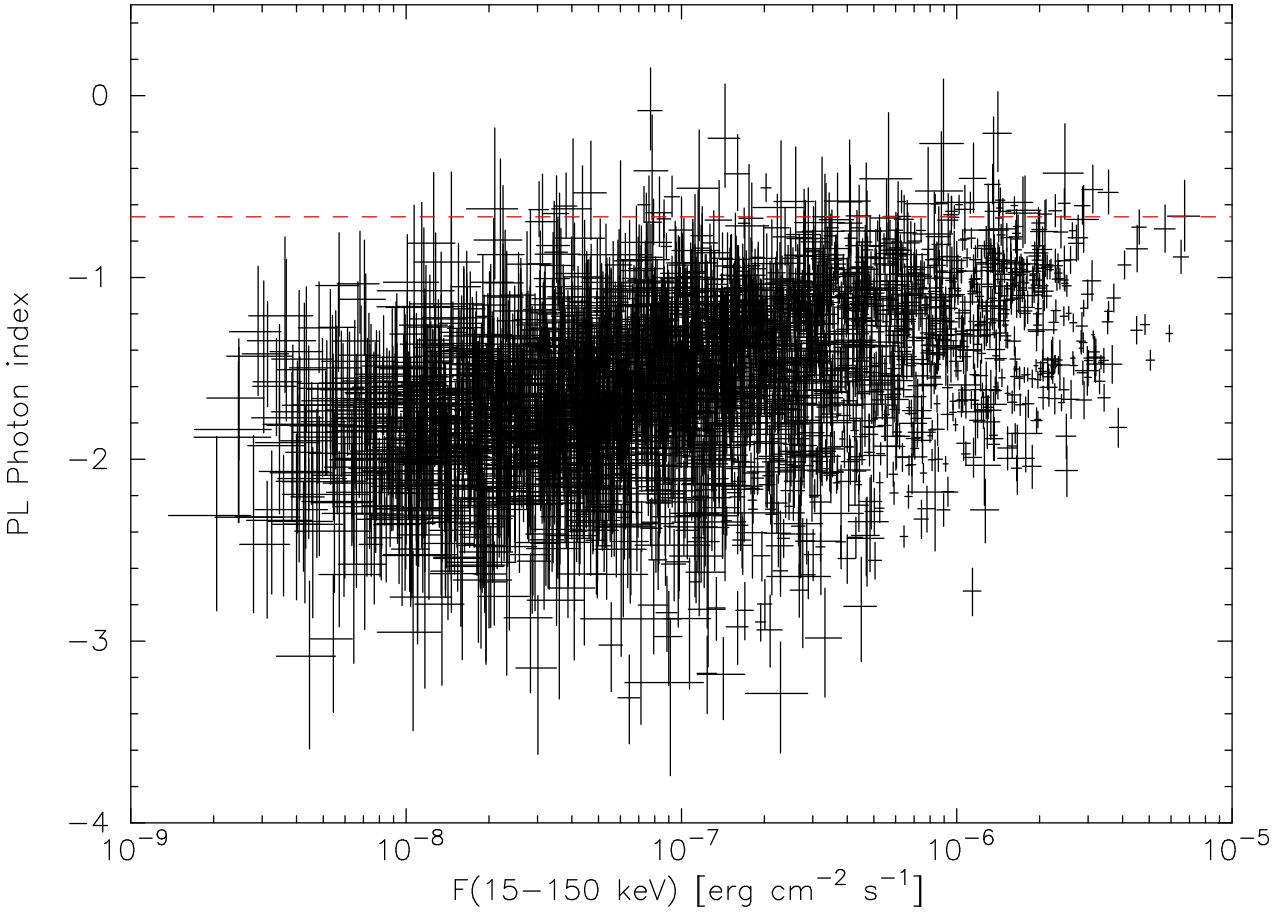

Fig. 19.— Distribution of the BAT photon index in a PL fit vs. energy flux in the 15-150 keV band. The red dashed line shows the photon index of -2/3. The total number of time-resolved spectra is 2968.

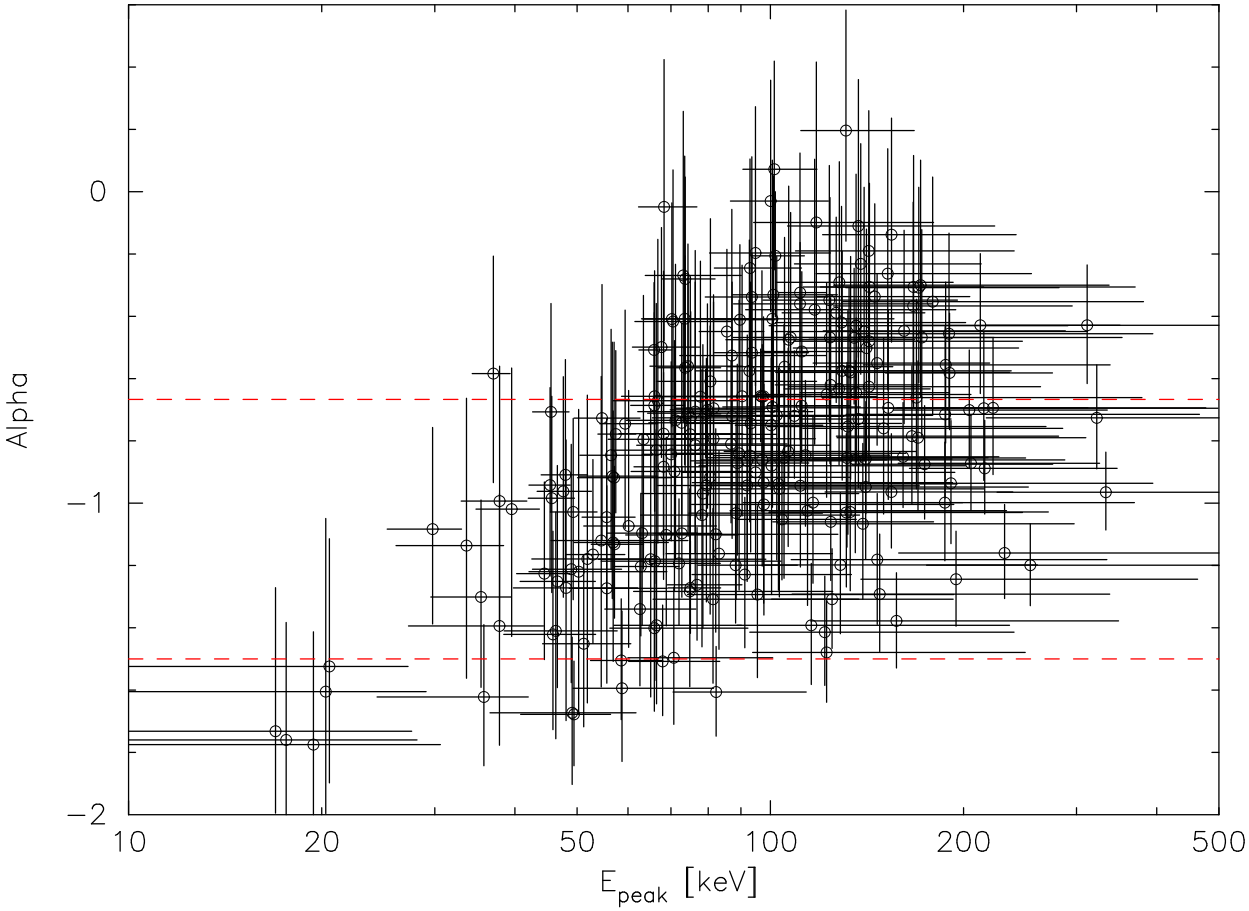

Fig. 20.— Distribution of the BAT photon index α and $E_{\rm peak}$ in a CPL fit. The red dashed lines show the photon index region from $-3/2$ to $-2/3$. The total number of time-resolved spectra is 234.

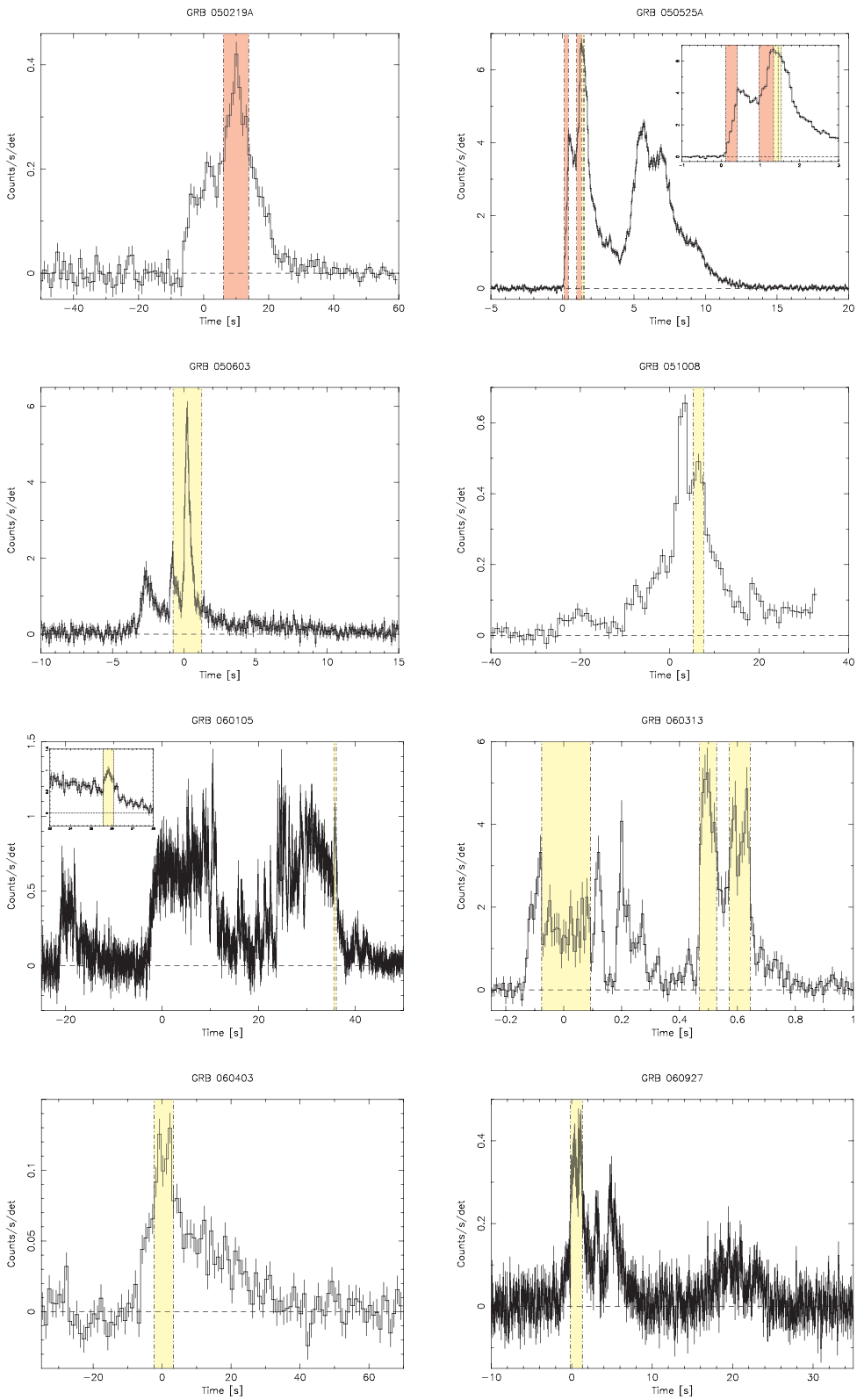

Fig. 21.— The BAT light curve with the interval showing the spectra exceeding the limits of the SSM as hatches. The red hatch is the interval exceeding the limit $> 3.2\ \sigma$. The yellow hatch is the interval exceeding the limit $> 1.6\ \sigma$ but $< 3.2\ \sigma$.

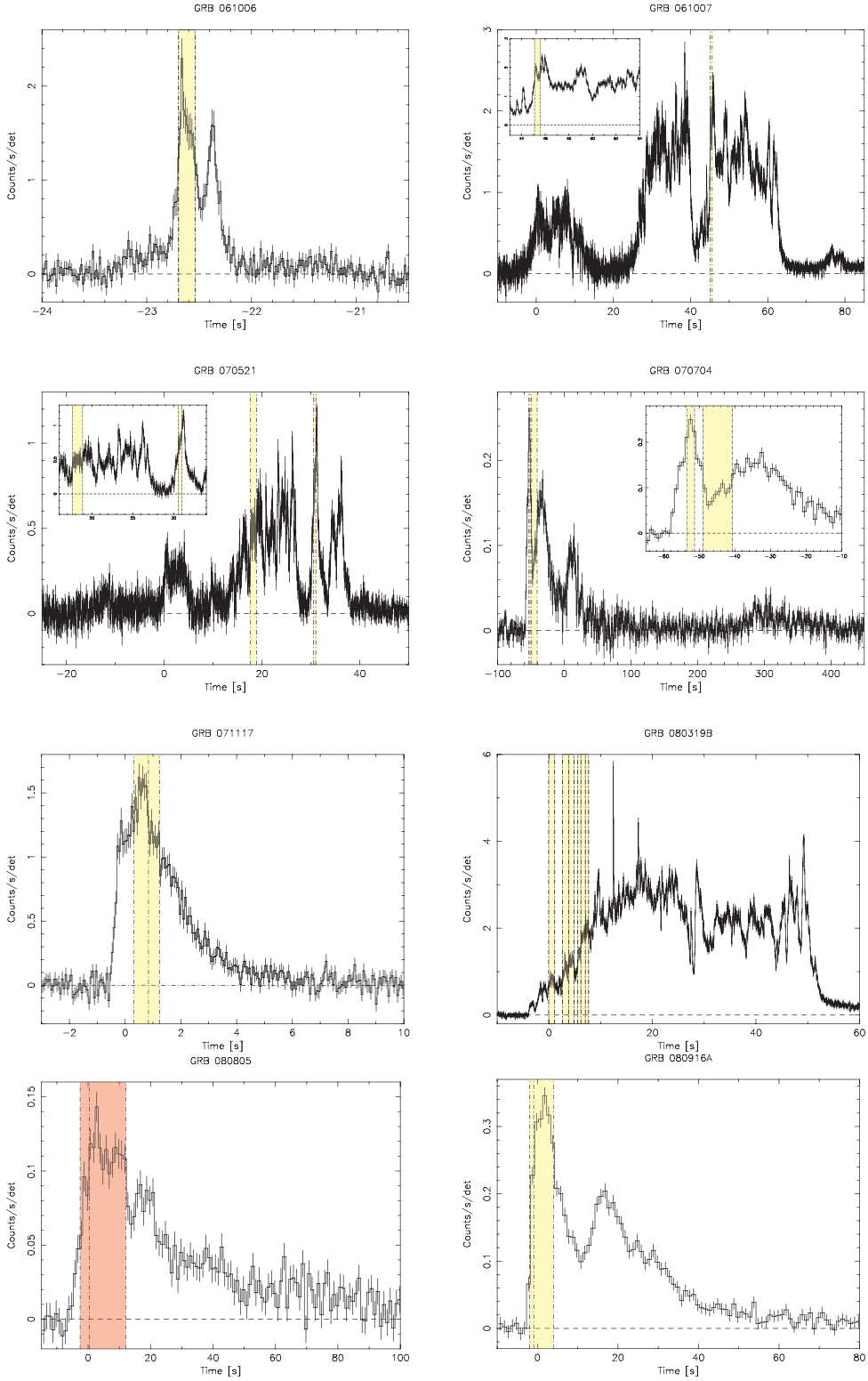

Fig. 22.— Continue

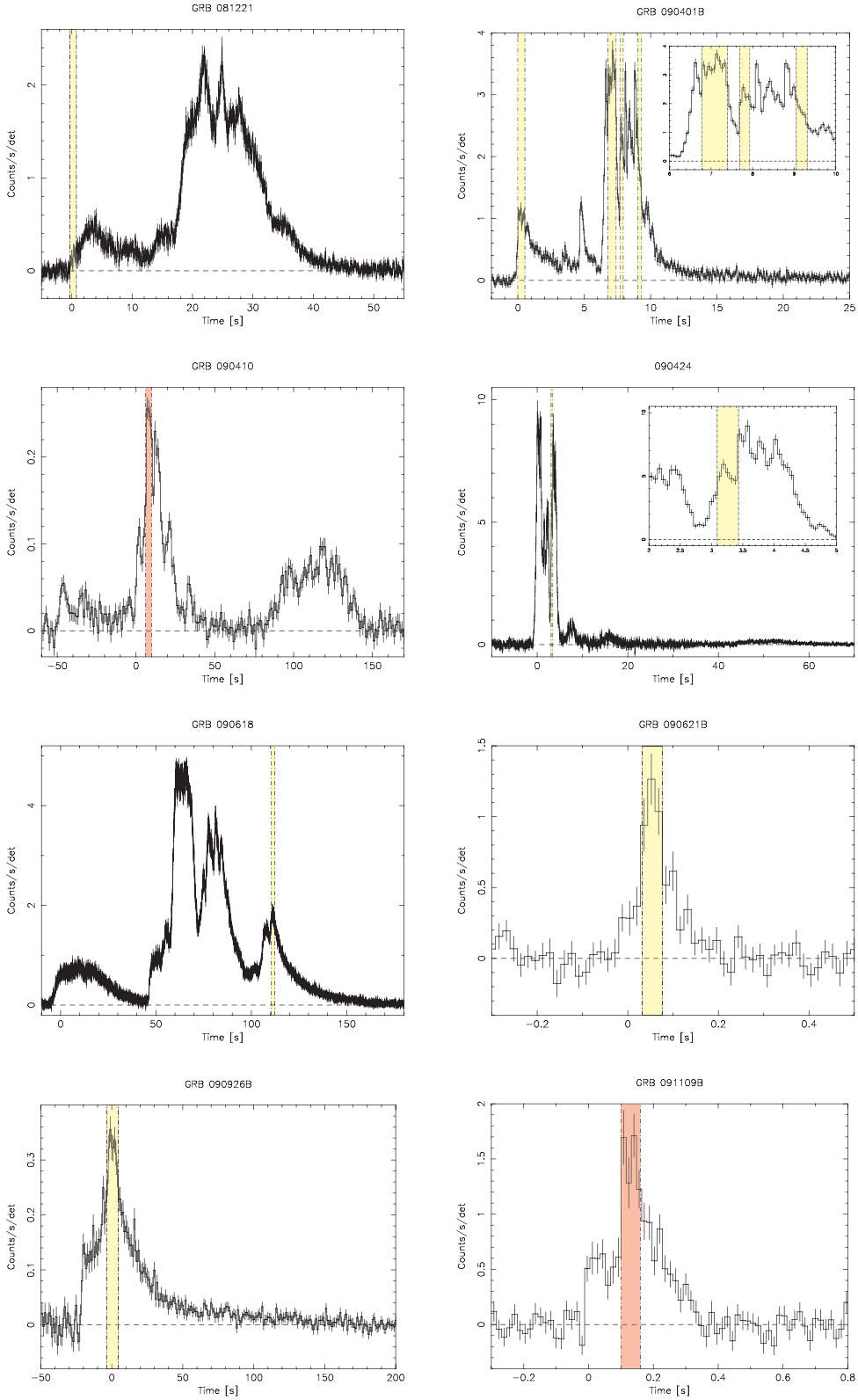

Fig. 23.— Continue

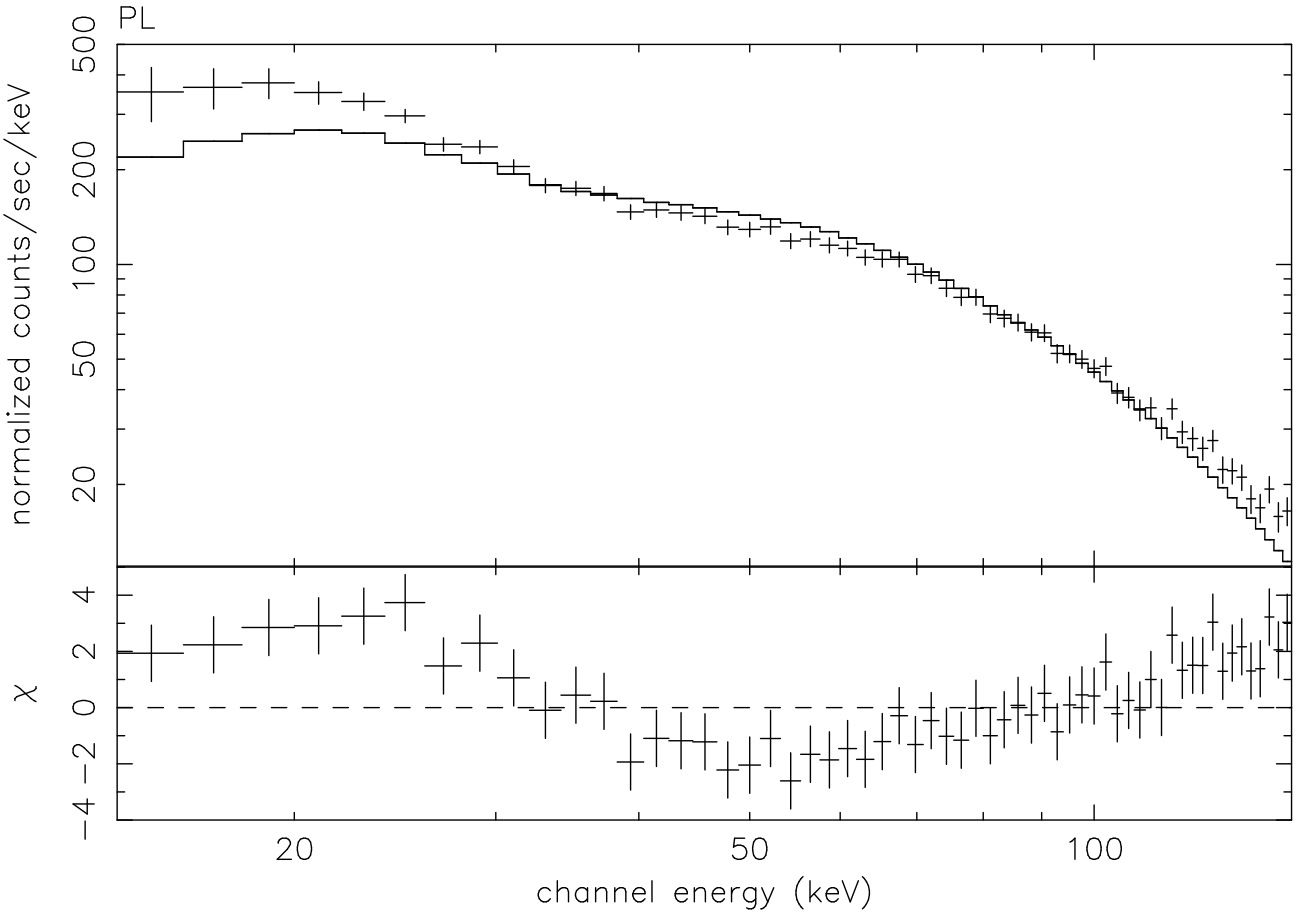

Fig. 24.— The simulated BAT spectrum of the *Fermi* GRB 090902B interval b spectral parameters as the input spectrum. The best fit spectral model (solid line) is a PL.

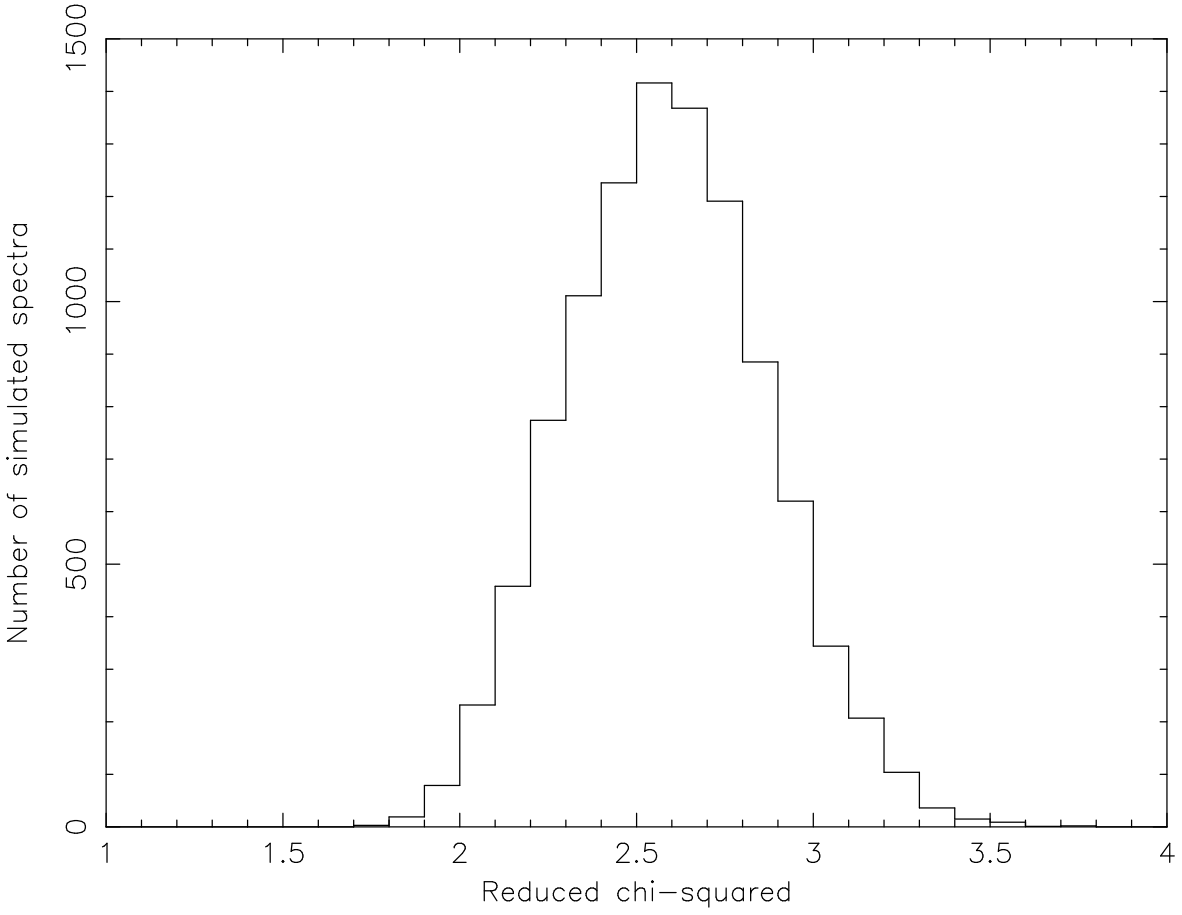

Fig. 25.— Histogram of reduced χ^2 in a PL fit of 10,000 BAT simulated spectra of the *Fermi* GRB 090902B interval b spectral parameters as the input spectrum.

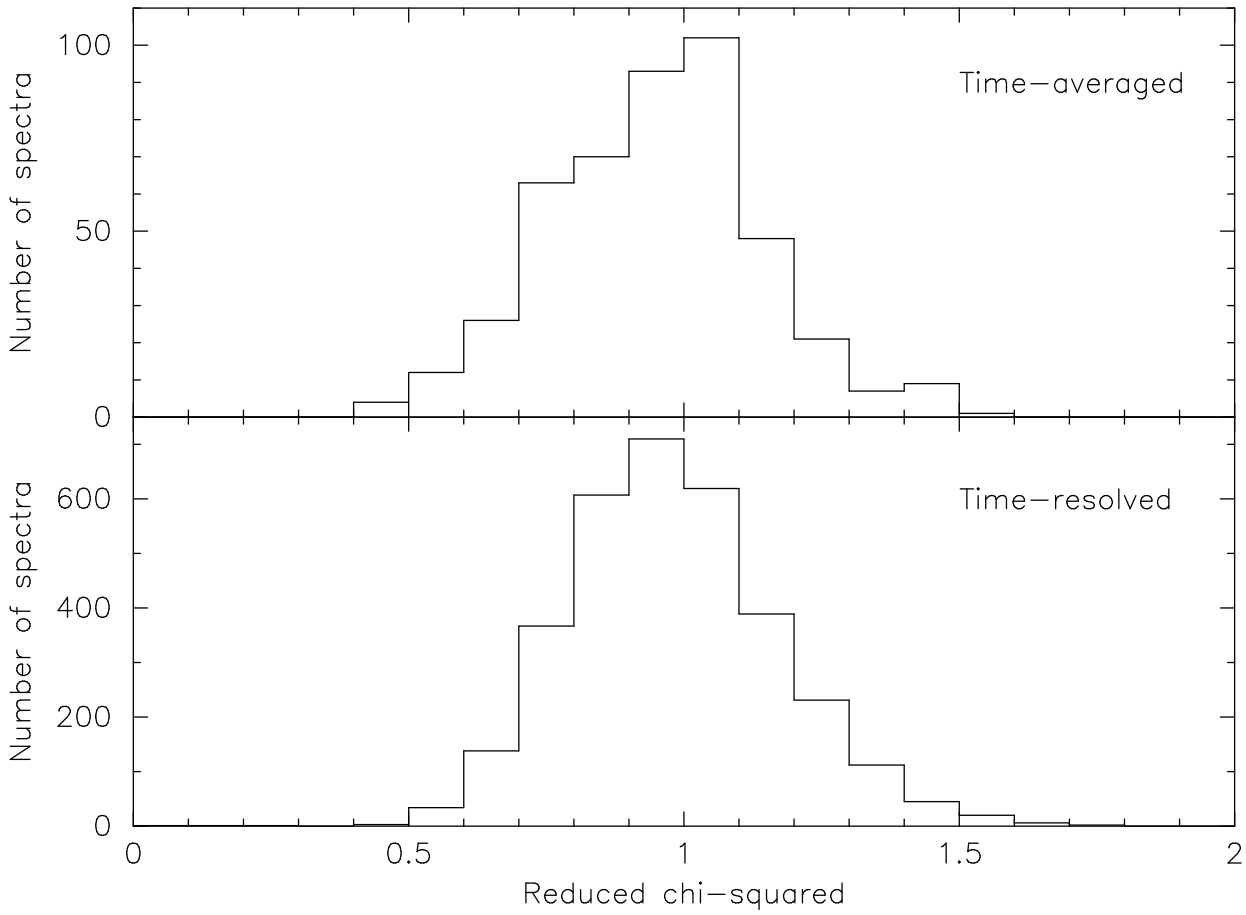

Fig. 26.— Histogram of reduced χ^2 in the best fit model (either a PL or a CPL model) for the time-averaged spectra (top) and the time-resolved spectra (bottom). The Gaussian fit to the histograms shows the peak of 0.95 with a σ of 0.19 and the peak of 0.96 with a σ of 0.18 respectively.

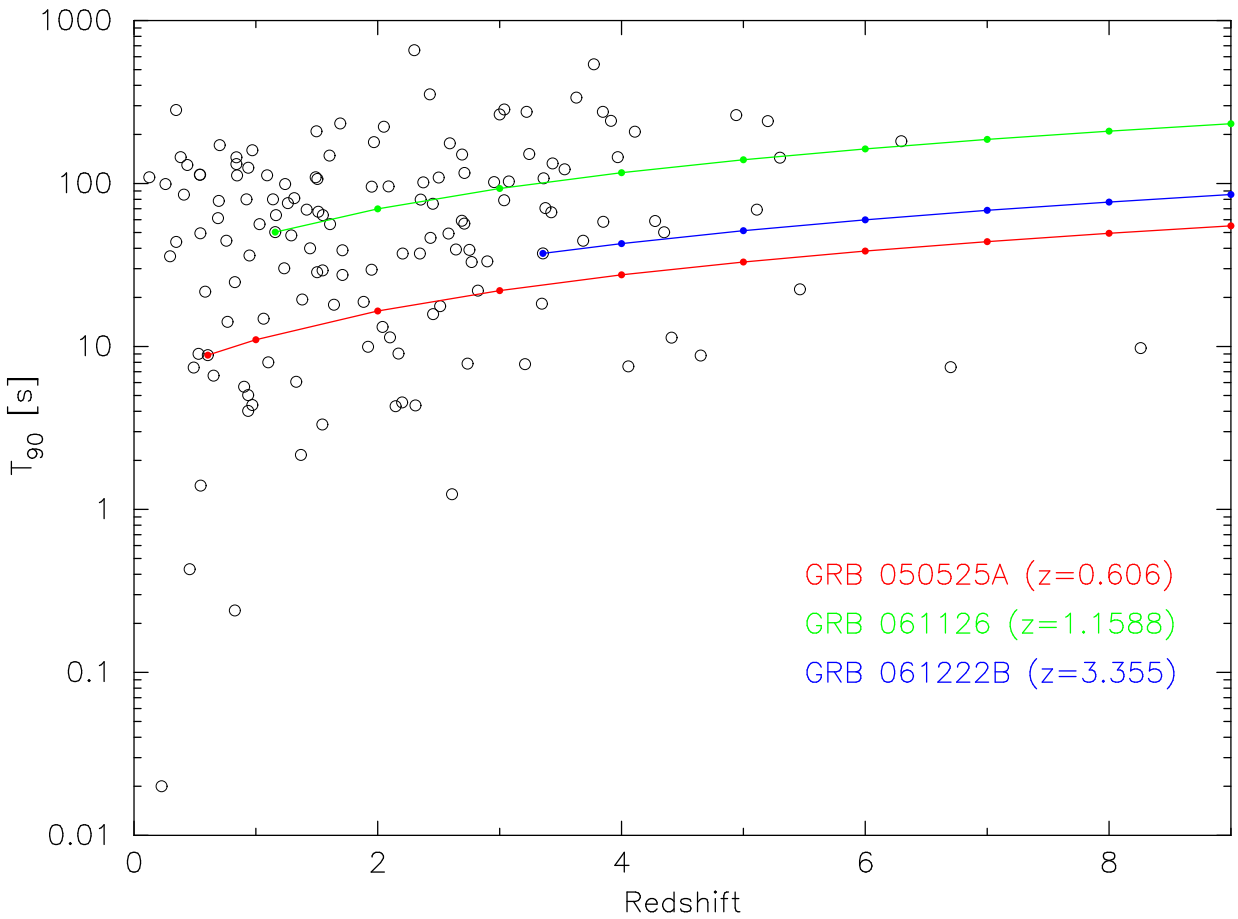

Fig. 27.— Distribution of the BAT observed T_{90} vs. redshift. For three known redshift GRBs, GRB 050525A (z=0.606), GRB 061126 (z=1.1588) and GRB 061222B (z=3.355), we calculated the trajectories of estimated observed T_{90} as a function of redshift assuming that the duration changes only by the time-dilation effect.

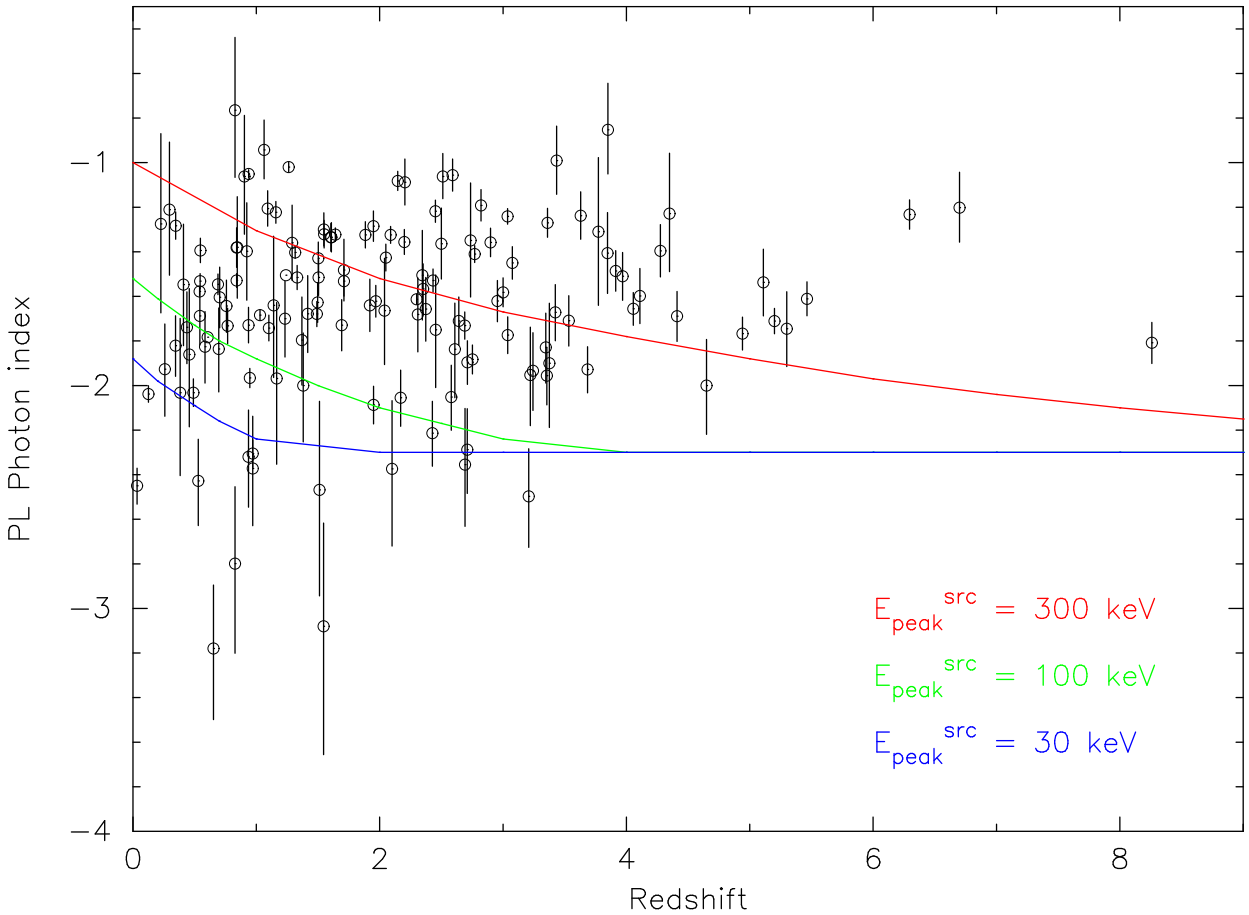

Fig. 28.— Distribution of the BAT observed PL photon index vs. redshift. The overlaid curves are the estimations of the BAT observed PL photon index as a function of redshift assuming the observed BAT PL photon index is the redshifted spectrum of the typical Band function shape with the rest-frame $E_{\rm peak}$ of 300 keV (red), 100 keV (green) and 30 keV (blue).

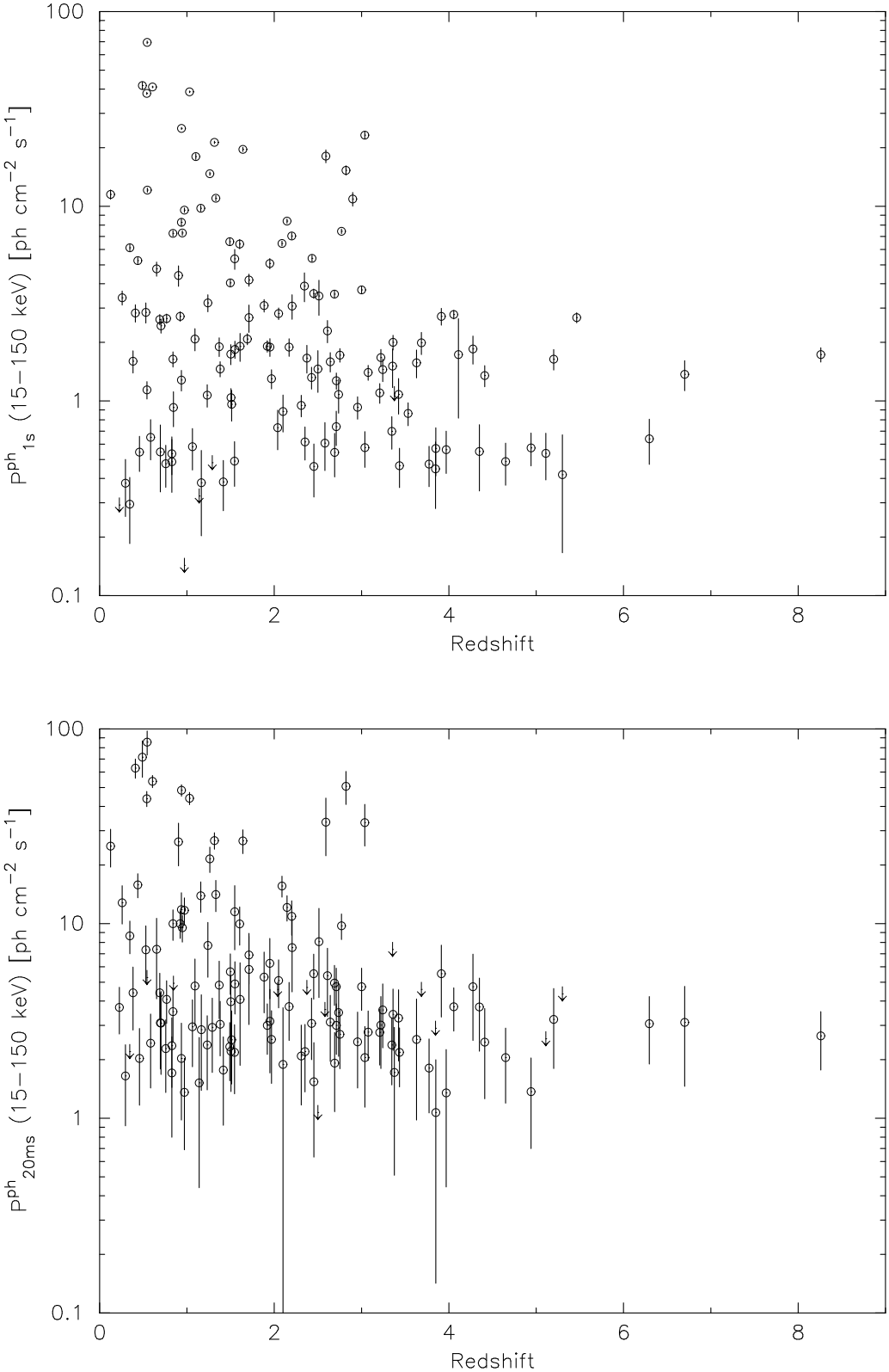

Fig. 29.— Distribution of 1 s (top) and 20 ms (bottom) observed peak photon flux in the 15-150 keV band vs. redshift.

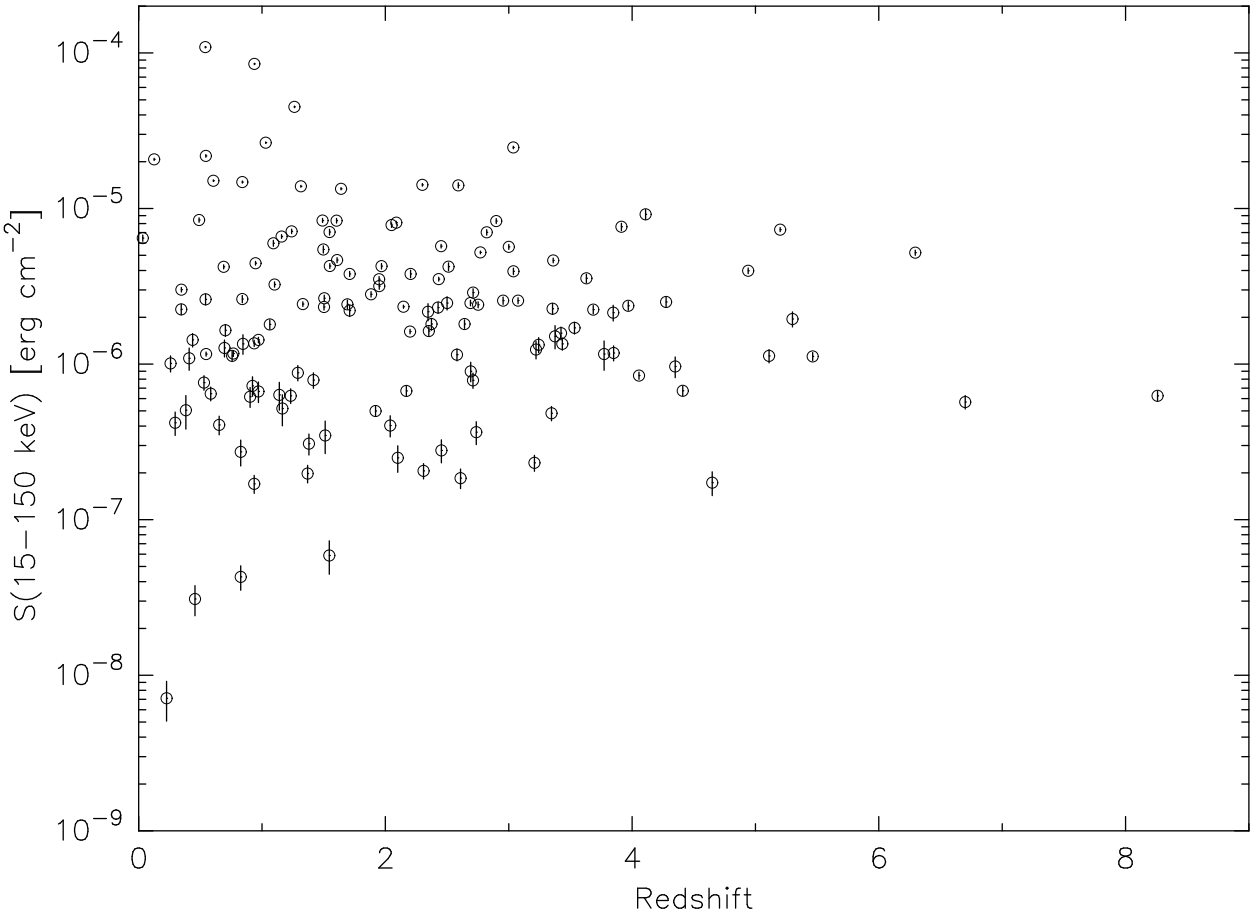

Fig. 30.— Distribution of the BAT observed energy fluence in the 15-150 keV band vs. redshift.

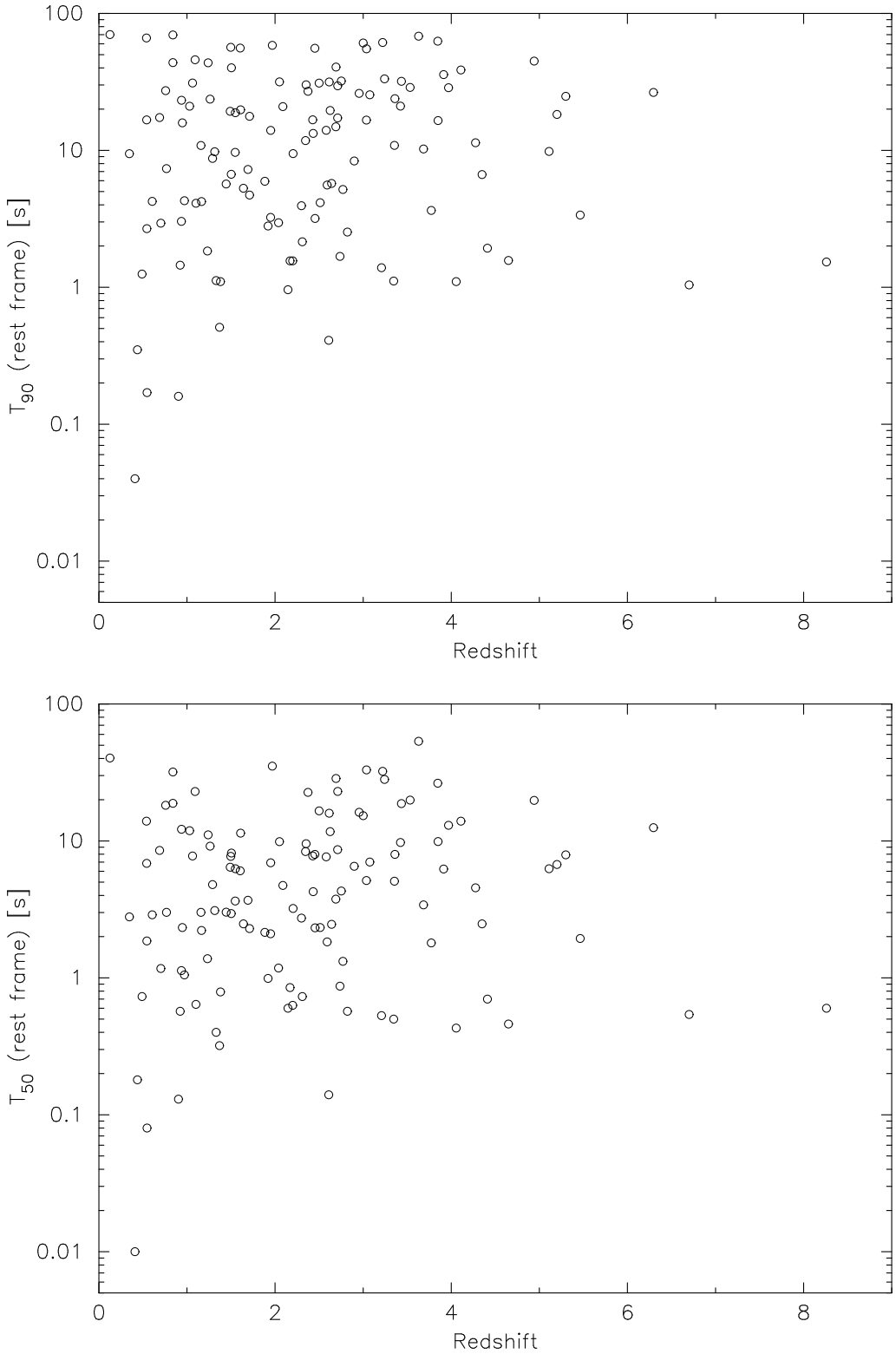

Fig. 31.— Distributions of T_{90} (top) and T_{50} (bottom) in the 140-220 keV band at the GRB rest frame vs. redshift.

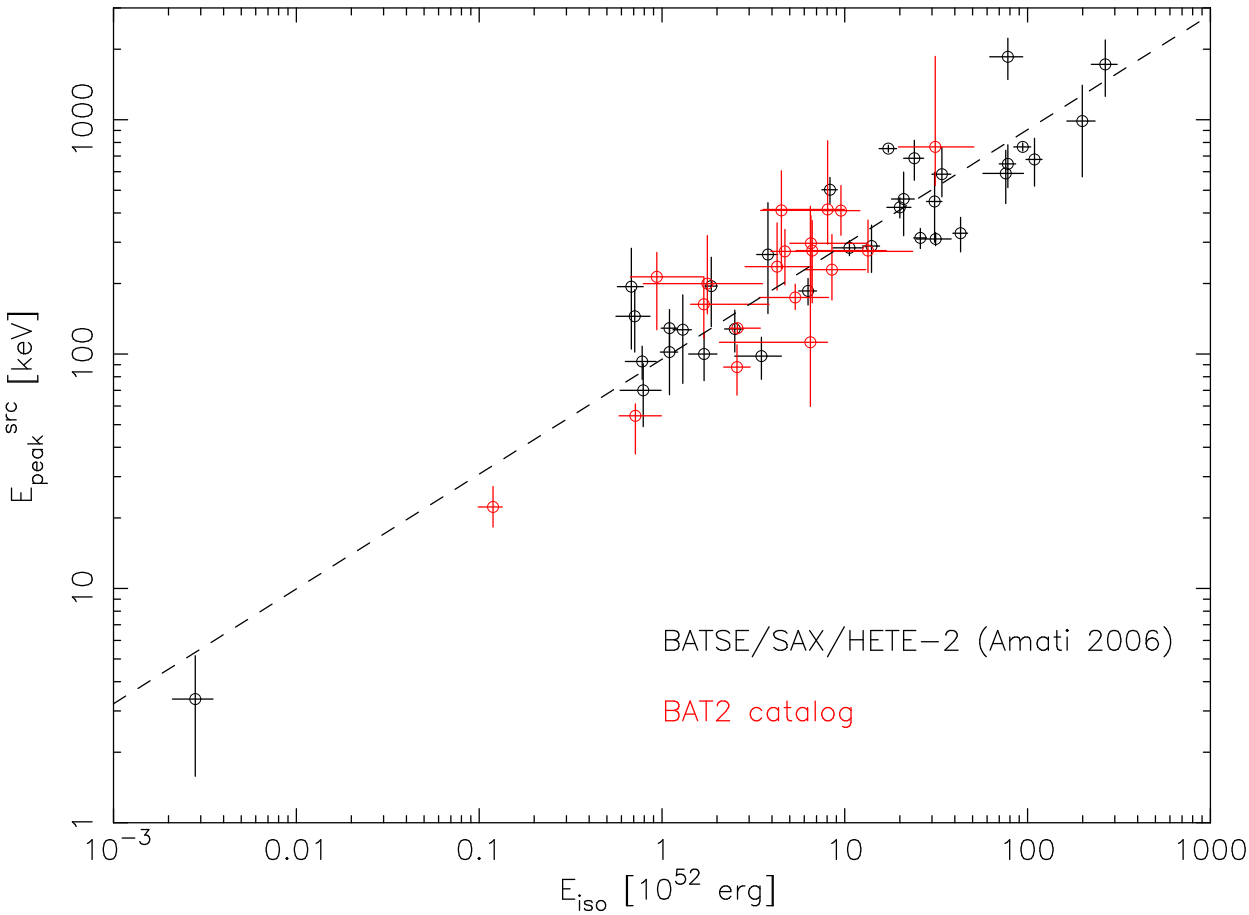

Fig. 32.— The correlation between $E_{\rm peak}^{\rm src}$ and $E_{\rm iso}$ for the *Swift* GRBs (red) and other GRB missions (black). The dashed line is the best fit correlation between $E_{\rm peak}^{\rm src}$ and $E_{\rm iso}$ reported by (Amati 2006): $E_{\rm peak}^{\rm src} = 95 \times (E_{\rm iso}/10^{52})^{0.49}$.